

Thermally Activated Walls for Reducing Energy Consumption of Cold-Climate Buildings

by

Mohammad Rezvanpour

A thesis submitted in partial fulfillment of the requirements for the degree of

Master of Science
in
Civil (Cross-disciplinary)

Department of Civil and Environmental Engineering
University of Alberta

© Mohammad Rezvanpour, 2023

Abstract

The global increase in energy usage and greenhouse gas (GHG) emissions is largely due to the ascending trend of energy consumption in buildings. To address the negative impacts of this trend, designing energy-efficient buildings is crucial. As a potential solution, thermal energy storage (TES) systems, specifically using active TES in buildings' mass have been proposed. This thesis focuses on reducing thermal loads (i.e., space cooling and heating loads) in cold-climate buildings by investigating the implementation of two methods of active TES in walls: the use of domestic cold water (DCW) for space cooling and ventilated concrete block wall (VBW) with supply air to zone (SAZ).

DCW can be circulated through thermally massive walls before regular household consumption (e.g., shower) (herein "DCW-wall") to provide free cooling without wasting DCW. The study evaluated the cooling potentials of DCW-wall system through 3D transient thermal simulations and revealed that the system is effective in providing cooling energy to the zone. With low inlet DCW temperatures, the system was able to deliver a significant amount of cooling energy per day, which could contribute to a substantial portion of the annual energy demand for space cooling in cities with cold climates like Toronto.

In VBW system air is circulated between a zone and the voided cores of a VBW, where the air exchanges heat with the wall before returning to the zone. To evaluate the system's performance, typical-day and annual energy analyses were conducted under various boundary conditions and air circulation speeds. The study found that a VBW with a 2 m/s air circulation speed throughout the day can lead to 67% more thermal energy storage when compared to having no air circulation. The annual analysis compared the energy performance between a VBW and a traditional wood-frame wall in different cold climates. In addition, an annual energy analysis showed that substituting a traditional wood-frame wall with a VBW can yield

a total assisting heating and cooling of 35 kWh/m² (wall area) for Edmonton, Canada throughout the year.

Overall, this thesis presents two methods that can potentially reduce space thermal loads in cold-climate buildings through active TES solutions in wall system. The results of this research can provide valuable insights for building design and energy management in order to create more energy-efficient buildings.

Preface

This thesis includes original research conducted by Mohammad Rezvanpour and is divided into four Chapters, with Chapters 1 and 4 serving as the introduction and conclusion, and Chapters 2 and 3 presenting the research in the form of journal papers.

Chapter 2 provides an overview of the research focused on evaluating the energy potential of the domestic cold water (DCW)-wall system for space cooling. The chapter covers the methodology, model validation, results, and discussion. It concludes with a summary of the main points and has been submitted for publication as “Space Cooling Energy Potential of Domestic Cold Water Before Household Consumption in Cold-Climate Regions” to the *Buildings* journal. In addition, some of the results have been published in the "Proceedings of 5th International Conference On Building Energy and Environment (COBEE 2022)".

Chapter 3 presents research on the generalizable thermal performance of a ventilated concrete block wall and the energy implications of its substitution for a traditional wood-frame wall in cold-climate buildings. The chapter covers the introduction, physical system, methodology, model validation, results, and discussion. It concludes by highlighting the key points and has been submitted for publication as “Generalizable Thermal Performance of a Ventilated Concrete Block Wall and the Energy Implication of Its Substitution for a Wood-Frame Wall in Cold-Climate Buildings” to the *Buildings* journal.

Both chapters are authored and communicated as “Mohammad Rezvanpour, Dr. Carlos Cruz-Noguez, and Dr. Yuxiang Chen”, with Rezvanpour being responsible for developing the methodology and numerical model, and analyzing the data, while Dr. Chen and Dr. Cruz-Noguez contributed through conceptualization, supervision, and manuscript revisions.

Dedication

To my loved ones,

my greatest gift

"It is not the mountain we conquer, but ourselves" -- Sir Edmund Hillary

Acknowledgments

I would like to express my deepest gratitude to my supervisor, Dr. Yuxiang Chen, and co-supervisor, Dr. Carlos Cruz-Noguez, for their exceptional guidance and support throughout my research. Their invaluable insights and expertise made the completion of this thesis possible.

I would also like to extend my appreciation to Dr. Tooba Shamsi, and my friends, *Bowen, Parnian, Mehdi, Vahid, Saeid, Amir* and *Ali* for their feedback and support throughout the journey. Your encouragement and constructive criticism were instrumental in shaping this thesis.

I am grateful to my family for their unwavering love and support throughout my academic journey. Your belief in me and my work has been a source of inspiration and motivation.

Finally, I would like to acknowledge the support of the University of Alberta, Natural Sciences and Engineering Research Council of Canada (NSERC), the Canadian Concrete Masonry Producers Association (CCMPA), and the Masonry Contractors Association of Alberta (MCAA) for their funding of this research. Their support has been invaluable in allowing me to pursue my passion for research in this field

Mohammad Rezvanpour

Table of Contents

Abstract.....	i
Preface.....	iv
Acknowledgments.....	vi
Table of Contents.....	vii
List of Tables	ix
List of Figures	x
Nomenclature.....	xii
List of Abbreviations	xii
List of Symbols.....	xiii
Chapter 1 Introduction	1
1.1.Thesis rationale and objectives..	4
1.2. Fundamentals, working principles and processes...	5
1.2.1. DCW-wall system.....	6
1.2.2.VBW with SAZ system	8
1.3.Thesis organization	10
Chapter 2 Space Cooling Energy Potential of Domestic Cold Water Before Household Consumption in Cold-Climate Regions	13
2.1. Introduction.....	13
2.2. Methodology.....	16
2.2.1. Description of the physical system	16
2.2.2.Variable DCW flow	17
2.2.3. Numerical model.....	18
2.2.4. Model validation	23
2.3. Results and discussion	25
2.3.1.Water outlet and average wall temperatures	25
2.3.2.Temperature uniformity and condensation prevention	27
2.3.3. Cooling heat flux density	28
2.3.4. Delivered cooling energy	29
2.3.5. Comparison of three configurations on the basis of model results.....	31
2.3.6. Influence of wall surface area on total DCE	39
2.4. Conclusion..	40

Chapter 3 Generalizable Thermal Performance of a Ventilated Concrete Block Wall and the Energy Implication of Its Substitution for a Wood-Frame Wall in Cold-Climate Buildings..	42
3.1. Introduction.....	42
3.2. Description of the physical system.	45
3.3. Methodology.....	48
3.3.1. Overview.....	48
3.3.2. Numerical model.....	56
3.3.3. Air speed.....	62
3.3.4. Model validation.....	65
3.4. Results and discussion.....	66
3.4.1. Typical-day thermal performance of VBW.....	67
3.4.2. Annual energy analysis for VBW and wood-frame wall.....	78
3.5. Conclusion..	86
Chapter 4 Conclusion.....	87
4.1. Future work.....	88
References.....	89
Appendix A – Calculation of thermal transmittances in DCW-wall system.....	95
Appendix B – Wood-frame wall.....	97
Appendix C – Predicted and measured indoor temperatures in annual energy analysis	100
Appendix D – Annual energy analysis for Vancouver and Toronto	102
Appendix E – A typical-day performance with drywall as the interior surface finishing	111

List of Tables

Table 2.1 Values for some parameters in three layers of the DCW-wall	22
Table 2.2 CV-RMSE of measured and simulated values in the present study and Merabtine et al.'s	24
Table 2.3 Allowable indoor RH to prevent condensation in spiral configuration	28
Table 2.4 Allowable indoor RH to prevent condensation in all configurations	35
Table 2.5 Maximum cooling capacity (W/m^2) for all scenarios	37
Table 2.6 Total DCE (MJ) per day for all scenarios	39
Table 2.7 Total DCE (MJ) per day for different wall surface areas	40
Table 3.1 Thermal properties of the materials used in VBW	47
Table 3.2 Criteria used for calculating the assisting heating and cooling energy	53
Table 3.3 Maximum and minimum average wall interior surface temperatures for different zone temperatures and air speeds	69
Table 3.4 Heat fluxes for exterior VBW with cement plaster	71
Table 3.5 Total net energy exchange of the exterior VBW with cement plaster	72
Table 3.6 Maximum and minimum average wall interior surface temperatures for different zone temperatures and air speeds	75
Table 3.7 Heat fluxes for interior VBW with cement plaster	76
Table 3.8 Total net energy exchange of interior VBW with cement plaster	77
Table 3.9 Monthly total assisting heating and cooling achieved by both walls for Edmonton.	84
Table D.1 Monthly total assisting heating and cooling achieved by both walls for Vancouver	105
Table D.2 Monthly total assisting heating and cooling achieved by both walls for Toronto	109
Table E.1 Maximum and minimum average wall interior surface temperatures for different zone temperatures and air speeds – Dry wall as the finishing layer	111
Table E.2 Heat fluxes for an exterior VBW – Dry wall as the finishing layer	113
Table E.3 Total net energy exchange of the exterior VBW – Dry wall as the finishing layer	113

List of Figures

Figure 1.1 Common forms of TES in buildings	2
Figure 1.2 DCW-wall system	7
Figure 1.3 VBW with SAZ system	9
Figure 2.1 Piping patterns	17
Figure 2.2 Daily pattern of average hourly water consumption for residential buildings	18
Figure 2.3 Schematic of the wall and thermal transmittances between a water node and its adjacent wall node.....	20
Figure 2.4 Measured and simulated average floor surface temperatures.....	24
Figure 2.5 Average wall surface temperature over the 24-hour period ($T_{sw} = 12^{\circ}\text{C}$, $T_{air} = 25^{\circ}\text{C}$, $S = 5\text{ cm}$).....	26
Figure 2.6 Wall surface temperature versus the distance from the inlet over the 24-hour period ($T_{sw} = 12^{\circ}\text{C}$, $T_{air} = 25^{\circ}\text{C}$, $S = 5\text{ cm}$)	27
Figure 2.7 Cooling capacity over the 24-hour period ($T_{sw} = 12^{\circ}\text{C}$, $T_{air} = 25^{\circ}\text{C}$, $S = 5\text{ cm}$).....	29
Figure 2.8 Cumulative DCE over the 24-hour period ($T_{sw} = 12^{\circ}\text{C}$, $T_{air} = 25^{\circ}\text{C}$, $S = 5\text{ cm}$)	30
Figure 2.9 Average wall surface temperature for all configurations over the period of 24 hours ($T_{sw} = 12^{\circ}\text{C}$, $T_{air} = 25^{\circ}\text{C}$, $S = 5\text{ cm}$)	32
Figure 2.10 Wall surface temperature versus the distance from the inlet for all configurations over the 24-hour period ($T_{sw} = 12^{\circ}\text{C}$, $T_{air} = 25^{\circ}\text{C}$, $S = 5\text{ cm}$)	34
Figure 2.11 Cooling capacity for all configurations during the 24-hour period ($T_{sw} = 12^{\circ}\text{C}$, $T_{air} = 25^{\circ}\text{C}$, $S = 5\text{ cm}$).....	36
Figure 2.12 Cumulative DCE for all configurations over the 24-hour period.....	38
Figure 3.1 Cross-sectional view of the VBW	46
Figure 3.2 Zone temperature profiles for typical-day performance (a cyclic temperature profile with a 24-hr cycle)	52
Figure 3.3 Heat loss values for VBW	50
Figure 3.4 Heat transfer mechanisms in VBW with SAZ	57
Figure 3.5 A schematic of the block dimensions, discretization, and nodes	59
Figure 3.6 Net energy exchange and pressure changes	64
Figure 3.7 Measured and simulated average wall surface temperatures	66
Figure 3.8 Zone air and average wall surface temperatures for an exterior VBW	68
Figure 3.9 Heat flux for an exterior VBW over a 24-hour period	70

Figure 3.10 Zone air and average wall surface temperatures for an interior VBW	74
Figure 3.11 Heat flux changes for an interior VBW over a 24-hour period	76
Figure 3.12 Outdoor, predicted indoor, and VBW surface temperatures for Edmonton, January	80
Figure 3.13 Heat flux of the VBW and wood-frame wall for Edmonton, January.....	81
Figure 3.14 Outdoor, predicted indoor, and VBW surface temperatures for Edmonton, July	82
Figure 3.15 Heat flux of the VBW and wood-frame wall for Edmonton, July	83
Figure B.1 Front view of the wood-frame wall and its discretization in three directions.....	98
Figure B.2 Cross-section of the Wood-frame wall	99
Figure C.1 Measured and predicted average indoor temperature for EcoTerra house- day86.....	100
Figure C.2 Measured and predicted average indoor temperature for EcoTerra house-day93	101
Figure C.3 Measured and predicted average indoor temperature for EcoTerra house-day	101
Figure D.1 Outdoor, predicted indoor, and VBW surface temperatures for Vancouver, January.....	102
Figure D.2 Heat flux of the VBW and wood-frame wall for Vancouver, January	103
Figure D.3 Outdoor, predicted indoor, and VBW surface temperatures for Vancouver, July	104
Figure D.4 Heat flux of VBW and wood-frame wall for Vancouver, July	105
Figure D.5 Outdoor, predicted indoor, and VBW surface temperatures for Toronto, January	107
Figure D.6 Heat flux of the VBW and wood-frame wall for Toronto, January	108
Figure D.7 Outdoor, predicted indoor, and VBW surface temperatures for Toronto, July ...	108
Figure D.8 Heat flux of VBW and wood-frame wall for Toronto, July	109
Figure E.1 Zone air and average wall surface temperatures for an exterior VBW with dry wall finishing.....	111
Figure E.2 Heat flux changes for an exterior VBW with dry wall finishing over a 24-hour period	112

Nomenclature

List of Abbreviations

CCD	Cooling degree days
CV	Control volume
CV-RMSE	Coefficient of variation of root-mean square error
DCE	Delivered cooling energy
DCW	Domestic cold water
FF	Framing factor
GHG	Greenhouse gas
GHI	Global Horizontal Irradiance
HDD	Heating degree days
HTF	Heat transfer fluid
NECB	National Energy Code of Canada for Buildings
RH	Relative humidity
SAZ	Supply air to zone
TABS	Thermally activated building systems
TES	Thermal energy storage
TMY	Typical meteorological year
VBW	Ventilated concrete block wall

List of Symbols

Δx	x-direction length of each control volume [m]
Δy	y-direction length of each control volume [m]
Δz	z-direction length of each control volume [m]
ΔT	Difference between the maximum and minimum average wall surface temperature [$^{\circ}\text{C}$]
ΔP	Pressure loss caused by fan [Pa]
F_{fr}	Friction factor
\dot{m}	Fluid (air or water) mass flow rate [kg/s]
λ_{wall}	Wall thermal conductivity [W/mK]
λ_{pipe}	Pipe thermal conductivity [W/mK]
λ_{water}	Water thermal conductivity [W/mK]
λ_{air}	Air thermal conductivity [W/mK]
ρ_{water}	Water density [kg/m^3]
ρ_{air}	Air density [kg/m^3]
F_v	View factor
d	Perpendicular distance between two facing surfaces inside the air channel [m]
\mathcal{L}	Length of each CV in contact with node f of the air inside the channel [m]
v	Fluid (air or water) speed [m/s]
ϑ	Fluid (air or water) kinematic viscosity [m^2/s]
σ	Stephan-Boltzmann constant [$\text{W}/\text{m}^2 \cdot \text{K}^4$]
ε	Emissivity
A_{AC}	Cross-sectional area of the air channel [m^2]

$C_{p_{air}}$	Air specific heat capacity [J/kg°C]
$C_{p_{water}}$	Water specific heat capacity [J/kg°C]
D_i	Pipe inside diameter [m]
D_h	Hydraulic diameter [m]
D_o	Pipe outside diameter [m]
E_{fan}	Fan energy consumption [kWh]
Gr	Grashof number
h_{air}	Air convective heat transfer coefficient inside the channel [W/m ² K]
h_{water}	Water convective heat transfer coefficient [W/m ² K]
h_{total}	Combined heat transfer film coefficient between zone air and wall surface [W/m ² K]
L_f	Length of the control volume f of the pipe in the direction of water flow [m]
M	Pipe spacing [m]
Nu	Nusselt number
Pr	Prandtl number
q	Heat flux density [W/m ²]
$Q_{advection}$	Heat flow rate between returning air from the air channel and the zone air [W]
$Q_{conduction}$	Heat flow rate between wall nodes [W]
$Q_{convection}$	Heat flow rate between air inside the channel and surrounding wall nodes [W]

$Q_{radiation}$	Heat flow rate between two facing wall nodes in contact with air [W]
$Q_{surface}$	Heat flow rate between zone air and nodes on the wall surface [W]
Q_{w2w}	Heat flow rate between water and wall control volume [W]
Ra	Rayleigh number
Re	Reynolds number
S	Wall thickness [m]
T_{AC}	Temperature of the air inside the air channel [°C]
T_{air}	Zone temperature [°C]
$T_{outside}$	Outside temperature [°C]
T_{sw}	Supply water (inlet) temperature [°C]
T_{wall}	Average wall surface temperature [°C]
$T_{wall.min}$	Minimum wall surface temperature [°C]
T_{water}	Average water temperature [°C]
U_{int}	Total thermal transmittance between zone air and wall surface [W/K]
U_p	Total thermal transmittance between water and adjacent wall node [W/K]
U_{p1}	Total thermal transmittance between water and the inside surface of the pipe [W/K]
U_{p2}	Total thermal transmittance between the inside and outside surfaces of the pipe [W/K]

U_{p3}	Total thermal transmittance between the cylindrical pipe surface and the adjacent wall node [W/K]
V_{wall}	The volume of one control volume [m ³]
W_f	Width of the control volume f of the wall in the direction transverse to the flow [m]
W_s	Width of the wall surfaces inside the air channel [m]
$X\text{-Step}$	Distance between two nodes in x direction [m]
$Y\text{-Step}$	Distance between two nodes in y direction [m]
$Z\text{-Step}$	Distance between two nodes in z direction [m]

Chapter 1 Introduction

Mitigating the negative impacts of climate change and global warming requires immediate attention and action. Despite the urgency of the situation, total world energy use and the resulting greenhouse gas (GHG) emissions are on the rise [1]. Energy expenditure in the building sector, specifically, has steadily increased by 1.1% per year since 2000 to account for 30-40% of the global energy use [2-4]. This increase has been the result of climate change and global warming, population growth, changes in building design, and increased demands for comfort [5-7]. Investigations by Levesque et al. [8, 9] revealed that the energy consumption of buildings will continue to rise unless strict policies are implemented and energy-efficient technologies are adopted.

The design of energy-efficient buildings is one of the proven ways to mitigate the adverse effect of the ascending trend of energy consumption in buildings. One of the promising approaches toward improving the energy efficiency of a building is implementing thermal energy storage (TES) systems [10]. TES systems can improve efficiency by compensating for mismatches between energy supply and demand, utilizing renewable energy sources, stabilizing zone temperatures, shifting peak loads, reducing heat losses, and enhancing the thermal comfort of occupants [10-13]. As an example, excess heat inside the zone can be stored in the storage medium during the day and then released at night. Therefore, the cooling demand during the day as well as the heating demand during the night can be reduced. Figure 1.1 shows the common forms of TES in buildings.

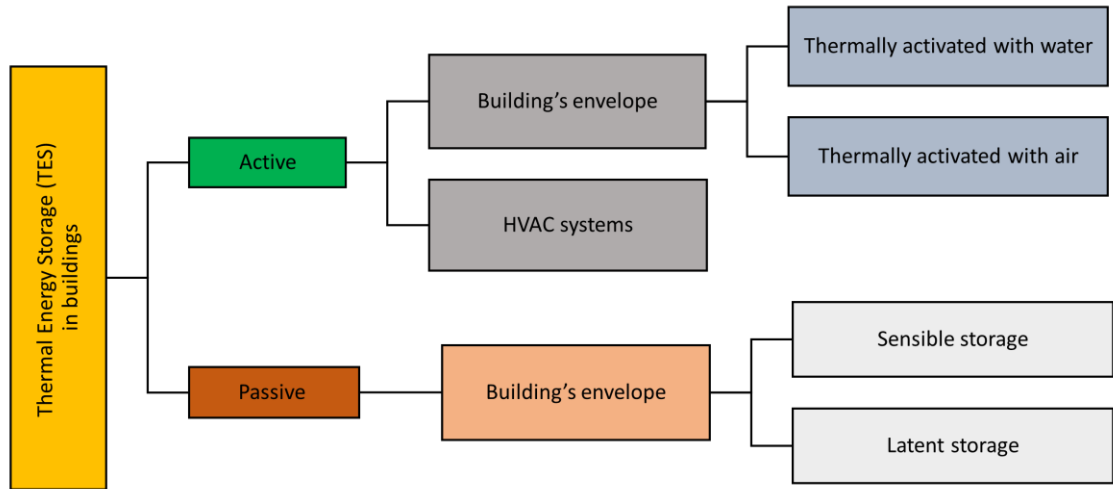


Figure 1.1 Common forms of TES in buildings

As shown in Figure 1.1, TES in buildings is generally classified into two categories: passive and active. Passive TES does not require any mechanical equipment to store heat in a building's envelope. In this type of TES, heat is transferred between the storage medium and the zone as a result of a temperature gradient. For example, direct or indirect storage of solar energy is an effective passive sensible TES. The integration of phase change materials (PCMs) in a building's envelope is an example of latent TES. In contrast, in active TES, mechanical equipment (e.g., a fan or a pump) is employed in order to deliberately provide cool/warm heat transfer fluid (HTF) to thermal mass. For instance, common methods for actively charging thermal mass are using pipe-embedded hydronic (i.e., water-based) or ventilated (i.e., air-based) systems in building envelopes.

A key factor in the high performance of TES systems is choosing a storage medium with good thermal capacity, density, and thermal conductivity [12]. Storage materials are generally divided into two categories of liquid and solid. In low temperature systems, water is the best option to be used both as the storage medium and HTF due to its low cost, availability, and

high thermal capacity. On the other hand, most solid storage materials have a lower thermal capacity than liquids but a higher density. Masonry, concrete, and brick are among the solids that are widely used in the building's envelope and can serve as thermal storage materials.

Building envelopes with significant thermal mass are capable of absorbing, storing, and gradually releasing heat based on the temperature difference between the mass and its surrounding zone. In light of that, the rate at which thermal mass gains or loses heat is known as thermal inertia. A material with high thermal inertia has a delayed reaction to rapid changes in the surrounding temperature. The delayed response results in a time lag between the maximum outdoor and indoor temperatures, which could be desirable. By taking advantage of this time lag, the building's mass can store energy during the day and gradually reject the heat at night or in the early hours of the following morning. Therefore, a building with a high thermal mass can offset temperature swings, improve thermal comfort, and reduce energy demand [14, 15]. However, when intense heat gain and loss occur, such as on very cold days with strong solar heat gain, thermal mass may not effectively regulate indoor temperature through passive storage and release [16]. In this case, the heat exchange between the mass and its zone can be improved by circulating the zone air through the thermal mass and returning it to the zone after exchanging heat with the core. This air flow into the zone not only provides ventilation but also results in faster and higher heat exchange rate. An example of this type of system is ventilated concrete block walls with air flow to the zone.

This thesis focuses on reducing thermal loads in cold-climate buildings through the use of active TES in walls by employing two methods. In these methods, water and air were chosen as the heat transfer fluid (HTF) to store heat in the wall system. The following subsection provides a brief explanation of these methods and their goals.

1.1. Thesis rationale and objectives

This thesis considers two active TES methods to reduce the space heating and cooling loads in cold-climate residential buildings. In its focus on the integration of active TES solutions in wall systems to reduce the thermal loads of buildings, this thesis attempts to bridge the current gaps in the relevant literature.

Due to the fact that cooling seasons are shorter than heating seasons in the cold regions, most of the studies in the area of space cooling are mainly focused on the regions with temperate and hot climates. However, climate change and global warming are changing the equations. For example, Canada, as one of the coldest countries on earth, has experienced longer heatwaves and higher summer temperatures during the past few years. Therefore, additional research with a focus on free space cooling approaches toward reducing the space cooling demand in countries with cold climate appears necessary.

Moreover, VBWs are able to provide dual functionality, acting as both structural support and thermal mass, storing excess thermal energy and buffer zone temperature fluctuation. VBWs enhance building performance through strong thermal coupling with the surrounding spaces and exposing more mass area for heat transfer, promoting effective thermal storage and release. Furthermore, VBWs' simplicity in design and minimal reliance on mechanical equipment make them a cost-effective option for improving the buildings' energy efficiency. Additionally, there is a scarcity of research on the use of VBWs in cold-climate buildings. The increased thermal energy storage and release of VBWs contribute to their enhanced efficiency. To maximize this benefit, substantial fluctuations in zone temperature are necessary. Cold-climate buildings experience significant zone temperature fluctuations during spring and fall, allowing the VBWs to demonstrate their full potential in maintaining thermal comfort and energy efficiency.

This thesis aims to close the above-mentioned gaps in the literature by introducing two active TES approaches, that have not been explored in the literature. To achieve this, the thermal mass of the wall will be actively charged using two independent systems, as follows:

- a) Domestic cold water (DCW)-wall system
- b) Ventilated concrete block wall (VBW) with supply air to zone (SAZ)

The fundamentals, working principles and processes of the two studied systems are presented in the next section.

1.2. Fundamentals, working principles and processes

Thermally activated building systems (TABS) refer to building components (e.g., concrete walls and floor) that are actively utilized in both heat transfer and storage. TABS mainly involve the incorporation of water pipes or air ducts into the building's elements to function as heat exchangers, effectively transferring heat to the surrounding zones and storing thermal energy within the structure. By storing the excess heat and releasing it later when needed, TABS with high thermal mass can smoothen the temperature fluctuation within the zone. Therefore, the workload of chillers or boilers can be reduced, resulting in energy and cost savings.

TABS with embedded water pipes exchange heat with the surrounding area only through the surface via convection and radiation mechanisms. Conversely, when air is used as HTF, heat exchange occurs through the surface via convection and radiation as well as through the supply air to the zone via advection (i.e., advection is a type of convection heat transfer resulted from the intensive bulk movement of air into each other). In the latter case, the circulating air exchanges heat with the building element before being supplied to the zone, thereby enhancing thermal coupling or heat exchange between the mass and the zone.

This thesis is a comprehensive study on the effectiveness of two types of thermally activated wall systems in reducing the space heating and cooling loads of cold-climate buildings. Specifically, the focus is on DCW-wall and VBW with SAZ systems, which were individually modeled and analyzed. In the following subsections, the working principles and processes of each system will be presented and discussed.

1.2.1. *DCW-wall system*

Cooling energy recovery from DCW prior to regular household consumption can offer a substantial amount of free cooling (herein as “DCW-based cooling”) in cold region countries such as Canada where the ground temperature is significantly lower than other climate regions. One of the DCW-based cooling approaches involves circulating DCW through pipes embedded in the middle layer of a thermally massive wall before it is dispensed by occupants for regular domestic usages such as shower and regular washing (herein as “DCW-wall”).

In this study, the pipe is made of copper and the wall is considered an exterior wall with one side exposed to zone air and the other side assumed to be adiabatic due to heavy insulation in cold-climate buildings and therefore negligible heat loss during a cooling season. The DCW-wall system aims to utilize the same amount of daily water consumption of households for space cooling, thereby preventing any wastage of DCW resulting from its implementation. Figure 1.2 shows how the DCW-wall system works.

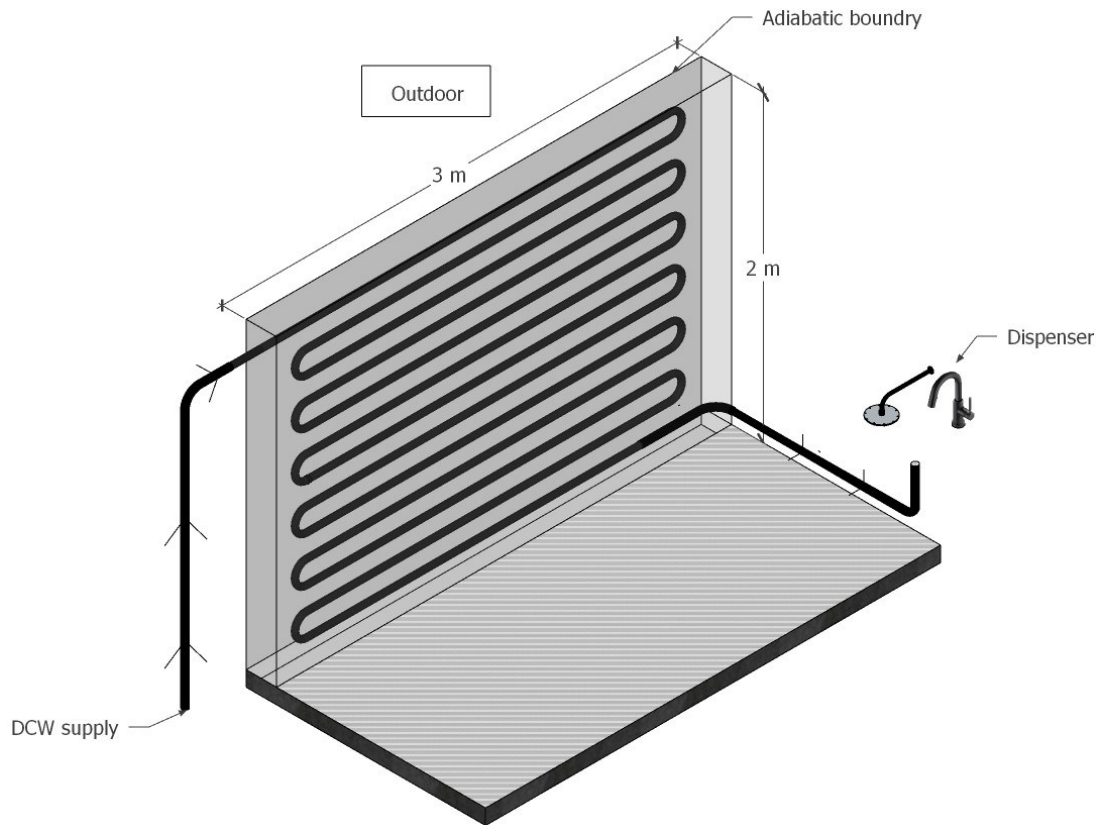


Figure 1.2 DCW-wall system

As illustrated in Figure 1.2, the DCW is pumped into pipes that are embedded within the thermally massive wall from the DCW supply. DCW circulates through the embedded pipes and the outlet water is directed to the dispensers for regular household use. Circulating DCW (which is typically colder than the zone air temperature) can absorb excess heat through the wall surface, thereby cooling the space before regular household activities, such as taking a shower.

Using thermally massive walls to recover cooling energy from DCW and assist space cooling does not require complex construction. A diverter valve can be installed to allow DCW to bypass the massive walls in the heating season. Therefore, DCW-walls could potentially reduce the capital and operating costs compared with other space cooling technologies, due to lower installation costs, down-sizing and potential elimination of mechanical cooling systems

and their maintenance requirements [17-19]. In cold regions like Canada, where the ground temperature is relatively lower than other regions, more cooling energy can be recovered. In addition, the outlet temperature of DCW will be warmed by room air to become more suitable for domestic usages (e.g., less mixing with domestic hot water in showers).

The second Chapter of the thesis aims to investigate the cooling potentials (i.e., cooling capacity and delivered cooling energy) of the DCW-wall system. In addition, parametric analysis is carried out to ascertain the impact of different influential factors on the performance of the system. The study examined the influence of four factors - pipe spacing, zone air temperature, DCW temperature, and three distinct piping patterns - on the thermal performance of the DCW-wall system.

1.2.2. *VBW with SAZ system*

Another type of TABS is VBW with SAZ (simply referred to VBW from now on) which can be constructed by stacking hollow concrete blocks on top of each other. Figure 1.3 shows the VBW system.

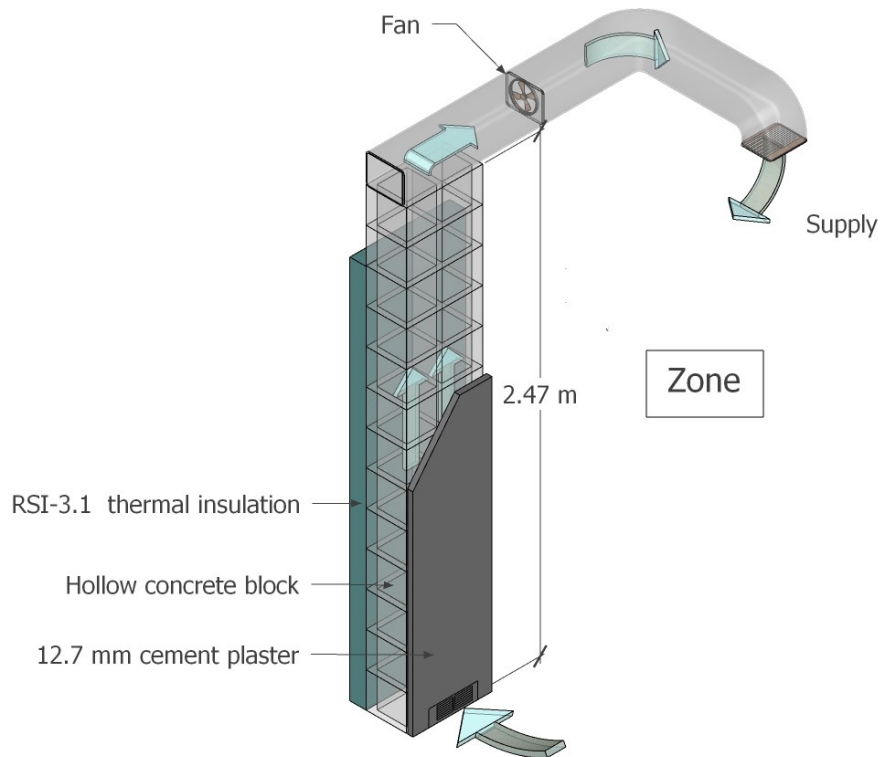


Figure 1.3 A schematic of VBW

As shown in Figure 1.3, by placing hollow blocks on top of each other, an air pathway can be created by connecting the voids within each block, enabling the free flow of air through the wall. Using a fan, zone air is drawn into each air channel from the bottom of the wall and moves upward in the wall height through the conduits, exchanges heat with the wall and returns to the zone from the top of the wall through a duct (i.e., supply air to zone).

In this process, the zone air carries the excess heat inside the zone and exchanges it with the wall (i.e., wall stores the heat) while moving upward through the air channel. Circulating air through these air channels can accelerate the heat transfer process in materials with slow rate of storage and release properties (e.g., concrete). This heat storage process buffers the temperature fluctuation within the zone and reduces the heating and cooling loads. The stored heat in the wall can be either released to the zone through the wall surface, through SAZ by the use of a fan, or a combination of both. When air moves up through the air channel, it releases

the zone excess heat to the wall. This heat is then stored by the wall, which helps to regulate temperature fluctuations within the zone, leading to a decrease in both heating and cooling loads. Furthermore, in this particular case, VBWs can significantly enhance the heat exchange rate between the wall and its surrounding zone compared to walls without SAZ. The increased heat exchange can reduce cooling and heating loads, improve thermal performance, and save money and space.

In the third chapter of the thesis, Similar to the DCW-wall system, a parametric study of the influential parameters is conducted. To that end, the thermal performance of one VBW strip (i.e., wall height of 2.47 m and one block width as shown in Figure 1.3) is investigated in a typical day (i.e., typical-day performance) and for an entire year (i.e., annual analysis). For the typical-day performance, two boundary conditions (i.e., exterior, and interior walls) with the adiabatic boundary conditions for the exterior wall (adiabatic boundary for the back of the wall strip shown in Figure 1.3), various zone air temperature profiles, different air speeds, and three interior surface finishing were investigated. The back surface of the interior wall is exposed to the same zone as the front surface. For annual energy analysis, a comparison was made between the thermal performance of an exterior VBW and a wood-frame wall in three different Canadian cities. In this analysis, the back surface of the wall strip is exposed to the real outdoor conditions.

1.3. Thesis organization

The thesis is structured into four chapters, with the research presented in Chapters 2 and 3 in a journal paper format. Chapter 4 concludes the thesis with a summary of key points and proposals for future work.

The remaining chapters of the thesis are arranged as follows:

Chapter 2 - Space Cooling Energy Potential of Domestic Cold Water Before Household Consumption in Cold-Climate Regions

This chapter aims to investigate the cooling potentials of a DCW-wall system during heatwaves in Canada, with a focus on the typical daily DCW usage in residential buildings. The chapter begins with an introduction and is followed by a description of the methodology used in the study. The methodology section consists of:

a) a description of the physical system, b) the variable DCW flow, c) the numerical model, and d) model validation. Then, a parametric analysis of influential factors such as pipe configuration, pipe spacing, wall thickness, and water supply temperature is carried out. For different operation scenarios, the following attributes are explored:

- a) water outlet temperature and average wall surface temperature;
- b) temperature uniformity on the wall and condensation prevention;
- c) cooling capacity of the DCW-wall system;
- d) delivered cooling energy of the DCW-wall system;
- e) The effect of wall surface area on delivered cooling energy.

The chapter concludes with a summary of its key findings in the conclusion section.

Chapter 3 - Generalizable Thermal Performance of a Ventilated Concrete Block Wall and the Energy Implication of Its Substitution for a Wood-Frame Wall in Cold-Climate Buildings

The main objective of this chapter is to evaluate the typical-day and annual thermal performance of a VBW. It begins with an introduction and is followed by a description of the physical system. Then, the methodology subsection begins with an overview of the two typical-day and annual performances. Following that, the methodology is divided into four

subsections: a) Overview; b) the development of the numerical model; c) finding the optimum air speed; and d) model validation.

The results and discussion section consists of two general parts: a typical-day thermal performance of the VBW, and an annual energy analysis of an exterior VBW and an exterior wood-frame wall. The results of the typical-day performance are further divided into the exterior and interior walls, and they analyze average wall surface temperature, heat flux density, and total net energy exchange with varying air speed and zone temperature profile. The annual energy analysis compares the energy performance of an exterior VBW and an exterior wood-frame wall in three Canadian cities and investigates the assisting heating and cooling potential of using VBWs instead of wood-frame walls.

Chapter 4 – Conclusion

Key findings from the results and discussion sections of both chapters 2 and 3 are summarized. Following that, potential future work is discussed.

Chapter 2 Space Cooling Energy Potential of Domestic Cold Water Before Household Consumption in Cold-Climate Regions

2.1. Introduction

Buildings account for 30–40% of the world's total energy expenditure as well as 20–30% of the total global greenhouse gas (GHG) emissions [2, 20]. The European Union (EU-28) saw an average annual increase of 6.3% in space cooling energy consumption from 2000 to 2015 [21]. Adopting energy-efficient measures, including free cooling techniques, can reduce a building's energy consumption. [22-24]. One such technique is ventilative cooling, which utilizes ambient air for space cooling [25, 26]. Although using ventilative cooling can reduce energy consumption, its overall effectiveness may be hampered by certain limitations. For example, during heat waves, outdoor temperatures may not be cool enough [27].

Cooling energy recovery from cold water can offer a substantial amount of free cooling. A 10°C change in water temperature and a daily water consumption of 1000 liters can produce approximately 42 MJ of free cooling energy. A recent application is the cooling of subway stations and shelters during heat waves [28]. Furthermore, some studies have examined the effect of cold recovery from domestic cold water (DCW) on GHG emissions, financial considerations, and water quality [29-31].

To recover cooling energy from DCW, DCW can be circulated through pipes embedded in a thermally massive wall before it is dispensed by occupants for regular domestic usage. Thermally massive building components, such as concrete walls and floors, have been widely used in providing hydronic panel heating and cooling [32]. They are often referred to as thermally activated building systems (TABS). TABS can reduce space heating/cooling energy consumption and mechanical system capacities through thermal energy storage (TES) [33-36]. TES stabilizes the cooling heat flux density (i.e., cooling capacity) fluctuations and sudden

changes in the wall surface temperature, preventing the surface temperature from falling too quickly to extremely low values. To that end, massive walls are preferable to metal panels for utilizing relatively low water inlet temperatures since the former can store higher amounts of thermal energy and delay the time the wall surface takes to reach its minimum temperature. TABS also enhance thermal comfort by creating a gradual change in indoor air temperature and evenly distributing heat flux density.

Several research studies have been conducted to identify the key parameters that affect the cooling performance of TABS. In a parametric study, Antonopoulos et al. [37] determined that water inlet temperature, pipe spacing, pipe depth, and zone air temperature had significant effects on thermal performance, while other parameters had negligible impact. These observations have been confirmed by similar studies [38-40]. In hydronic pipe-embedded systems, the water inlet temperature greatly affects the cooling capacity (i.e., water and wall surface). Antonopoulos et al. [37] discovered that the lowering supply water temperature from 15°C to 5°C resulted in an increase in cooling heat flux density from 45 W/m² to 120 W/m². Furthermore, different studies have also investigated the use of relatively high-temperature water (18°C to 25°C) for space cooling in an effort to reduce energy consumption. Šimko et al. [41] conducted an experiment to determine the maximum cooling capacity for a 16°C to 25°C water inlet temperature range. Similar studies [42-44] carried out experiments with a supply water temperature range of 18°C to 21°C. An increase in water supply temperatures would decrease energy consumption for space cooling, but it would also significantly decrease the cooling capacity of the system. Moreover, some studies [38, 43, 45] have demonstrated that pipe spacing significantly affects cooling capacity. They found that decreasing the pipe spacing in the same area would result in greater cooling capacity, due to an increase in heat transfer area. Changes in influential parameters affect the performance of TABS.

Using thermally massive walls to recover cooling energy from DCW (herein as “DCW-wall”) and assist space cooling does not require complex construction. A diverter valve can be installed to allow DCW to bypass the massive walls in the heating season. Therefore, DCW-walls could potentially reduce the capital and operating costs compared with other space cooling technologies due to lower installation costs, downsizing and the potential elimination of mechanical cooling systems and their maintenance requirements [17-19]. In cold regions like Canada, where the ground temperature is relatively lower than other regions, more cooling energy can be recovered. In addition, the outlet temperature of DCW will be warmed by room air to become more suitable for domestic usage (e.g., less mixing with domestic hot water in showers). However, to the best of the authors' knowledge, there is a lack of study on the cooling energy potential of DCW-walls in residential buildings for cold-climate regions. Therefore, the present paper provides such a study with a focus on thermal performance - cooling capacity and recoverable cooling energy. Findings from the extant literature indicate that it is essential to consider a reasonable range of values for influential parameters when evaluating performance. In light of this, the current study investigates not only different recommended values for influential parameters but also the effect of various piping patterns on DCW-walls' cooling potentials.

In terms of the paper's organization, the research methodology is discussed first, followed by the development and validation of the numerical model. Then, the following results and discussion section has six subsections discussing water outlet temperature, average wall temperature, temperature uniformity, condensation prevention, cooling capacity, delivered (recovered) cooling energy (DCE), the performance difference of three piping configurations, and the influence of wall surface area on total DCE.

2.2. Methodology

A zone temperature is the main boundary parameter that influences the cooling performance of a DCW-wall if direct solar radiation on the wall is not present. Running whole building thermal simulations can provide such a zone temperature profile and the corresponding DCW-wall performance; however, this approach will only provide the performance for the chosen specific building characteristics (e.g., physical construction, room temperature settings, and location of the DCW-wall) and climate conditions. This study aims to generalize the performance of DCW-walls by providing a performance envelope for DCW-walls through a parametric analysis. Zone temperature is included as one of the parameters, thereby avoiding the time-consuming and not very meaningful whole-building thermal simulations. By estimating the performance of a DCW-wall based on a range of zone temperatures, the performance can be interpreted for a broader range of zone conditions. The following sections describe the physical system, the selected DCW flow pattern, and the numerical model and its configurations used for parameter analysis.

2.2.1. Description of the physical system

In this system, DCW is routed through copper pipes embedded in the middle layer of a wall to cool the zone by exchanging heat with the warm indoor environment. The wall is considered an exterior wall, with one side exposed to zone air. For the parametric analysis, wall thicknesses of 5 cm and 10 cm were chosen. Figure 2.1 shows copper pipes embedded in the middle layer of a wall in three different patterns: spiral, serpentine, and parallel.

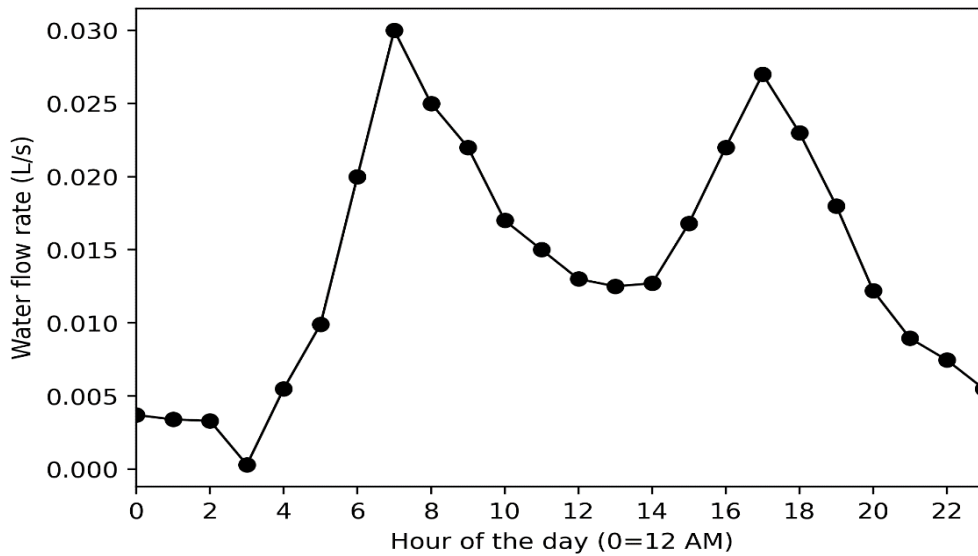


Figure 2.2 Daily pattern of average hourly water consumption for residential buildings

The hourly values correspond to the average values of families of four, for a total of 1200 liters of water flowing per day [31]. The maximum flow rate is 0.03 L/s at 7 a.m. Two peak hours can be observed, one in the morning and the other in the evening. The flow rate gradually decreased from 5 p.m. to 3 a.m. the following day, eventually reaching near zero. The thermal models presented in this paper use this variable DCW flow and assume it is steady periodic with a cycle of 24 hours.

2.2.3. Numerical model

The following configurations were incorporated into the thermal models:

- In cold-climate regions, such as Canada, municipal domestic water lines are buried around 1.5 to 2 meters deep in the ground. Therefore, the temperature of domestic water entering households is similar to the ground temperature at these depths. Two water inlet temperatures (T_{sw}) of 12°C & 15°C were selected based on the mean monthly ground temperatures for the summer months (June to August) in Toronto, Canada [50]. Two fixed zone temperatures (T_{air}) of 25°C and 30°C are used for thermal simulations.

- The temperature of 26°C is considered a safe threshold for an indoor environment [51]. In this context, an increase in emergency medical calls and premature mortality rates were associated with indoor temperatures above 26°C [52]. In addition, heat warnings are usually issued when maximum daily temperatures reach 30°C in Canada [52]. Zone temperature is likely to reach 30°C in the heat warning periods without mechanical cooling. Therefore, in this study, zone temperatures (T_{air}) of 25°C and 30°C are used as the lower and higher limits of the zone temperatures during cooling seasons. The results obtained based on these two fixed zone temperatures represent the performance envelope of the DCW-walls. It offers a range for the cooling potentials of the DCW-wall for zone temperatures between 25°C and 30°C.
- The dimensions of the modelled wall are 2 m in height and 3 m in width. The impact of different wall areas on total DCE will be discussed in [subsection 2.3.6](#). Furthermore, the simulations were conducted with two wall thicknesses of 5 cm and 10 cm to assess the impact of TES on cooling potentials and wall temperature.
- The exterior side of the DCW-wall is assumed to be adiabatic because of the thick thermal insulation used in cold-climate buildings, and the temperature difference between the wall and the exterior is not significant during a cooling season.
- As discussed above, pipe spacings of 10 cm and 30 cm are used to determine the cooling potentials of the DCW-wall system. In this paper, the results are presented for both the top and bottom of the optimal spacing range. The pipe is placed in the middle layer of the wall.
- The temperature of each control volume of water or wall is assumed to be uniform. Temperature nodes were placed at the center of each control volume.
- The convective thermal resistance between the water and the pipe (h_{water}) was considered in all thermal models.

- Under a steady-periodic daily water flow pattern and constant boundary conditions, transient thermal simulations were conducted. When the temperature profiles stabilized (i.e., the temperatures of all control volumes converged), the results of the last 24-hour period were used for analysis.

Using the method of rectangular control volumes [53], a 3D numerical model was developed to analyze the cooling potentials of using DCW as a cooling medium in a thermally activated wall system in cold-climate residential buildings. Figure 2.3 depicts a 3D schematic of the wall that includes temperature nodes, control volumes (CVs), and the thermal transmittances between a water node and its adjacent wall node.

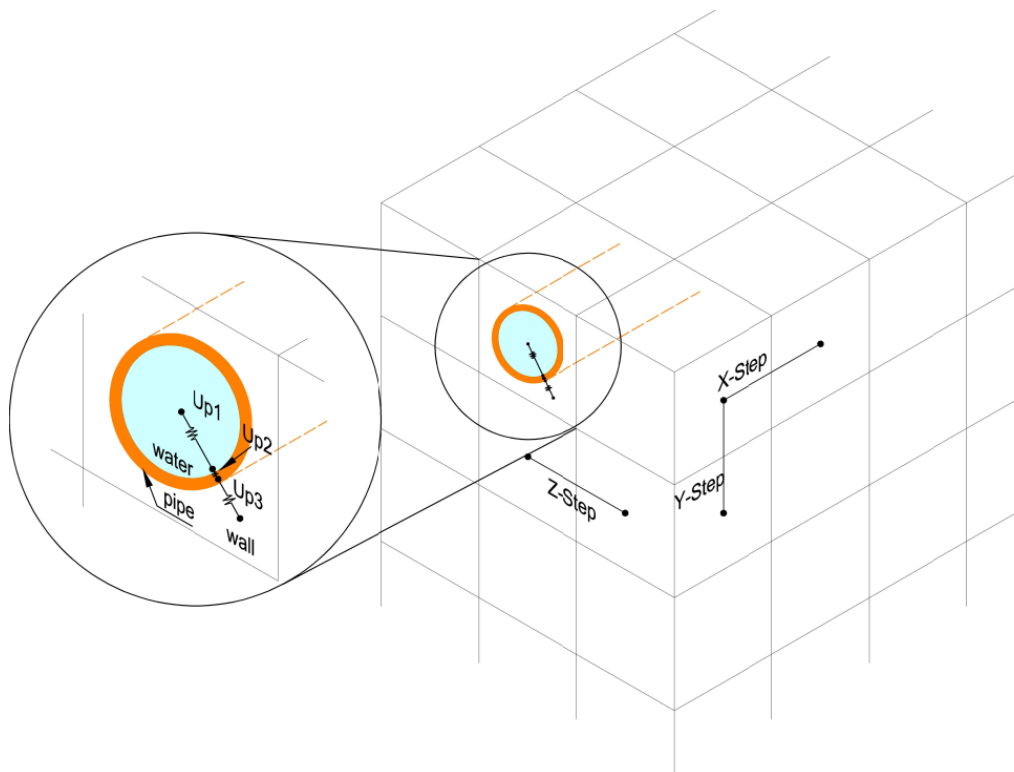


Figure 2.3 Schematic of the wall and thermal transmittances between a water node and its adjacent wall node

As shown in Figure 2.3, X-Step, Y-Step, and Z-Step refer to the distances between the two nodes in the x, y, and z directions, respectively. The X-Step and Y-Step were set at 5 cm, but the Z-Step can be equal or unequal for different layers along the thickness depending on the

objectives or required accuracy for the thermal simulations or model validation. For this study, the number of layers for the 5 cm- and 10 cm-thick walls were one and three, respectively, with unequal Z-Step used in the latter.

2.2.3.1. Water nodes

Water temperature can be obtained using Eq. (2.1) [53], which can be discretized into a finite difference equation and solved explicitly [54].

$$(\rho C_p)_{\text{water}} \left(\pi \frac{D_i^2}{4} \times L_f \right) \frac{dT_{\text{water}}^f}{dt} = U_p (T_{\text{wall}}^{i,j,k} - T_{\text{water}}^f) - \dot{m} C_{p_{\text{water}}} (T_{\text{water}}^f - T_{\text{water}}^{f-1}) \quad (2.1)$$

$$f = 1, 2, 3, \dots, n_{\text{pipe}}$$

where ρ_{water} and $C_{p_{\text{water}}}$ are the density and specific heat capacity of the water, respectively. D_i and L_f denote the inside diameter of the pipe and the length of the CV that correspond to node f on the pipe in the direction of water flow, respectively. Indices i, j, k and f represent the node counter for the wall in three directions and pipe in the direction of water flow. In Eq. (2.1), i, j, k are the node coordinates of the wall CV that is in contact with the node f of the pipe. T_{wall} , T_{water} , \dot{m} , and U_p denote the wall temperature and water temperature in their respective CVs, the water mass flow rate, and the total thermal transmittance between the water node and adjacent wall node, respectively. Eq. (2.2) can be used to calculate the U_p .

$$U_p = \frac{1}{\frac{1}{U_{P1}} + \frac{1}{U_{P2}} + \frac{1}{U_{P3}}} \quad (2.2)$$

As illustrated in Figure 2.3; U_{P1} , which is the total thermal transmittance between water and the pipe; U_{P2} , which is the total thermal transmittance between the inner and outer surfaces of the pipe, and; U_{P3} which is the total thermal transmittance between the cylindrical pipe's surface and the adjacent wall node. U_{P3} considers the shape factor for an accurate calculation of heat energy exchange between a circular cylinder (i.e., pipe) centered in a solid square (i.e.,

control volumes) [54]. More details on calculating the thermal transmittances of U_{P1} , U_{P2} , and U_{P3} can be found in [Appendix A](#).

2.2.3.2. Wall nodes

The wall temperature at any given location (i.e., node) can be determined using Eq. (2.3).

$$(\rho C_p)_{wall} V_{wall} \frac{dT_{wall}^{i,j,k}}{dt} = Q_{w2w}^{i,j,k} + Q_{surface}^{i,j,k} + Q_{conduction}^{i,j,k} \quad (2.3)$$

where V_{wall} is the volume of each CV, Q_{w2w} denotes the heat flux between water and wall which is positive, $Q_{surface}$ represents the heat flux from zone towards the wall nodes which is positive at the stated direction, and $Q_{conduction}$ is the conduction heat transfer between the wall nodes, which can be calculated using Eq.

(2.4).

$$Q_{conduction}^{i,j,k} = \lambda_{wall} \times \left\{ \begin{array}{l} \frac{\Delta z \Delta y}{\Delta x} (T_{wall}^{i+1,j,k} + T_{wall}^{i-1,j,k} - 2T_{wall}^{i,j,k}) \\ + \frac{\Delta z \Delta x}{\Delta y} (T_{wall}^{i,j+1,k} + T_{wall}^{i,j-1,k} - 2T_{wall}^{i,j,k}) \\ + \frac{\Delta y \Delta x}{\Delta z} (T_{wall}^{i,j,k+1} + T_{wall}^{i,j,k-1} - 2T_{wall}^{i,j,k}) \end{array} \right\} \quad (2.4)$$

where Δx , Δy , Δz stands for x-direction, y-direction, and z-direction length of each CV, respectively.

Table 2.1 shows the value of Q_{w2w} , $Q_{surface}$, and V_{wall} for the layers along the wall thickness. A wall with a thickness of 10 cm consists of 3 layers, while a wall with a thickness of 5 cm has only one layer.

Table 2.1 Values for some parameters in three layers of the DCW-wall

Wall thickness	Layer	Q_{w2w}	$Q_{surface}$	$V_{wall}^{i,j,k}$
10 cm	Front	0	$U_{int}(T_{air} - T_{wall}^{i,j,k})$	$\Delta z \times \Delta x \times \Delta y$

	Middle	$U_p(T_{wall}^{i,j,k} - T_{water}^f)$	0	$(\Delta z \times \Delta x \times \Delta y) - (\pi \frac{D_o^2}{4} \times L_f)$
	Back	0	0	$\Delta z \times \Delta x \times \Delta y$
5 cm	-	$U_p(T_{wall}^{i,j,k} - T_{water}^f)$	$U_{int}(T_{air} - T_{wall}^{i,j,k})$	$(\Delta z \times \Delta x \times \Delta y) - (\pi \frac{D_o^2}{4} \times L_f)$

where U_{int} is the total thermal transmittance between the wall surface and the zone air. U_{int} can be obtained using Eq. (2.5).

$$U_{int} = h_{total} \times \Delta y \times \Delta x \quad (2.5)$$

h_{total} is the combined heat transfer film coefficient between the wall surface and the zone air. A constant value of 9.09 W/m².K was used for h_{total} in the model because the air speed inside the zone was assumed to be low. As a result, h_{total} was not subjected to substantial variation [46, 55].

2.2.4. Model validation

Merabtine et al. [56] conducted an experimental study on the thermal characteristics of a floor heating system. The floor in that study has a configuration similar to the wall modelled here. From top to bottom, the floor consisted of anhydrite concrete screed (4 cm), polyethylene at raised temperature resistance (PE-RT) pipes embedded in the screed in a spiral pattern, and polyurethane insulation (5.6 cm). All specifications mentioned in the experimental study were taken into account by modifying the numerical model parameters using those proposed in the experiment. Among these specifications were transient water inlet and zone temperatures; water flow rate; pipe material; pipe spacing; piping pattern; floor dimensions; floor thickness; and the precise location of the pipes embedded in the floor. The average floor surface temperature was measured every 10 minutes for 5 hours. Figure 2.4 illustrates the changes in measured and simulated average floor surface temperatures. The coefficient of variation of the

root-mean square error (CV-RMSE) statistical measure was chosen to represent the error between the simulated and the measured values. The CV-RMSE is calculated by dividing the root mean square error by the average of the measured data. The CV-RMSE can be determined using Eq. (2.6) [57].

$$CV - RMSE = \frac{\sqrt{\frac{\sum_{i=1}^n (y_i - \hat{y}_i)^2}{n}}}{\bar{y}} \quad (2.6)$$

where n is the number of data points; y_i is the measured value; \hat{y}_i is the simulated value; and \bar{y} is the average of all measured values.

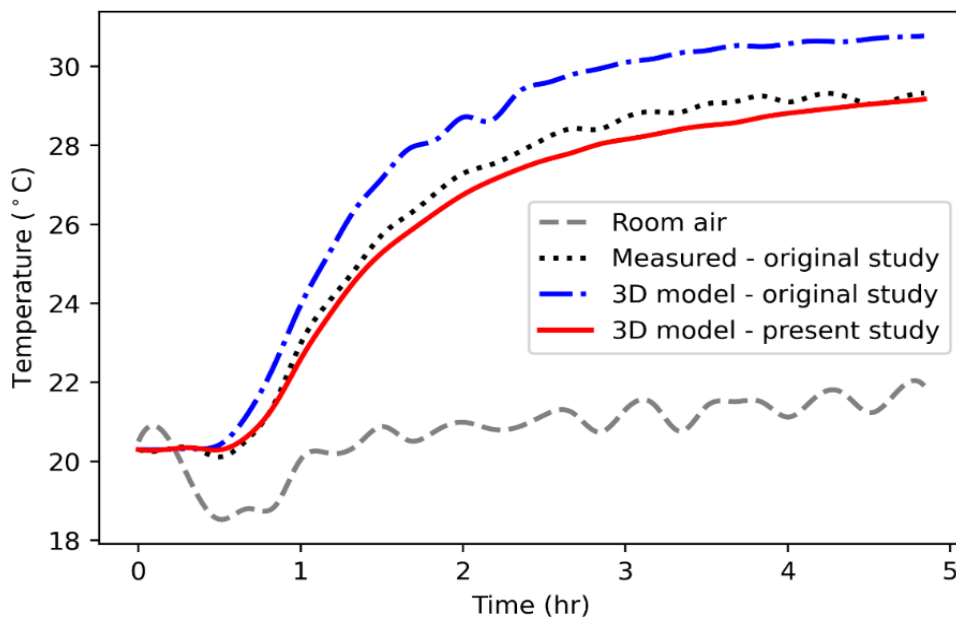


Figure 2.4 Measured and simulated average floor surface temperatures

Table 2.2 compares the CV-RMSE of measured and simulated data for floor average surface temperatures between the present study and Merabtine et al.'s.

Table 2.2 CV-RMSE of measured and simulated values in the present study and Merabtine et al.'s

CV-RMSE (%)	Measured	Simulated (original study)	Measured	Simulated (present study)
-------------	----------	----------------------------	----------	---------------------------

As shown in Table 2.2 CV-RMSE values proved that the model presented in this study is reliable for transient simulation of similar thermally activated wall systems.

2.3. Results and discussion

This section presents the main results and associated analyses of spiral configuration in four subsections: water outlet and average wall temperatures; wall surface temperature uniformity; a general guideline for preventing condensation on the wall; and cooling potentials (i.e., cooling heat flux density and delivered cooling energy) based on the following parameters:

- Supply water temperature (T_{sw})
- Zone temperatures (T_{air})
- Wall thickness (S),
- Pipe spacing (M)

At the end of this section, the performance of the three configurations is compared. The descriptions and figures in the following subsections present the results for the temperature scenario of $T_{sw} = 12^\circ\text{C}$, $T_{air} = 25^\circ\text{C}$, and $S = 5$ cm for two pipe spacings. The results for the other temperature scenarios, wall thickness, and pipe spacing are tabulated in the last subsection.

2.3.1. *Water outlet and average wall temperatures*

Depending on the configuration of the system, the wall surface temperature behaves differently. Calculating the surface temperature of the wall is crucial as the cooling capacity of the system is directly related to the temperature difference between the wall surface and the zone. In addition, calculating the minimum wall temperature is critical to knowing the

minimum allowable humidity level of the zone air to avoid condensation on the wall surface. Condensation also reduces the effectiveness of radiant cooling systems [58]. Moreover, thermal comfort can be impacted by the uniformity of the surface temperature. Figure 2.5 shows the average surface temperature fluctuations for a spiral configuration over a 24-hour period.

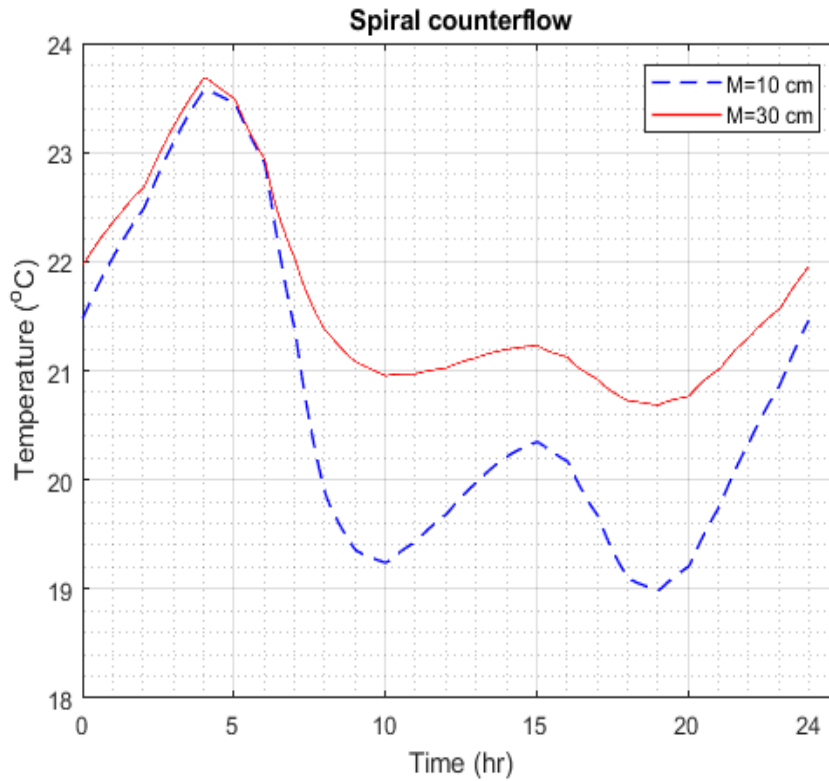


Figure 2.5 Average wall surface temperature over the 24-hour period ($T_{sw} = 12^{\circ}\text{C}$, $T_{air} = 25^{\circ}\text{C}$, $S = 5\text{ cm}$)

The average wall surface temperature reaches its low values approximately 2 to 3 hours after the water flow rate reaches its high values, as shown in Figure 2.5. The average surface temperature dropped to 19°C and 20.6°C at 19:00 for spacings $M = 10\text{ cm}$ and $M = 30\text{ cm}$, respectively. The 10 cm-thick wall is 1°C less than the 5 cm-thick wall in this situation. As the flow rate approached zero, the surface temperature was close to the zone temperature due to insignificant heat rejection from the wall to the pipe. At the same time, the wall absorbed a significant amount of heat from the zone. On the other hand, as the flow rate increased, the wall surface temperature decreased due to a higher heat flux from the wall to the water. This

results in a rise in the water outlet temperature. The temperature range for the water outlet in both spacings of the spiral configuration varied between 16.8°C and 24.2°C.

2.3.2. Temperature uniformity and condensation prevention

Temperature distribution on the wall surface is crucial not only for the comfort of the occupants, but also for reducing the risk of condensation [59, 60]. Figure 2.6 plots the wall surface temperature along the water flow path versus its distance from the water inlet and time for the spiral configuration over the 24-hour period.

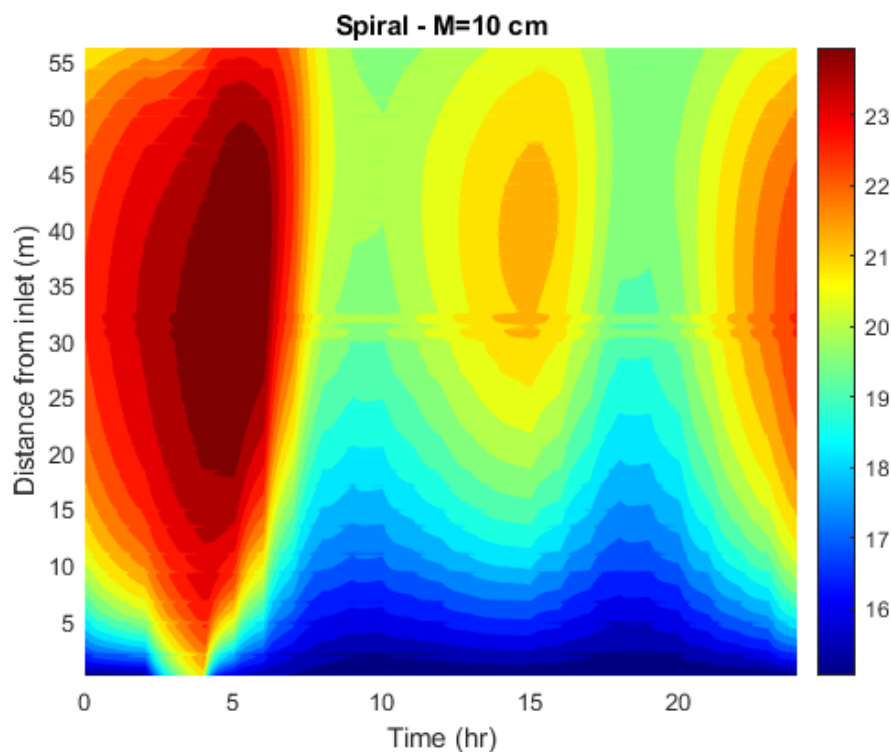


Figure 2.6 Wall surface temperature versus the distance from the inlet over the 24-hour period ($T_{sw} = 12^{\circ}\text{C}$, $T_{air} = 25^{\circ}\text{C}$, $S = 5\text{ cm}$)

Figure 2.6 shows a maximum surface temperature difference of 3.5°C across the wall at the pipe spacing of 10 cm and a difference of 3°C at 30 cm. To avoid condensation, the minimum wall surface temperature should be higher than the dewpoint temperature of the air inside the zone. To establish a conservative yet simple guideline, two minimum wall surface temperatures of all operation scenarios were used as dewpoint temperatures. Thereby, the corresponding RH

is found from a psychrometric chart based on the zone air temperature, as shown in Table 2.3 Allowable indoor RH to prevent condensation in spiral configuration. To avoid condensation on the wall surface, indoor RH should not exceed 53.8% and 44.2% when the zone temperature is 25°C and 30°C, respectively. These findings are in agreement with the ideal indoor RH, which is between 30% and 50% [61].

Table 2.3 Allowable indoor RH to prevent condensation in spiral configuration

$T_{\text{wall.min}} / T_{\text{air}}$ (°C)	Allowable RH (%)
15/25	≤ 53.8
16.5/30	≤ 44.2

2.3.3. Cooling heat flux density

In this study, the amount of heat absorbed by the wall surface from the zone per square meter of wall (W/m^2) is referred to as cooling heat flux density (i.e., cooling capacity). Cholewa et al. [62, 63] argued that due to heat loss towards the backside of the cooled/heated walls, calculations of cooling capacity based on water temperature and flow rate do not always accurately represent the heat flux towards the zone. Cooling capacity can be obtained using Eq. (2.7). According to this equation, the cooling capacity (q) is always positive when cooling is being delivered to the zone air (i.e., the zone air temperature is higher than the average wall surface temperature).

$$q = h_{\text{total}}(T_{\text{air}} - T_{\text{wall}}) \quad (2.7)$$

The combined heat transfer coefficient (h_{total}) between zone and wall surface was set to $9.09 \text{ W}/\text{m}^2\cdot\text{K}$ [46]. Figure 2.7 shows the changes in cooling capacity for the spiral configuration over the 24-hour period.

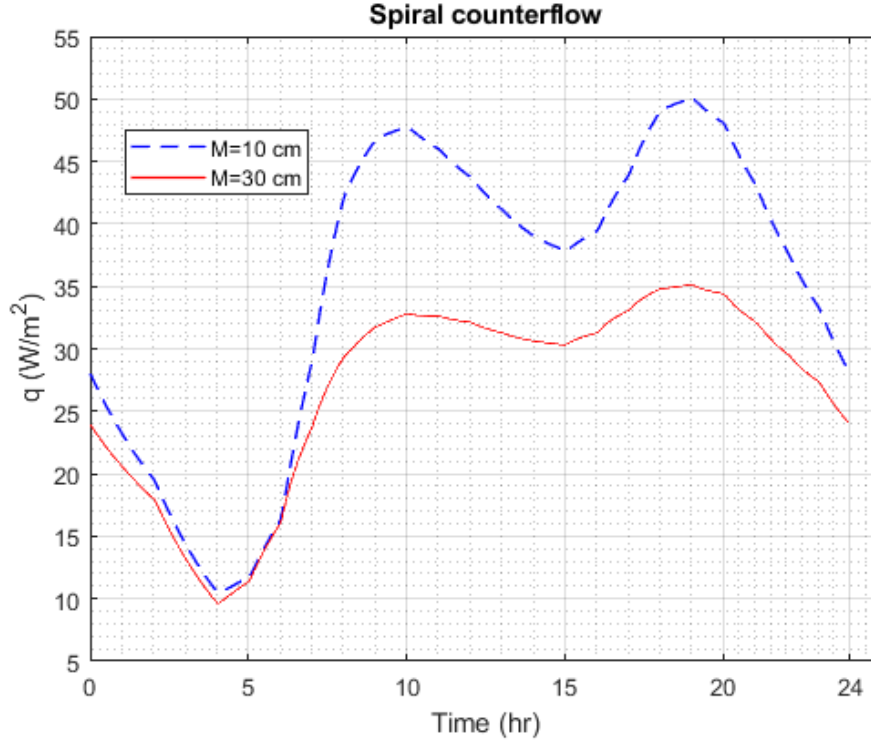


Figure 2.7 Cooling capacity over the 24-hour period ($T_{sw} = 12^\circ\text{C}$, $T_{air} = 25^\circ\text{C}$, $S = 5$ cm)

As shown in Figure 2.7, the cooling capacity peaked at 50 W/m^2 for $M = 10$ cm and 35 W/m^2 for $M = 30$ cm. With $M = 10$ cm, the cooling capacity was significantly greater than that of $M = 30$ cm. This is due to the longer pipe length (i.e., greater heat transfer area) and a more uniform surface temperature (fewer hot spots). For both spacings, the minimum cooling capacity was around 10 W/m^2 when the flow rate was almost zero.

2.3.4. Delivered cooling energy

The delivered cooling energy (DCE) in this study is defined as the amount of cooling energy from the water delivered to the room and the wall (i.e., heat loss from the water flow) and can be calculated using Eq. (2.8).

$$DCE = \dot{m}C_{p_{\text{water}}}(T_{\text{outlet water}}(t) - T_{\text{inlet water}})\Delta t \quad (2.8)$$

where Δt is the simulation timestep (i.e., 60 sec).

Figure 2.8 illustrates the cumulative DCE (“Total DCE”), the portion of DCE that goes to the room (“DCE to room”), and the amount of energy stored in the wall (“Energy stored in wall”) during a 24-hour period. DCE to room equals to the amount of heat transferred between the room and the surface of the wall. Furthermore, the energy stored in the wall is calculated based on the difference between the total DCE and the DCE to room, which can either be heat storage (i.e., wall temperature increases, negative values in Figure 2.8) or cold storage (i.e., the wall temperature decreases, positive values in Figure 2.8). As shown in Figure 2.8, in the first five hours, the accumulated energy stored in wall (“Energy stored in wall”) is negative (i.e., wall became warmer) because the heat gain from the room is greater than the heat loss to the water due to the low water flow rate. According to Figure 2.8, the total DCE for $M = 10$ cm increased throughout the day to a value of 20 MJ at the end of the day. For $M = 30$ cm, the total DCE reached 15 MJ after 24 hours.

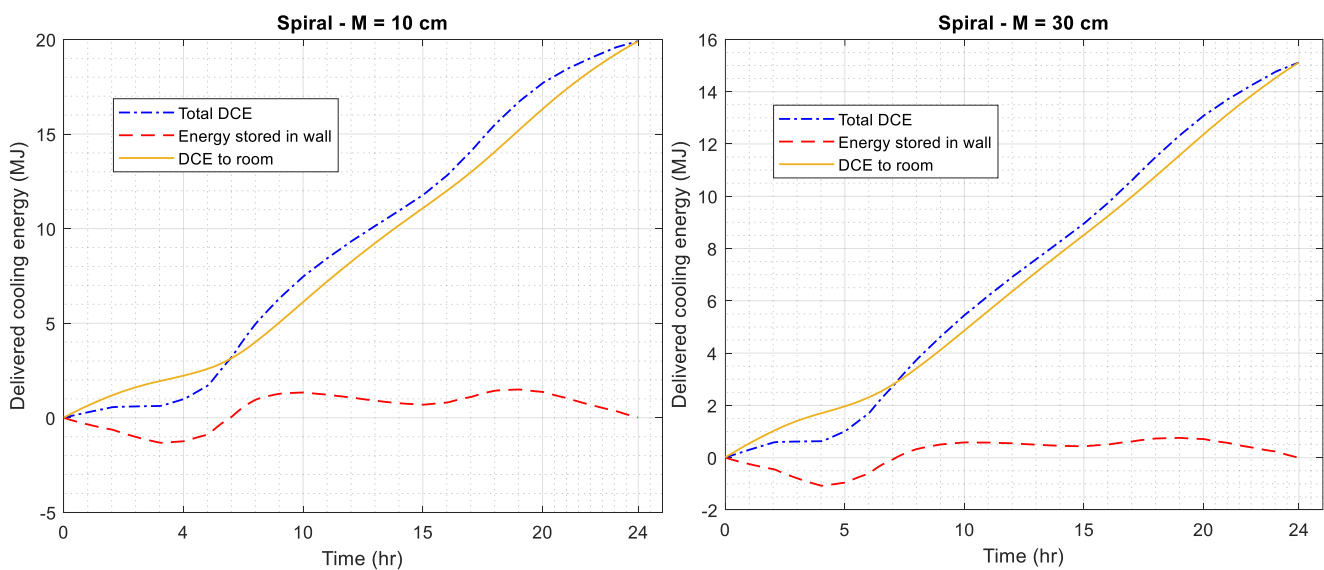


Figure 2.8 Cumulative DCE over the 24-hour period ($T_{sw} = 12^{\circ}\text{C}$, $T_{air} = 25^{\circ}\text{C}$, $S = 5$ cm)

In order to evaluate the significance of the cooling energy that DCW-wall can provide, the cooling energy is compared to the space energy demand of Toronto, Ontario, Canada as a

benchmark city for the cold climate. To determine the space cooling energy demand in Toronto, calculations were performed using the average space cooling energy consumption of households in the province of Ontario. According to Natural Resources Canada and Statistics Canada [64, 65], the average energy consumption per household for space cooling in Ontario was 1.9 GJ in 2019. To calculate the energy demand for space cooling, an energy efficiency rating for cooling equipment is necessary.

The efficiency of cooling devices is commonly determined using the Seasonal Energy Efficiency Ratio (SEER) [66]. The SEER is calculated by dividing the amount of heat removed from the air in British Thermal Units (BTUs) by the total energy consumed in watt-hours (Wh). SEER is similar to the Coefficient of Performance (COP), which is a unitless measurement. [66]. With a SEER of 10 BTU/Wh (equivalent to a COP of 2.9) [67], the energy demand for space cooling can be calculated as 5.6 GJ (i.e., 2.9×1.9). Toronto experienced 23 days with mean ambient temperatures above 25°C [68]. If a DCW-wall in the abovementioned configuration was operated in these 23 days, it can provide 0.026 GJ cooling energy per day, and ~0.6 GJ for 23 days. This is approximately 11% of the space cooling energy demand for the entire cooling season in Toronto. More cooling energy can be provided if the wall is operated in the other days of the summer. In other words, DCW-wall system would be credited with a higher contribution percentage if only the cooling demand during heat waves was considered. In this context, the proposed DCW-wall could even eliminate the need for mechanical cooling systems in cities with fewer days of heat waves, such as Edmonton, Alberta, Canada.

2.3.5. Comparison of three configurations on the basis of model results

This subsection compares the three configurations with respect to water outlet temperature, average wall surface temperature, wall surface temperature distribution, permissible indoor RH to avoid condensation, and cooling potentials.

2.3.5.1. Water outlet and average wall temperatures

Figure 2.9 depicts the changes in average wall temperature for the three configurations during the 24-hour period.

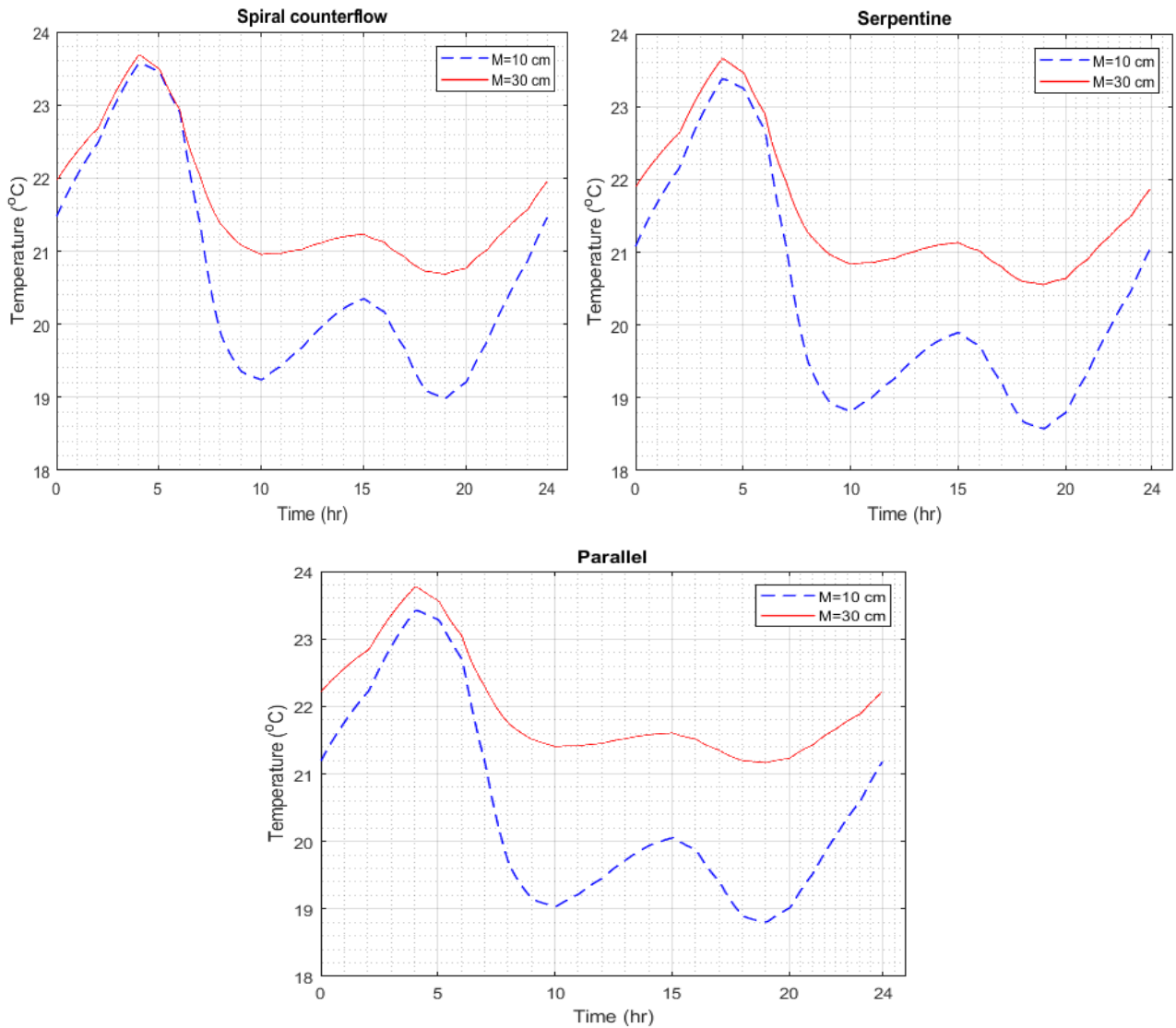


Figure 2.9 Average wall surface temperature for all configurations over the period of 24 hours ($T_{sw} = 12^{\circ}\text{C}$, $T_{air} = 25^{\circ}\text{C}$, $S = 5\text{ cm}$)

When the cooling capacity was at its maximum and the pipe spacing was 10 cm, the average temperature of the wall surface decreased to 19°C , 18.6°C , and 18.8°C for spiral, serpentine, and parallel configurations, respectively. In addition, when the pipe spacing was 30 cm, the spiral and serpentine configurations experienced the same minimum surface

temperature of 20.6°C, while the parallel configuration had a minimum temperature of 21.2°C. When the cooling capacity reached its maximum value, the surface temperature of a 10 cm-thick wall was 1°C warmer than that of a 5 cm-thick wall. Also, as the wall thickness was increased from 5 cm to 10 cm, a slower decrease rate of the wall surface temperature and a delay in reaching the minimum temperature by one hour were observed. These changes have a continuous effect on the temperature of the outlet water as well. The water outlet temperature for all operation scenarios varied between 16.5°C and 29°C. When the flow rate is low, the outlet temperatures approach the zone temperatures.

2.3.5.2. Temperature uniformity and a condensation prevention

Figure 2.10 illustrates the wall surface temperature contours for all configurations throughout the day.

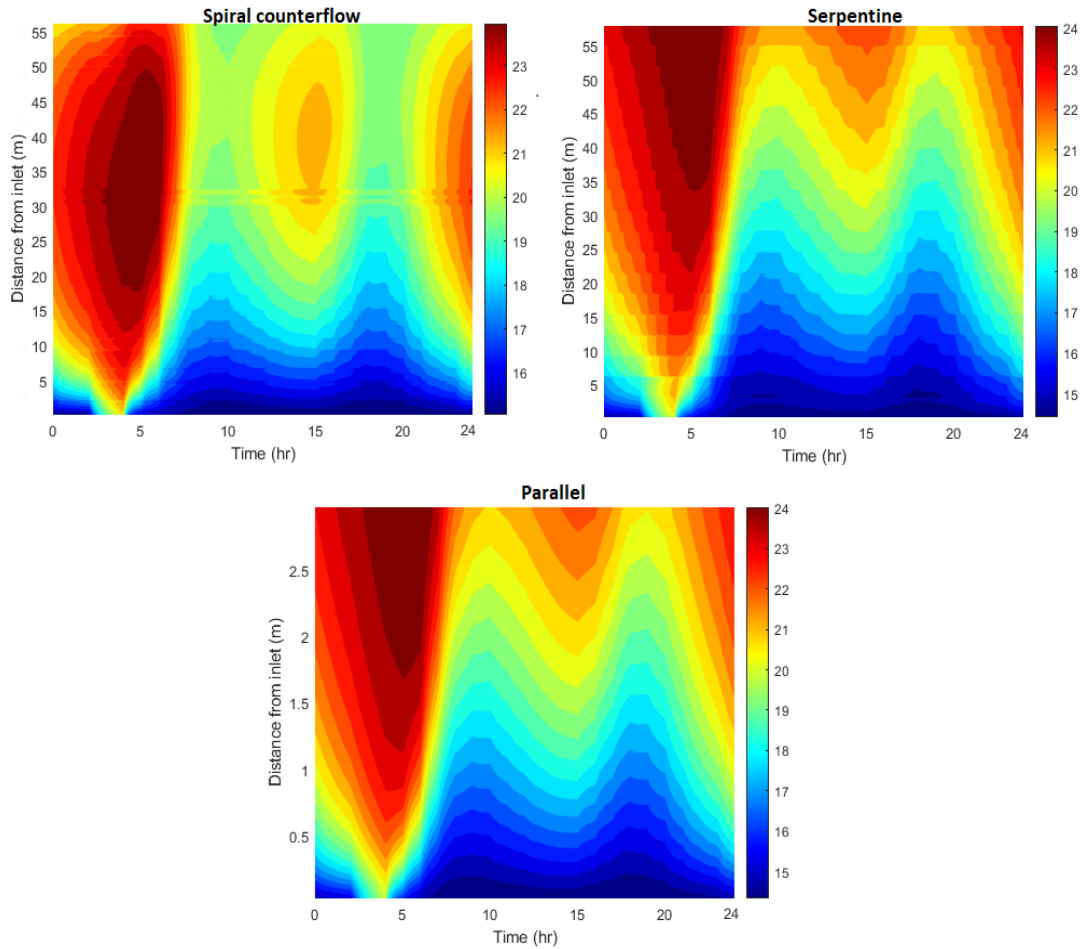


Figure 2.10 Wall surface temperature versus the distance from the inlet for all configurations over the 24-hour period ($T_{sw} = 12^{\circ}\text{C}$, $T_{air} = 25^{\circ}\text{C}$, $S = 5\text{ cm}$)

As depicted in Figure 2.10, the spiral configuration had a more evenly distributed temperature, with a maximum difference of 4°C across the wall, when compared to the serpentine and parallel configurations, which had maximum temperature differences of 6.5°C and 6.7°C , respectively. The variation in temperature uniformity between configurations is caused by the arrangement of pipes in the wall. In a spiral configuration, the cool supply water and less cool return water are in parallel and therefore provide a more uniform cooling flux density to the wall. This difference in pipe layout also affects the minimum wall surface temperature, which is crucial for determining the permissible indoor RH.

Table 2.4 provides a guide to determining the allowable indoor RH to minimize the risk of condensation on the wall surface, based on all temperature scenarios for the three piping configurations.

Table 2.4 Allowable indoor RH to prevent condensation in all configurations

Configuration	$T_{\text{wallmin}} / T_{\text{air}}$ (°C)	Allowable RH (%)
spiral	15/25	≤ 53.8
	16.5/30	≤ 44.2
serpentine	14.5/25	≤ 52.1
	15.6/30	≤ 41.7
parallel	14.37/25	≤ 51.7
	15.25/30	≤ 40.8

In zone with temperatures between 25°C and 30°C, the spiral configuration permits a higher indoor humidity level compared to the other configurations. While the serpentine configuration allows for a 1% higher humidity level than the parallel configuration.

2.3.5.3. Cooling heat flux density

Figure 2.11 shows the variation of cooling capacity in all modelled configurations for 24 hours. For all configurations,

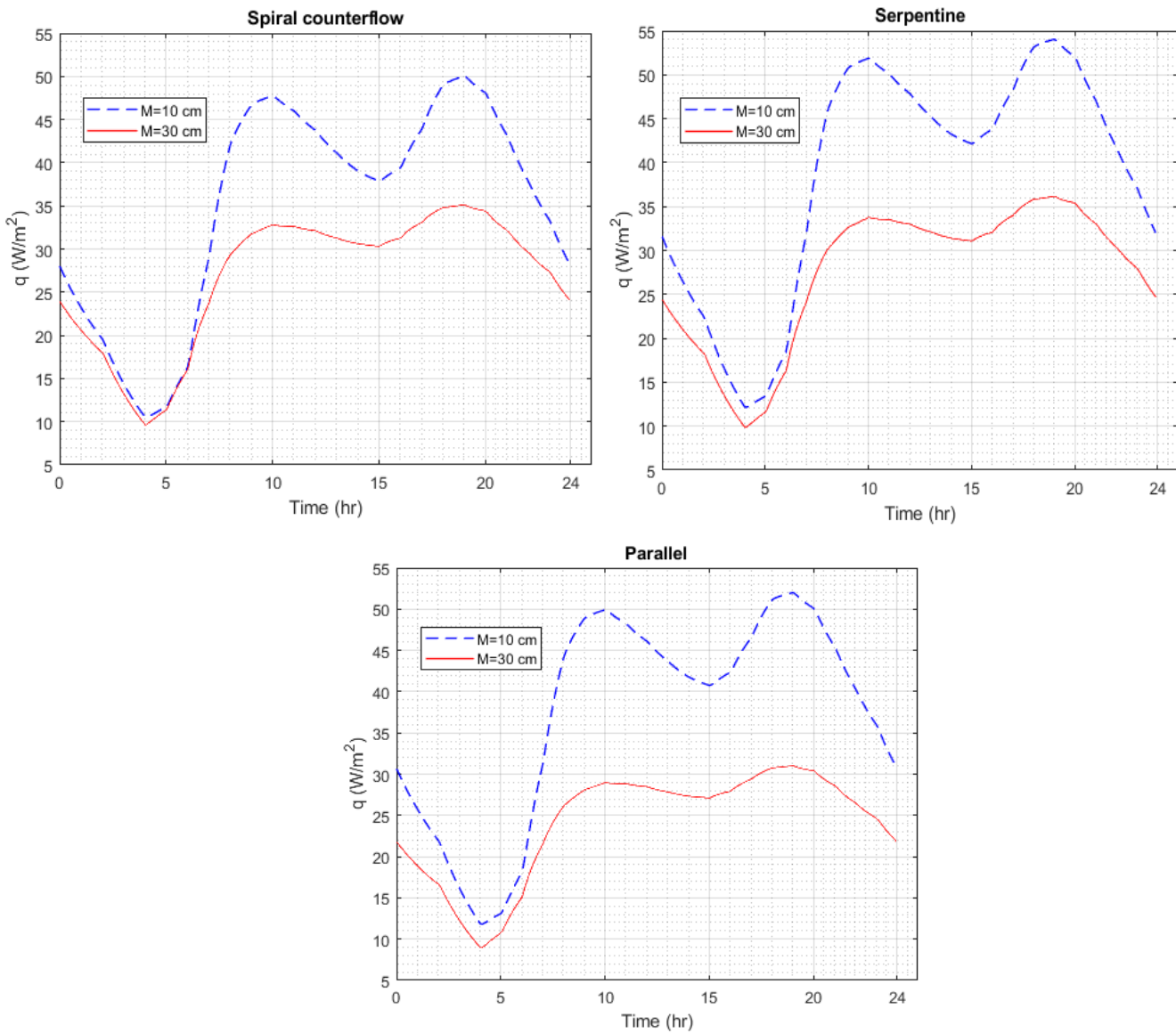


Figure 2.11 Cooling capacity for all configurations during the 24-hour period ($T_{sw} = 12^{\circ}\text{C}$, $T_{air} = 25^{\circ}\text{C}$, $S = 5$ cm)

As shown in Figure 2.11, the peak cooling capacity was reached approximately two hours after the water flow rate reached its maximum. For a spacing of $M = 10$ cm, the serpentine configuration had the highest cooling capacity, followed by the parallel and spiral configurations. Additionally, the difference in cooling capacity between the two spacings (i.e., the maximum distance between the two curves in Figure 2.11) was greater for the parallel configuration compared to the other two configurations. Similar to $M = 10$ cm, the serpentine configuration delivered the highest cooling capacity for $M = 30$ cm, followed by the spiral and

parallel configurations. Table 2.5 presents the maximum cooling capacity for all scenarios simulated in this study.

Table 2.5 Maximum cooling capacity (W/m^2) for all scenarios

Temperature	serpentine				parallel				spiral			
	$S^* = 5$		$S = 10$		$S = 5$		$S = 10$		$S = 5$		$S = 10$	
scenarios	M^{**}	$M =$	$M =$	$M =$	$M =$	$M =$	$M =$	$M =$	$M =$	$M =$	$M =$	$M =$
	$= 10$	30	10	30	10	30	10	30	10	30	10	30
$T_{sw} = 12^\circ C$ $T_{air} = 25^\circ C$	54	36	46.1	33.9	53.8	31.9	45.8	30	50	35	41.2	32.6
$T_{sw} = 12^\circ C$ $T_{air} = 30^\circ C$	80	53.5	68	49.7	79.1	46.8	67.6	44.4	73.9	51.9	60.8	48
$T_{sw} = 15^\circ C$ $T_{air} = 25^\circ C$	40.5	27	34.5	25.2	40.2	24.9	34.3	22.7	37.5	26.4	31	24.4
$T_{sw} = 15^\circ C$ $T_{air} = 30^\circ C$	65	43.9	55.8	40.8	64.8	38.5	55.4	36.5	60.8	42.7	49.9	39.3

* Wall thickness in *cm*

** Pipe spacing in *cm*

Based on Table 2.5, the greatest decrease in maximum cooling capacity occurred at $S = 5$ cm when the pipe spacing was changed from 10 cm to 30 cm. As a result of increased spacing, the cooling capacity for the serpentine configuration decreased by 33% for $S = 5$ cm and 27% for $S = 10$ cm. Additionally, for both $S = 5$ cm and $S = 10$ cm, the reductions in cooling capacity were 40% and 34% for the parallel configuration, and 30% and 21% for the spiral configuration when the pipe spacing was increased from 10 cm to 30 cm. The results indicated that the maximum cooling capacity is more affected by the pipe spacing than by the wall thickness.

2.3.5.4. Delivered cooling energy

Figure 2.12 shows the changes in the cumulative total DCE, DCE to room, and energy stored in the wall over a 24-hour period for all configurations.

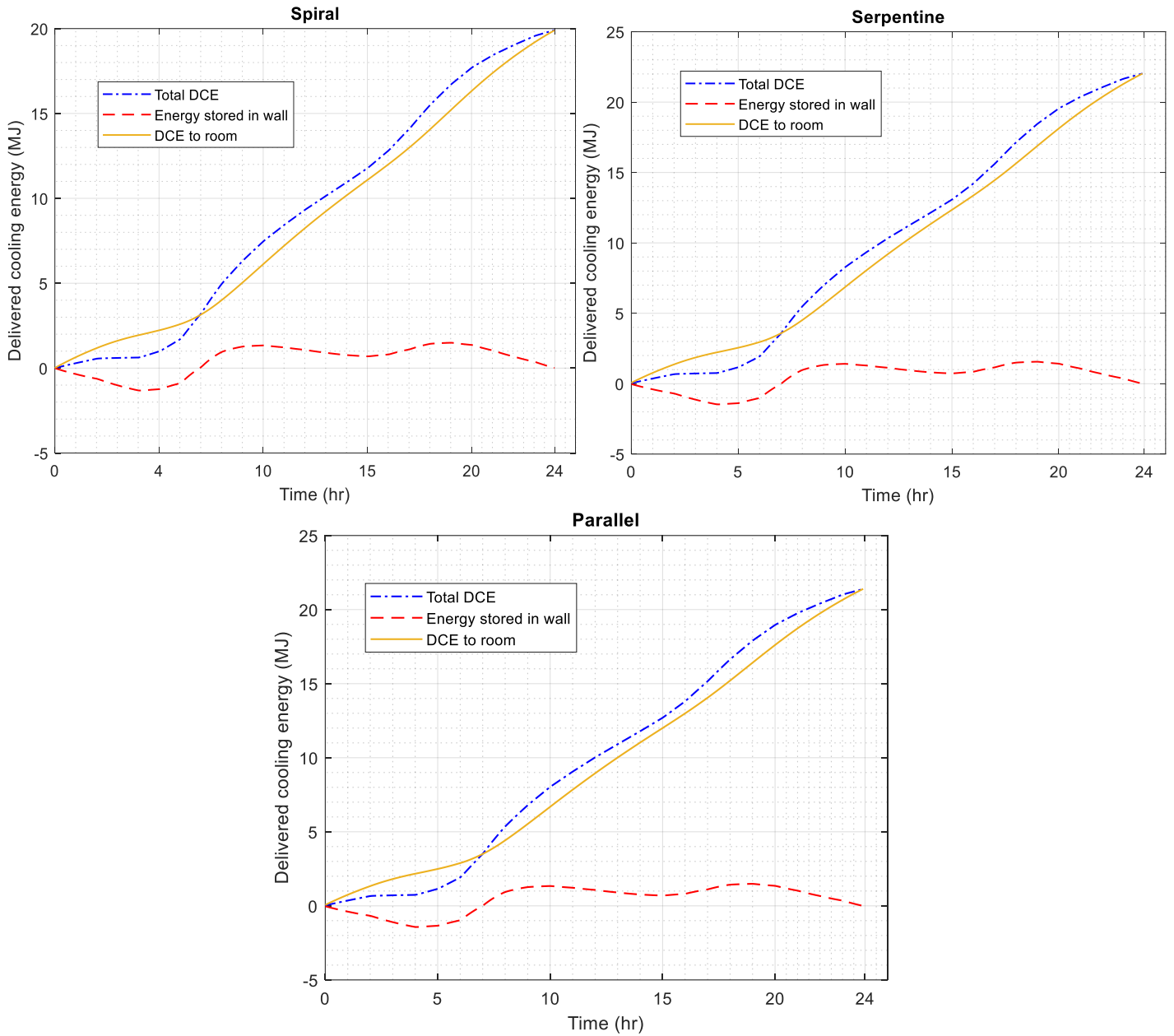


Figure 2.12 Cumulative DCE for all configurations over the 24-hour period

$$(T_{sw} = 12^{\circ}\text{C}, T_{air} = 25^{\circ}\text{C}, S = 5 \text{ cm})$$

The cumulative DCE trends depicted in Figure 2.12 exhibit a similar behavior for all configurations and are discussed in [subsection 2.3.4](#). In this context, although thermal mass did not significantly contribute to heat/cold storage, it could stabilize the wall surface temperature and cooling capacity throughout the day. Table 2.6 presents the total DCE values for all scenarios. Similar to cooling capacity, the serpentine configuration showed the highest cooling energy delivered by the system in all temperature scenarios.

Table 2.6 Total DCE (MJ) per day for all scenarios

Temperature scenarios	serpentine				parallel				spiral			
	S = 5		S = 10		S = 5		S = 10		S = 5		S = 10	
	M = 10	M = 30	M = 10	M = 30	M = 10	M = 30	M = 10	M = 30	M = 10	M = 30	M = 10	M = 30
$T_{sw} = 12^{\circ}\text{C}$ $T_{air} = 25^{\circ}\text{C}$	22	16	21	16	21	14	20	14	20	15	19	15
$T_{sw} = 12^{\circ}\text{C}$ $T_{air} = 30^{\circ}\text{C}$	30	23	29	22	29	20	28	20	26	22	26	22
$T_{sw} = 15^{\circ}\text{C}$ $T_{air} = 25^{\circ}\text{C}$	17	13	16	12	15	11	15	10	16	12	14	12
$T_{sw} = 15^{\circ}\text{C}$ $T_{air} = 30^{\circ}\text{C}$	25	18	24	18	24	16	23	16	23	18	22	18

2.3.6. Influence of wall surface area on total DCE

In addition to the previously mentioned influential parameters, changes in wall dimensions affect the total DCE due to the change in pipe length and therefore the area of heat transfer. For the temperature scenario of $T_{sw} = 12^{\circ}\text{C}$ and $T_{air} = 25^{\circ}\text{C}$ with a wall thickness of 5 cm, Table 2.7 shows the simulation results of the total DCE for all configurations with respect to changes in wall surface area (wall height was fixed at 2 m, but length was subjected to change).

Table 2.7 Total DCE (MJ) per day for different wall surface areas

Configuration	Wall surface area (m ²)									
	4		6		8		10		12	
	M =	M =	M =	M =	M =	M =	M =	M =	M =	M =
	10	30	10	30	10	30	10	30	10	30
spiral	16	12	21	16	22	18	24	20	25	22
serpentine	18	11	22	15	25	18	27	20	28	22
parallel	17	11	22	15	24	17	26	19	28	21

As shown in Table 2.7, on average, expanding the wall surface area from 4 m² to 6 m² resulted in a 21% increase in total DCE for pipe spacing of $M = 10$ cm and a 29% increase for $M = 30$ cm. Furthermore, when the wall surface area was increased from 6 m² to 8 m², 8 m² to 10 m², and 10 m² to 12 m², the total DCE increased by 10%, 7.2%, and 4.4%, respectively, for $M = 10$ cm. For $M = 30$ cm, the values are 11.1%, 10%, and 8.9%, respectively. Table 2.7 reveals that while both an increase in wall surface area and a decrease in pipe spacing lead to an increase in total DCE, the impact of the latter is more pronounced.

2.4. Conclusion

The primary objectives of this Chapter were to evaluate the cooling potentials of a DCW-wall system and establish a general guideline for preventing condensation on the wall surface. This paper used a 3D transient thermal model that was validated using transient experimental data from a similar study. A typical DCW flow rate pattern was incorporated to calculate the maximum cooling capacity, DCE, water outlet temperature, and average wall surface temperature for different operation and boundary scenarios.

Results showed that smaller pipe spacing, lower water inlet temperature, and thinner walls all contributed to higher cooling capacity and total DCE. With a maximum cooling capacity of 80 W/m² and a total DCE of 30 MJ/day, the serpentine configuration offered the highest cooling

potentials. The free cooling energy provided by the DCW-wall system can effectively reduce or even eliminate the reliance on mechanical cooling systems during a cooling season in cold-climate residential buildings without wasting DCW resources. Findings revealed that the DCW-wall system with spiral configuration supplied almost 11% of the energy demand for space cooling during the cooling season in Toronto, Canada. In addition, the three configurations demonstrated the lowest average wall surface temperature, ranging from 18.6°C to 21.2°C across all operation and boundary scenarios. At peak cooling capacity, the surface temperature of a 10 cm-thick wall was found to be 1°C higher than a 5 cm-thick wall. Furthermore, the spiral counterflow configuration displayed the most uniform temperature on the wall surface, which is essential for thermal comfort and condensation prevention. Based on this, a conservative yet simple guideline was proposed to prevent condensation. Maintaining indoor RH levels between 40.8% and 53.8% would minimize the likelihood of condensation regardless of the operation and boundary scenario.

Chapter 3 Generalizable Thermal Performance of a Ventilated Concrete Block Wall and the Energy Implication of Its Substitution for a Wood-Frame Wall in Cold-Climate Buildings

3.1. Introduction

Buildings account for approximately 40% of global energy use and 30% of greenhouse gas (GHG) emissions [69]. Unless strict policies are implemented and energy-efficient technologies are adopted, the energy consumption of buildings will continue to increase, posing a serious threat to the global environment and economy [8, 9]. Using thermal energy storage (TES) is a cost-effective approach to enhance the energy efficiency of buildings. TES in buildings can improve the thermal performance by balancing energy supply and demand, using renewable energy sources, smoothing zone temperature fluctuations, and improving thermal comfort for occupants [10-13]. Particularly, using building envelope (i.e., walls, floor, ceiling) for TES is one of the promising methods to reduce the space heating and cooling demands. Reduction in heating and cooling demands can be achieved by storing and releasing significant amounts of thermal energy through the thermal mass of the envelope. Storing excess thermal energy in the envelope can buffer zone temperature fluctuations and reduce space heating and cooling loads. The stored heat can be used later to warm the zone when indoor temperature drops, such as at night and early in the morning. The process of storing and releasing heat can be passive, active, or a combination of both strategies. Passive strategies rely on the natural convection through the surfaces of a building's envelope, while active strategies use mechanical equipment like pumps or fans to circulate heat transfer fluids (HTFs) like water or air through pipes or conduits embedded in the envelope to facilitate the exchange of heat. Active TES systems offer several advantages over passive TES systems, including greater control and improved responsiveness. With more precise control over the storage and release of thermal

energy, active systems enable better management of energy supply and demand, while their ability to quickly respond to varying environmental conditions and occupant's needs ensures optimal thermal comfort. This improved control and responsiveness lead to higher energy efficiency in buildings, reducing energy consumption and associated costs. Furthermore, enhanced thermal comfort results from active TES systems maintaining more consistent indoor temperatures. In addition, active TES systems can be more easily integrated with other energy-efficient technologies, such as renewable energy sources, creating a comprehensive energy management system that further improves building performance.

The use of active TES as a means of reducing the thermal loads of buildings has received significant attention in recent years. In particular, researchers have been studying the use of ventilated block walls (VBW) as an active TES solution in building envelope [16, 70-73]. In these types of walls, the hollow cores of the blocks are aligned to create air channels. Circulating air through these channels can accelerate the heat transfer and therefore thermal energy storage and release. By actively moving air through the channel, the heat transfer coefficient between the thermal mass and air is increased, allowing for increased heat transfer rate and thus greater storage and release of thermal energy. This increased rate of heat transfer enables the wall to store thermal energy more effectively during periods of high temperature and release it more rapidly during cooler periods, improving the overall thermal performance of the building. The stored thermal energy in the wall can be released to the zone through the wall surface, through supply air to zone by the use of a fan (i.e., the air is drawn into the channel where it exchanges heat with the wall before being returned back into the zone), or a combination of both. Sources for air ventilation include ambient air, exhaust air from an air conditioning system, and zone air [16, 72]. In the last case, zone air is drawn into the air channel within the wall, exchanges heat with the mass, and then returns to the zone. In this particular case, air circulation can significantly enhance the heat exchange rate between the wall and its

surrounding zone compared to walls without air circulation [16, 71]. The majority of research on using active TES in buildings' mass has focused on ventilated concrete floor and ceiling slabs [74-79]. However, a few studies were conducted to assess the thermal performance of VBWs without supplying air to the zones.

Huang et al. [71] examined the thermal performance of an exterior VBW without supply air to zone in a hot region in China. The exhaust air from the ventilation system passes through the air channel, therefore, it was assumed that the temperature of the circulated air would be the same as the indoor temperature. Air circulation enables the wall to store the indoor excess thermal energy during warm period and release when the indoor temperature drops. Their findings showed that the impact of air speed on the thermal storage performance is much higher than the impact of airflow temperature for a given cavity size.

Moreover, VBWs can also serve as an interior wall. The thermal performance of an interior VBW without SAZ was examined in a few studies [72, 73, 80]. Yu et al. [73] investigated the dynamic thermal performance of an interior VBW. Authors placed and stacked hollow concrete blocks in a way to create serpentine air channel. Then, they charged the wall with heated air at a constant temperature and speed. The constructed wall was placed in the middle of two identical rooms. The maximum total heat flux of 112.9 W/m^2 between the wall surface and zone was achieved when the air speed was 2.9 m/s, supply air temperature was 40°C , and zone air temperature was fixed at 17°C .

The benefits of using VBWs without SAZ in reducing thermal loads of buildings have been presented in literature. However, a review of extant literature has shown that there are no studies that have evaluated the performance of VBW with air circulating between the VBW and its associated zones (simply referred to as VBW from now on). VBWs are able to provide dual functionality, acting as both structural support and thermal mass, storing excess thermal energy and buffer zone temperature fluctuation. VBWs enhance building performance through

strong thermal coupling with the surrounding spaces and exposing more mass area for heat transfer, promoting effective thermal storage and release. Furthermore, VBWs' simplicity in design and minimal reliance on mechanical equipment make them a cost-effective option for improving the buildings' energy efficiency. Additionally, there is a scarcity of research on the use of VBWs in cold-climate buildings. The increased thermal energy storage and release of VBWs contribute to their enhanced efficiency. To maximize this benefit, substantial fluctuations in zone temperature are necessary. Cold-climate buildings experience significant zone temperature fluctuations during spring and fall, allowing the VBWs to demonstrate their full potential in maintaining thermal comfort and energy efficiency. Therefore, this study aims to evaluate the typical-day and annual thermal performance of a VBW in a cold region. Evaluating the performance of a VBW on a typical day involves investigating the heat flux density and total net energy exchange between the VBW (exterior and interior) and the associated zone over a 24-hour period. By analyzing different zone temperature profiles, air speeds, and interior finishes, this parametric analysis enables a comprehensive understanding of the VBW's performance under various conditions, ensuring its effectiveness in diverse situations. Additionally, the study of annual thermal performance aims to quantify the annual total assisting heating and cooling loads in Canadian residential buildings by replacing traditional wood-frame walls with VBWs. To achieve this, three Canadian cities of Edmonton, Vancouver, and Toronto have been selected for the simulations.

3.2. Description of the physical system

Figure 3.1 shows a schematic of the VBW configuration studied in this thesis. One column of blocks is shown in this schematic, but more columns can be connected in parallel or series. This study is focused on the thermal performance of one column VBW, the height of which equals a typical floor-to-ceiling height of approximately 2.5 meters. The performance of

multiple columns in parallel will be approximately equal to the one-column performance multiplied by the number of columns.

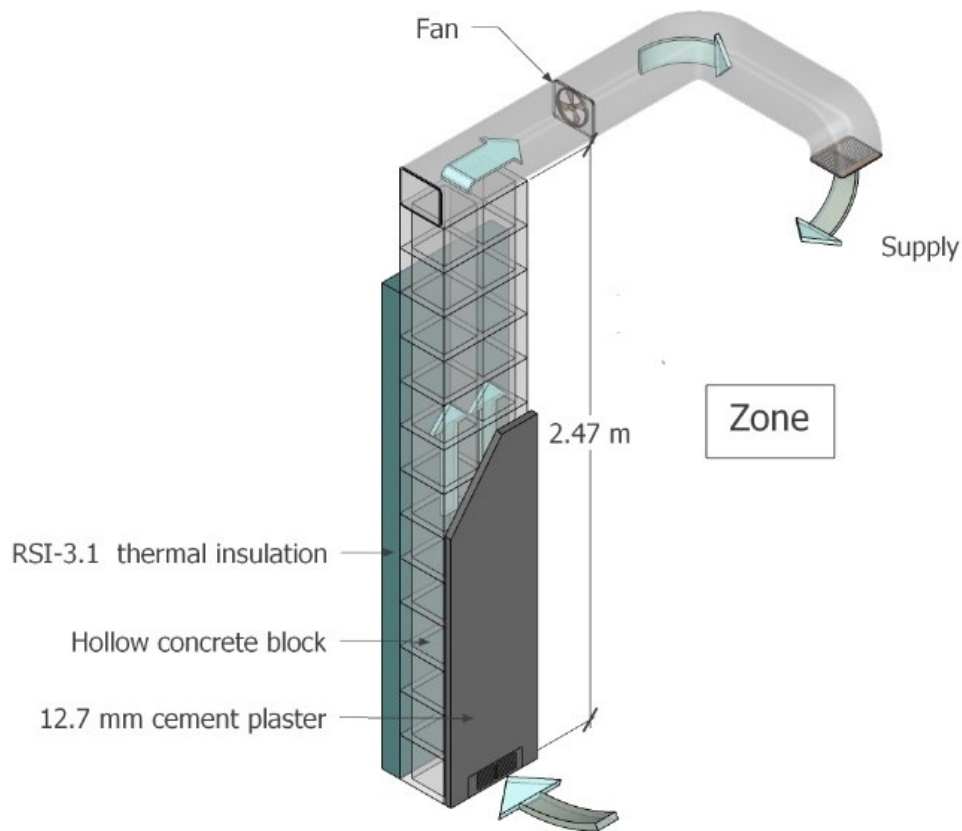


Figure 3.1 A schematic of the VBW

As illustrated in Figure 3.1, a wall of ~2.5 meters in height is constructed by stacking 13 hollow concrete blocks on top of each other [81]. By stacking hollow blocks on top of each other, two air channels are created by connecting the hollow cores. Using a fan, zone air is drawn into each air channel from the bottom and moves upward in the wall height, exchanges heat with the wall, and returns to the zone from the top through a duct.

As shown in Figure 3.1, the modelled VBW consists of a cement plaster finishing on the interior side, hollow concrete blocks, and RSI-3.1 thermal insulation on the exterior side. The choice of RSI-3.1 was made to meet the minimum standard requirement of RSI-3.5 for exterior walls when combined in series with hollow concrete blocks and cement plaster. In this study,

the RSI value for exterior walls was chosen based on the minimum requirement set by the National Energy Code of Canada for Buildings (NECB) in 2020 [82]. The RSI value is a measure of a material's thermal resistance in metric units, with higher values indicating better insulation.

Table 3.1 presents the thermal properties of all layers of the VBW.

Table 3.1 Thermal properties of the materials used in VBW

Materials	Thermal properties			Ref.
	Thermal conductivity coefficient (W/m.K)	Density (kg/m ³)	Specific heat capacity (J/kg.K)	
Cement plaster	0.72	1860	840	[83]
Concrete	1.5	2240	840	[83]
Thermal insulation	0.038	25	1400	[84]

The system depicted in Figure 3.1 is designed to effectively exchange heat with its associate zones and store it to prevent space over heating and cooling, thereby reducing space heating and cooling loads. Throughout the day, as the indoor temperature rises primarily due to the direct and indirect solar heat gain, zone air is directed into the VBW where it exchanges heat with the block mass. The process allows the wall to store excess thermal energy and to cool the air before it is supplied to the zone. This cooled air helps maintain a comfortable temperature and reduces the need for additional cooling. At night and in the early morning, as the indoor temperature drops mainly due to lower outdoor temperature, the zone air takes the stored heat

and returns it to the zone. The continuous process of storing and releasing heat ensures a stable indoor temperature and leads to reduction in space thermal loads.

3.3. Methodology

This section elaborates on the research methodology, beginning with an overview of the types of performance evaluations. It continues with an explanation of the boundary conditions used to evaluate thermal performance. The next part of the section describes the heat transfer equations and the air speeds for evaluating thermal performance. The section concludes with a discussion of the model's validation.

3.3.1. Overview

Two types of thermal performance are evaluated: a) a typical-day thermal performance of an interior and an exterior VBW, and b) the annual energy analysis of an exterior VBW and an exterior wood-frame wall.

The typical-day approach can evaluate the VBW performance across different zone temperature profiles, air speeds, and interior wall finishes. By accounting for the common indoor temperature variations, this approach can generalize the findings and enables the application of results to a broader range of circumstances and building structures. Without it, determining the outdoor boundary conditions becomes challenging due to the numerous potential outdoor conditions. Focusing on cold-climate buildings in Canada, the annual energy analysis aims to investigate the yearly performance of the VBW and a traditional wood-frame wall, considering close-to-actual zone temperature and actual outdoor conditions in three Canadian cities of Edmonton, Vancouver, and Toronto.

3.3.1.1. Typical-day performance

This approach examines the thermal performance of an interior and an exterior VBW over the course of a typical day. The performance consists of determining the average wall surface temperature, heat flux density, and energy exchange. In this analysis, the zone temperature is

assumed to follow a steady-periodic operation, which involves maintaining a consistent zone temperature and air speed for several days. Transient simulations were conducted for a sufficiently long period (i.e., several days) until the wall surface temperature converged. The results of the last 24-hour period are used for the typical-day performance.

3.3.1.1.1 Boundary conditions

In typical-day analysis, interior and exterior VBWs are exposed to different boundary conditions. An interior VBW exchanges heat with the zone on both sides. In contrast, one side of an exterior VBW is exposed to the outdoor environmental conditions. Because of the wide range of outdoor temperatures and varying overall thermal resistances, it can be challenging to cover all possible boundary conditions or select suitable ones to produce generalizable performance evaluation when it comes to exterior walls.

a) Exterior wall

This study assumed an adiabatic boundary condition for the exterior wall. The assumption of adiabatic boundary condition can be considered accurate in summer due to the thick insulation of exterior walls in cold-climate buildings and insignificant temperature difference between indoors and outdoors. In the case of outdoor temperatures dropping below freezing, there would be significant heat loss through the exterior walls which cannot be ignored. This is because indoor temperatures are typically kept relatively mild, around 21°C, thus creating a large temperature difference between indoors and outdoors during cold winter months. To account for the heat loss, the typical-day analysis includes the a “heat loss percentage” factor when calculating the total energy exchange values. The “total energy exchange” represents a single number and is defined as the cumulative absolute amount of heating and cooling energy that can be supplied to the zone (or absolute variation of thermal energy stored in the VBW) by the VBW during a 24-hour period.

In cold climates, buildings can experience significant heat loss through their exterior walls when the outdoor temperature drops far below freezing. Therefore, accurately determining the heat loss is crucial when evaluating the thermal performance of a VBW. The “heat loss percentage” was determined using a conservative method that accounts for the coldest outdoor temperatures while maintaining a constant indoor temperature. The heat loss values for an exterior VBW with no insulation and an RSI value of 3.5 are shown in Figure 3.2. The values are simulated with the transient thermal model developed in this study, to be described in detail in the following “Numerical model” section.

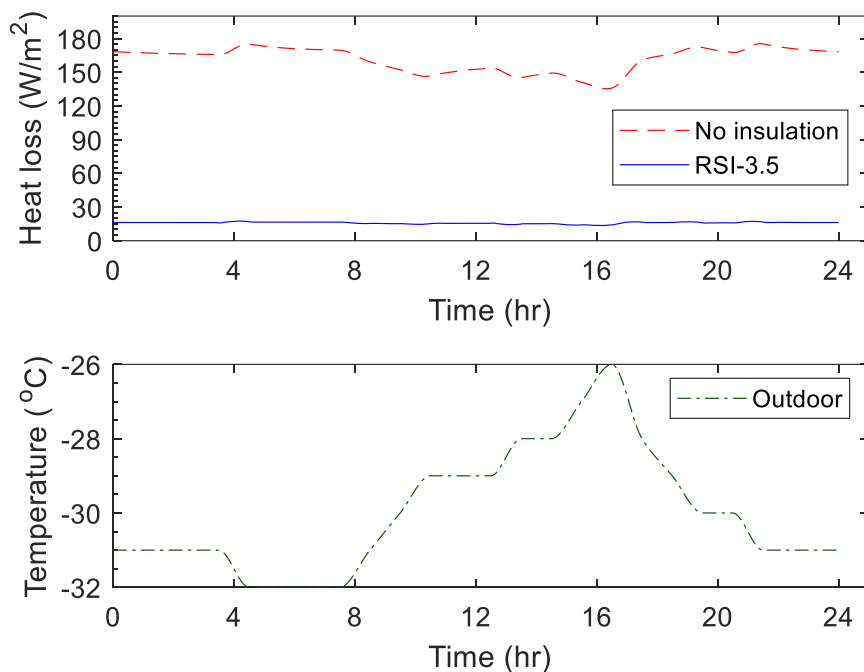


Figure 3.2 Heat loss values for VBW

As shown in Figure 3.2, utilizing extremely low outdoor temperature, and maintaining a constant indoor temperature of 21°C maximize the heat loss. It can be observed that, at any given point during the day, the heat loss for an uninsulated wall is nearly 90% greater than that for an insulated one. In other words, by meeting the minimum overall thermal resistance recommended by NECB, 90% of heat loss can be saved. This means that the exterior insulated

VBW loses only 10% of the heat in the zone, which refers to the “heat loss percentage” in this study. When evaluating typical-day performance in thermal models, it is assumed that the back of the VBW is adiabatic and a heat loss percentage (i.e., 10%) is applied to the total energy exchange results. However, for annual energy analysis, the exterior wall is not assumed to be adiabatic, and its behavior is influenced by outdoor temperature fluctuations.

The calculated heat loss percentage factor of 10% in the typical-day performance analysis is notably conservative, resulting in the lowest wall performance observed throughout the day. This conservative estimate is primarily due to the consideration of an exceptionally low outdoor temperature range for a day, as illustrated in Figure 3.2. By adopting such an approach, the study aims to provide a comprehensive understanding of wall performance under extreme conditions, thereby offering a more rigorous evaluation of the wall systems' potential in cold-climate buildings throughout the year without considering numerous scenarios for outdoor conditions.

b) Interior wall

As an interior wall, VBW is exposed to the same temperature on both sides throughout the day. Similar to exterior wall, air speeds of 0 m/s, 1 m/s, and 2 m/s and; minimum zone temperature of 20°C and peak zone temperatures of 22°C, 24°C, and 26°C (as shown in Figure 3.3) were selected for the sensitivity analysis.

3.3.1.1.2 Zone temperature profiles

The thermal performance of a VBW is greatly impacted by its zone temperature profile. To provide a satisfactory level of thermal comfort, various organizations have established minimum and maximum zone temperatures for residential buildings. For this study, Canada was selected as the benchmark country and the temperature range for the zone was set to be between 20°C and 26°C [51, 52, 85-87]. A sensitivity analysis of VBW performance was

conducted to assess the impact of diverse zone temperature profiles, utilizing the typical-day methodology. This sensitivity analysis incorporated a minimum zone temperature of 20°C, with peak temperatures set at 22°C, 24°C, and 26°C, respectively. A sensitivity analysis can reveal how well VBW performs in terms of reducing the space thermal loads in different ranges of indoor temperature and air speeds. Variations in outdoor temperature are primarily responsible for indoor temperature swings. Figure 3.3 illustrates the setup of indoor temperature swings according to the typical fluctuation in outdoor temperature throughout the day. The outdoor temperature is generally lower in the late hours of the night until early morning than during the rest of the day. In addition, as a result of solar radiation, the outdoor temperature usually rises from late morning until evening. Therefore, the sensitivity analysis evaluated three indoor temperature profiles to determine the impact of temperature variations within the set limits.

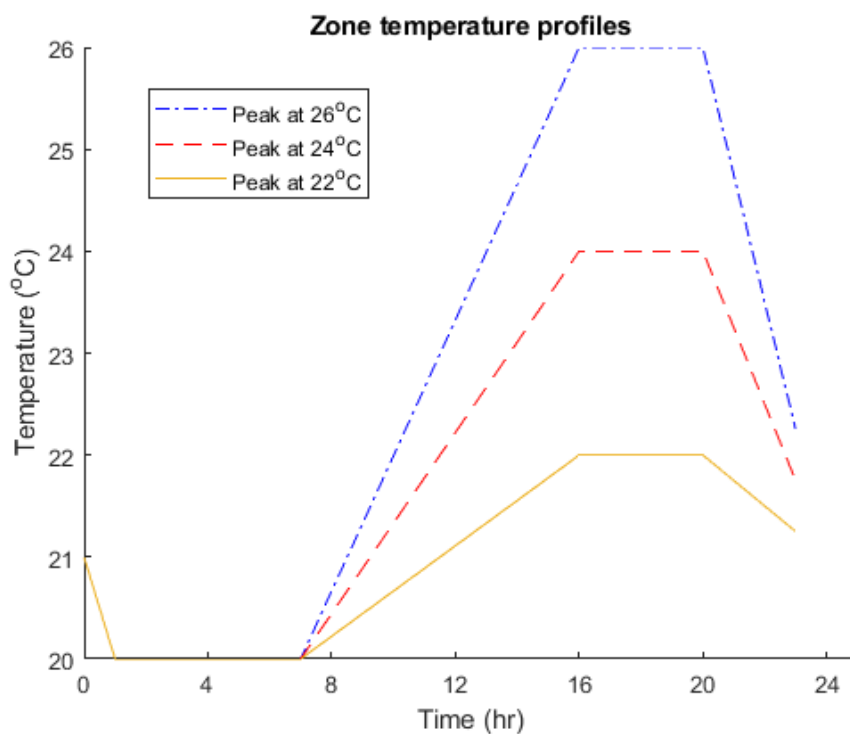


Figure 3.3 Zone temperature profiles for typical-day performance (a cyclic temperature profile with a 24-hr cycle)

3.3.1.2 Annual energy analysis

The annual energy analysis aims to quantify and compare the yearly impacts of VBW and traditional wood-frame walls on space heating and cooling loads over the course of a year. In order to evaluate the thermal performance of a VBW versus a traditional wood-frame wall, two indicators of performance were introduced: assisting heating and assisting cooling. These measures refer to the amount of thermal energy stored in each wall that contributes to reduced space heating and cooling needed over the course of a year. [Appendix B](#) provides more details about the modelled wood-frame wall.

The yearly performance of the two wall systems is simulated under a close-to-actual zone temperature profile and actual outdoor environmental conditions. Table 3.2 outlines the criteria utilized to determine the assisting heating and cooling energy (kWh/m² of the wall) for both walls. Notably, one scenario was considered for assisting heating, while two scenarios were used for assisting cooling.

Table 3.2 Criteria used for calculating the assisting heating and cooling energy

Scenario	Criteria
Heating (H)	$T_{\text{outside}} < T_{\text{air}}$
	$T_{\text{wall}} > T_{\text{air}}$
Cooling – scenario 1 (C #1)	$T_{\text{outside}} > T_{\text{air}}$
	$T_{\text{wall}} < T_{\text{air}}$
Cooling – scenario 2 (C #2)	$T_{\text{outside}} > T_{\text{air}}$
	$T_{\text{wall}} < T_{\text{air}}$
	$20 < T_{\text{outside}} < T_{\text{air}}$
	$T_{\text{wall}} < T_{\text{air}}$

For outdoor environmental conditions, three Canadian cities - Edmonton, Vancouver, and Toronto - were selected to consider the variations in conditions across different climate regions in Canada. The annual energy analysis employs typical meteorological year (TMY) data from 1996 to 2015. TMY is a compilation of selected meteorological data for a specific location over the course of one year.

Zone temperature greatly affects the thermal behavior of wall systems. The zone temperature at any time depends on the zone temperature at the preceding time. In addition to zone temperature, outdoor temperature and solar radiation have a continuous influence on the temperature of a zone. Conducting whole building thermal simulations can yield zone temperature profiles and related wall performance data. However, this approach is limited to the specific building characteristics chosen (e.g., physical construction, room temperature settings, and wall placement) as well as the prevailing climate conditions. To overcome this limitation, this study aims to establish a performance envelope for VBW and wood-frame walls using a parametric analysis. By incorporating zone temperature as one of the parameters, the study bypasses the need for time-consuming whole-building thermal simulations. Estimating wall performance across a spectrum of outdoor and zone temperatures allows for interpretation and application to a wider array of zone conditions. To obtain a close-to-actual zone temperature profile under varying outdoor conditions, the measured outdoor temperature and GHI data for the EcoTerra house (located in Eastman, QC, Canada) [88] were used to develop a prediction function Eq. (3.1) for zone temperature.

$$T_{air}^t = (0.72 * T_{air}^{t-1}) + (0.03 * T_{outside}^{t-1}) + (0.0005 * GHI^{t-1}) + (0.01 * T_{outside}^t) + (0.0004 * GHI^t) + 6.4 ; 20 \leq T_{air}^t \leq 26 \quad (3.1)$$

where T_{air}^t is the zone temperature in the current timestep (10 minutes in this study) in °C, T_{air}^{t-1} denotes the zone temperature in the past timestep, GHI^t and GHI^{t-1} stand for the global horizontal irradiance in the current and past timesteps in W/m^2 , respectively, and $T_{outside}^t$ and $T_{outside}^{t-1}$ is the outdoor temperature in the current and past timesteps in °C, respectively.

Based on Eq. (3.1), the indoor temperature data in the current timestep were chosen as the dependent variable, while the indoor temperature in the past timestep, outdoor temperature in the current and past timestep, and also GHI in the current and past timestep, were considered as independent variables. Moreover, the impact of outdoor temperature and solar radiation in the current timestep has been considered in order to minimize the response delay in the predicted temperature.

The goodness of fit was assessed by calculating the R-square parameter, which indicates how well independent variables explain variations in dependent variable. An R-square of 0.952 was obtained for the comparison between the measured (from EcoTerra house) and predicted indoor temperature, implicating that the proposed function can predict the indoor temperature with an acceptable level of accuracy. The comparison between the predicted indoor temperatures and the actual indoor measurements at EcoTerra house for selected days is shown in [Appendix C](#).

This prediction function is used to predict the temperature of a zone located in the three chosen climates/cities with corresponding meteorological data. EcoTerra serves as an exemplary case study due to its combination of heavy thermal mass and wood-frame walls within the same structure. This coexistence of both wall systems allows for a direct comparison of their performance under the same conditions, making the analysis more accurate and reliable. Using actual data from the EcoTerra house enhances the accuracy of predicted zone temperature at any given time, which not only increases the reliability of the performance

analysis but also bolsters the robustness and relevance of our study in understanding the real-world implications of these wall systems.

3.3.2. Numerical model

As shown in Figure 3.1, thermal models are developed for a wall strip (i.e., one block width with a 2.47 m height) using the following assumptions and considerations for boundary conditions and heat transfer equations.

3.3.2.1. Heat transfer equations

Figure 3.4 illustrates a schematic cross-section of the air channel, displaying all of the involved heat transfer mechanisms. As depicted in Figure 3.4, heat is transferred between the air inside the channel and the surrounding wall via convection. Heat is also transferred between the wall nodes facing each other in the channel through radiation. Additionally, the air returning to the zone exchanges heat with the zone air through advection. Advection is a type of convection heat transfer mechanism resulting from the intensive bulk movement of air. The zone also conducts heat transfer with the wall surface through both convection and radiation.

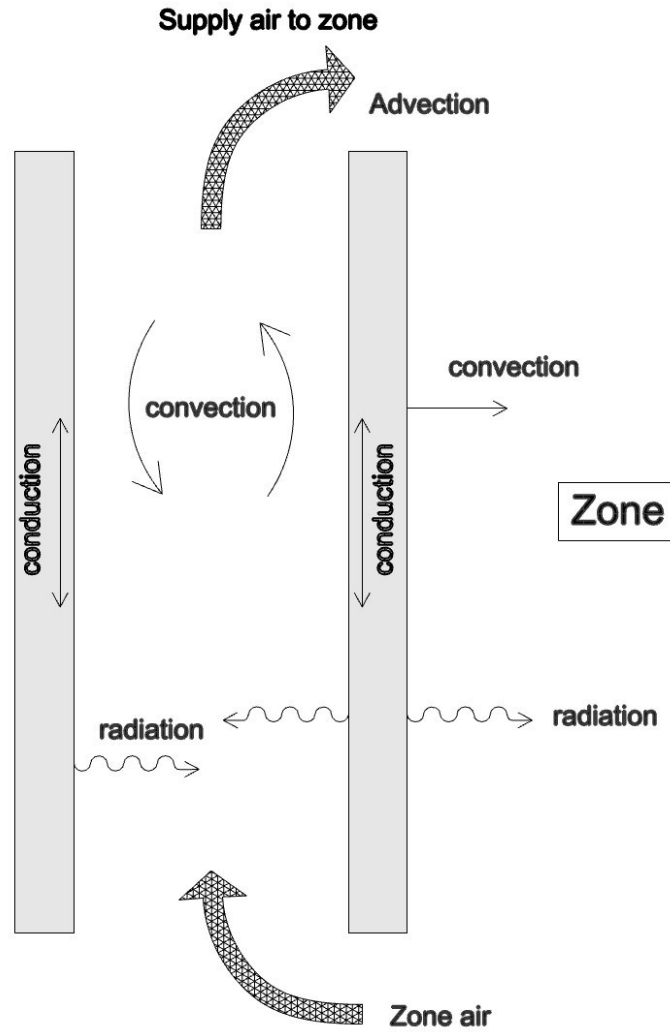


Figure 3.4 Heat transfer mechanisms in VBW

3.3.2.1.1. Heat transfer inside the air channel

The temperature of air inside the channel can be determined by solving Eq. (3.2).

$$(\rho C_p)_{\text{air}}(A_{AC}\Delta y) \frac{dT_{AC}^f}{dt} = \sum_m (h_{\text{air}} \mathcal{L}^{i,j,k} \Delta y (T_{\text{wall}}^{i,j,k} - T_{AC}^f)) - \dot{m} C_{p_{\text{air}}} (T_{AC}^f - T_{AC}^{f-1}) \quad (3.2)$$

$$f = 1, 2, 3, \dots, n_{\text{air}}$$

In Eq. (3.2), ρ_{air} and $C_{p_{\text{air}}}$ represent the density and specific heat capacity of the air inside the channel, respectively. A_{AC} and Δy are the cross-sectional area of the air channel and the height

of each control volume (CV) that corresponds to node f , respectively. The indices i, j, k and f denote the node counters for the wall in three directions (corresponding to $\Delta x, \Delta y, \Delta z$) and for the air within the channel. In Eq. (3.2), i, j, k are the node coordinates of the wall that is in contact with the node f of the air. Furthermore, the summation index m refers to the number of wall nodes surrounding the air node. $T_{\text{wall}}, T_{\text{AC}}, \dot{m}, h_{\text{air}}$, and \mathcal{L} denote the wall temperature, air temperature inside the channel, air mass flow rate, the convective heat transfer coefficient of the air inside the channel, and the length of each CV (either in Δx direction or Δz direction) in contact with node f of air inside the channel, respectively. h_{air} can be determined using Eq. (3.3).

$$h_{\text{air}} = \frac{Nu \times \lambda_{\text{air}}}{D_h} \quad (3.3)$$

where $D_h, \lambda_{\text{air}}$ and Nu are hydraulic diameter, air thermal conductivity and Nusselt number, respectively. The Nusselt number can vary depending on the flow regime (i.e., laminar, or turbulent). Eqs. (3.4) and (3.5) determine the Nusselt number [89].

$$Nu = 4.364 \text{ (Laminar flow; } Re_D \leq 2300) \quad (3.4)$$

$$Nu = \frac{\frac{F_{fr}(Re-1000)Pr}{8}}{1+12.7\left(\frac{F_{fr}}{8}\right)^{0.5} (Pr^{2/3}-1)} \text{ (Turbulent flow; } 3000 \leq Re_D \leq 5 \times 10^6 \text{ \& } 0.5 \leq Pr \leq 2000) \quad (3.5)$$

Re represents the Reynolds number, Pr denotes the Prandtl number, and F_{fr} is the friction factor. Eqs. (3.6) to (3.8) can be used to calculate Re, Pr , and F_{fr} [89, 90].

$$Re_D = \frac{v \times D_h}{\vartheta} \quad (3.6)$$

$$Pr = \frac{\vartheta}{\lambda_{\text{air}} / (\rho C_p)_{\text{air}}} \quad (3.7)$$

$$\frac{1}{\sqrt{F_{fr}}} = -2\log\left(\frac{\epsilon}{3.7D_h} + \frac{2.51}{Re_D\sqrt{F_{fr}}}\right) \quad (3.8)$$

where v is the air speed, ϑ is the kinematic viscosity, and ϵ is the roughness which was set at 0.3 mm [91].

3.3.2.1.2. Heat transfer between wall nodes

Figure 3.5 illustrates a schematic of the block, showing its dimensions, discretization, and nodes.

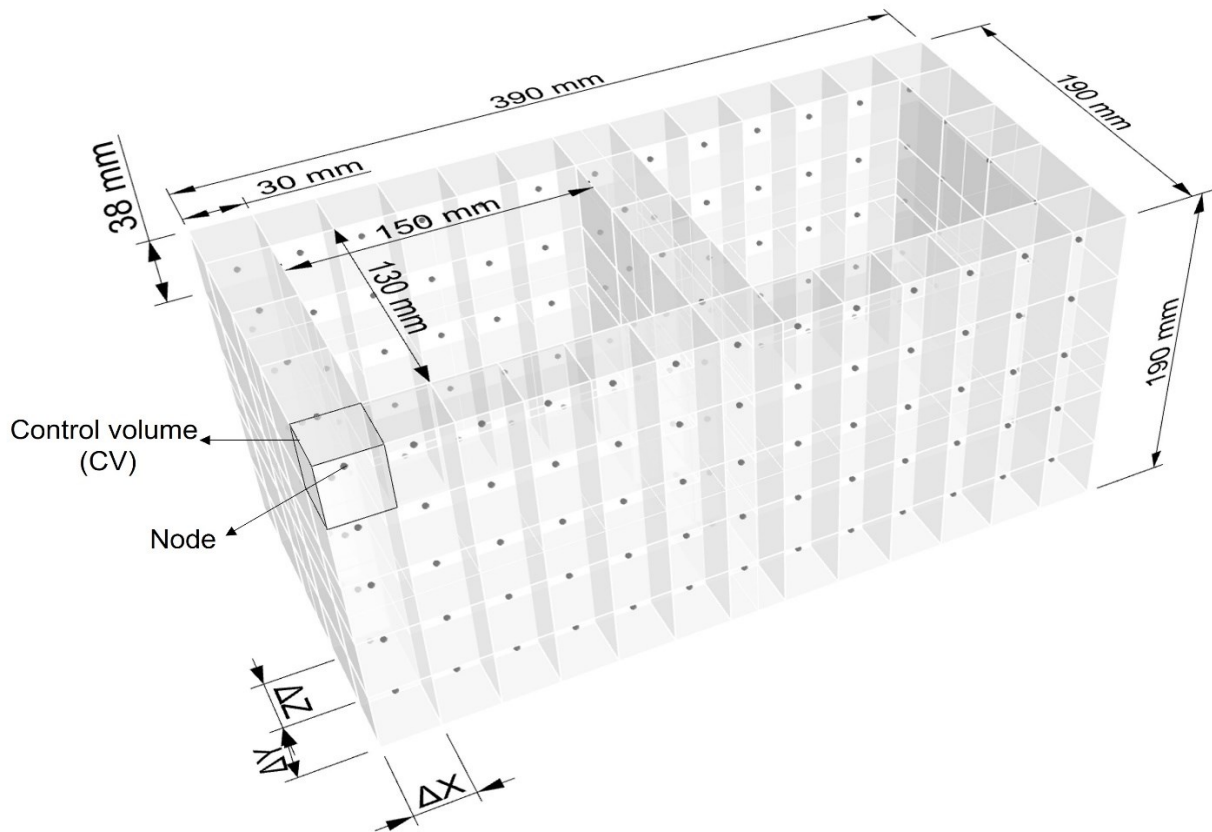


Figure 3.5 A schematic of the block dimensions, discretization, and nodes

As shown in Figure 3.5, the block is discretized equally in three directions with nodes spaced by 30 mm in x-direction and 38 mm for y direction. In the z-direction, the block CVs in the face shells have a width of 30 mm , while the block CVs in contact with air inside the

channel have a width of $\frac{130}{3}$ mm. The discretization of other continuous layers such as the cement plaster and rigid thermal insulation, mirrors that of the block. Also, the dimensions of the block are selected based on those commonly used in construction [81].

Heat transfer between the wall nodes takes place through conduction, convection with the air inside the channel, radiation between wall nodes that are exposed to air and are facing each other, and also the convection heat transfer between the wall surface nodes and the zone air. The latter will be discussed further in [subsection 3.3.2.2.3](#). The overall impact of all input and output heat fluxes continuously alters the temperature of the CVs. The wall temperature at any given location (i.e., nodes) can be determined by using Eq. (3.9) while considering all heat fluxes entering and exiting the CVs.

$$(\rho C p)_{wall} V_{wall} \frac{dT_{wall}^{i,j,k}}{dt} = Q_{conduction}^{i,j,k} + Q_{convection}^{i,j,k} + Q_{radiation}^{i,j,k} + Q_{surface}^{i,j,k} \quad (3.9)$$

where V_{wall} represents the volume of each CV, $\Delta x, \Delta y, \Delta z$ are length, height, and width of the CVs as shown in Figure 3.5, $Q_{convection}$ is the exchanged heat flow rate between air inside the channel and surrounding wall nodes, $Q_{surface}$ denotes the heat flow rate from the zone towards the nodes on the wall surface, $Q_{radiation}$ is the radiation heat flow rate between two facing wall nodes in contact with air, and $Q_{conduction}$ represents the conduction heat flow rate between the wall nodes, which can be calculated using Eq. (3.10).

$$Q_{conduction}^{i,j,k} = \lambda_{wall} \times \left\{ \begin{array}{l} \frac{\Delta z \Delta y}{\Delta x} (T_{wall}^{i+1,j,k} + T_{wall}^{i-1,j,k} - 2T_{wall}^{i,j,k}) \\ + \frac{\Delta z \Delta x}{\Delta y} (T_{wall}^{i,j+1,k} + T_{wall}^{i,j-1,k} - 2T_{wall}^{i,j,k}) \\ + \frac{\Delta y \Delta x}{\Delta z} (T_{wall}^{i,j,k+1} + T_{wall}^{i,j,k-1} - 2T_{wall}^{i,j,k}) \end{array} \right\} \quad (3.10)$$

$Q_{convection}$ and $Q_{radiation}$ can be calculated using Eq. (3.11) and Eq. (3.12), respectively.

$$Q_{convection}^{i,j,k} = h_{air} \mathcal{L}^{i,j,k} \Delta y (T_{wall}^{i,j,k} - T_{air}^f) \quad (3.11)$$

$$Q_{radiation}^{i,j,k} = \sigma \Delta y \mathcal{L}^{i,j,k} F_v F_\varepsilon (T_{wall}^4 - T'_{wall}{}^4) \quad (3.12)$$

where σ is the Stephan-Boltzmann constant (i.e., $5.67 \times 10^{-8} \text{ W/m}^2 \cdot \text{K}^4$) and F_ε is the emissivity factor (i.e., $F_\varepsilon = \frac{1}{\frac{2}{\varepsilon} - 1}$ for $\varepsilon = 0.85$). $(T_{wall} - T'_{wall})$ is the difference between average temperature of every two facing and adjacent interior surfaces of the channel for every Δy (i.e., 38 mm). In simpler terms, the nodes on each interior surface of the air channel, consisting of three nodes in the Δz direction and five nodes in the Δx direction, are combined with their corresponding Δy values to form a single surface. The average temperature of this surface is then calculated for further analysis of radiation heat transfer. F_v represents the view factor between each pair of channel interior surfaces (facing and adjacent) for every Δy [89, 92]. The view factor between two facing surfaces in the channel can be obtained using Eq. (3.13) [89].

$$\mathcal{F}_{facing} = \frac{2}{\pi \bar{X} \bar{Y}} \left\{ \ln \left[\frac{(1+\bar{X}^2)(1+\bar{Y}^2)}{1+\bar{X}^2+\bar{Y}^2} \right]^{0.5} + \bar{X}(1+\bar{Y}^2)^{0.5} \tan^{-1} \frac{\bar{X}}{(1+\bar{Y}^2)^{0.5}} + \bar{Y}(1+\bar{X}^2)^{0.5} \tan^{-1} \frac{\bar{Y}}{(1+\bar{X}^2)^{0.5}} - \bar{X} \tan^{-1} \bar{X} - \bar{Y} \tan^{-1} \bar{Y} \right\} \quad (3.13)$$

$$\bar{X} = \frac{\Delta y}{d}, \bar{Y} = \frac{W_s}{d}$$

where d is the perpendicular distance between two facing surfaces of the air channel either in length (Δx) or width (Δz) direction, and W_s denotes the width of each surface. The view factor for the adjacent surfaces can be determined using Eq. (3.14).

$$\mathcal{F}_{v-adjacent} = \frac{1 - \mathcal{F}_{v-facing}}{2} \quad (3.14)$$

3.3.2.1.3. Heat transfer between the wall and zone air

Two mechanisms are involved for the heat transfer between wall and zone air: a) convection and radiation through the wall surface, b) advection through the SAZ. Eq. (3.15) can be used to determine the heat transfer between the wall surface and the zone air.

$$Q_{surface}^{i,j,k} = h_{total} \times \Delta y \times \Delta x (T_{wall}^{i,j,k} - T_{air}) \quad (3.15)$$

T_{air} is the zone temperature and h_{total} is heat transfer film coefficient (combined convective and radiant heat transfer) between the wall surface and the zone air and other interior zone surfaces. The value for h_{total} can be obtained by solving Eq. (3.16) or Eq. (3.17) depending on the Rayleigh number [83].

$$h_{total} = 1.33 \left(\frac{|T_{air} - T_{wall}|}{H} \right)^{0.25} + 5.5 \quad 10^5 < Ra < 10^9 \quad (3.16)$$

$$h_{total} = 1.26 |T_{air} - T_{wall}| + 5.5 \quad Ra > 10^9 \quad (3.17)$$

In both Eqs. 3.13 and 3.14, the first term represents the convective heat transfer coefficient, while the constant term represents the radiative heat transfer coefficient [17, 93, 94]. H is the wall height and Ra is the Rayleigh number which can be calculated using Eq. (3.18).

$$Ra = GrPr \quad (3.18)$$

Gr is the Grashof number. Eq. (3.19) can be used to determine the Gr .

$$Gr = \frac{g\beta|T_{air} - T_{wall}|H^3}{(\rho\nu)^2} \quad (3.19)$$

where g and β are the gravitational acceleration and thermal expansion coefficients, respectively. Along with convection and radiation, wall and zone also exchange heat through advection. Eq. (3.20) can be used to determine the heat transfer between SAZ and zone air.

$$Q_{advection} = \dot{m}Cp_{air}(T_{AC}^{f,end} - T_{air}) \quad (3.20)$$

where $T_{AC}^{f,end}$ is the air temperature at the outlet of the air channel.

3.3.3. Air speed

A major factor influencing the thermal performance of VBW is the air speed [71]. The literature reports air speed values ranging from 0.2 m/s to 3 m/s for investigating the thermal performance of ventilated walls [71, 73, 95-97]. Nevertheless, each case study requires an

optimum air speed in accordance with the design, the system's energy consumption (e.g., fan), as well as its net energy exchange. To determine the optimal air speed, the "total net energy exchange" was calculated as the difference between total energy exchange from the wall (e.g., sum of the exchanged energy through surface and SAZ) and fan energy consumption in typical-day zone temperature profiles. Eq. (3.21) can be used to obtain the fan energy consumption in a day.

$$E_{fan} = \Delta P \times v \times A_{AC} \times (24/1000) \quad (3.21)$$

where E_{fan} is the fan energy consumption in kWh, v denotes the air speed in m/s and ΔP is the total pressure loss caused by the fan in Pa. ΔP can be obtained using Eq. (3.22) (*Darcy-Weisbach equation*) [98].

$$\Delta P = \frac{f \times L}{2D_h} \rho v^2 \quad (3.22)$$

Different ΔP and net energy exchange values are calculated for air speeds ranging from 0.2 m/s to 5 m/s. Figure 3.6 shows the changes in ΔP and net energy exchange based on the different air speeds for a one wall strip.

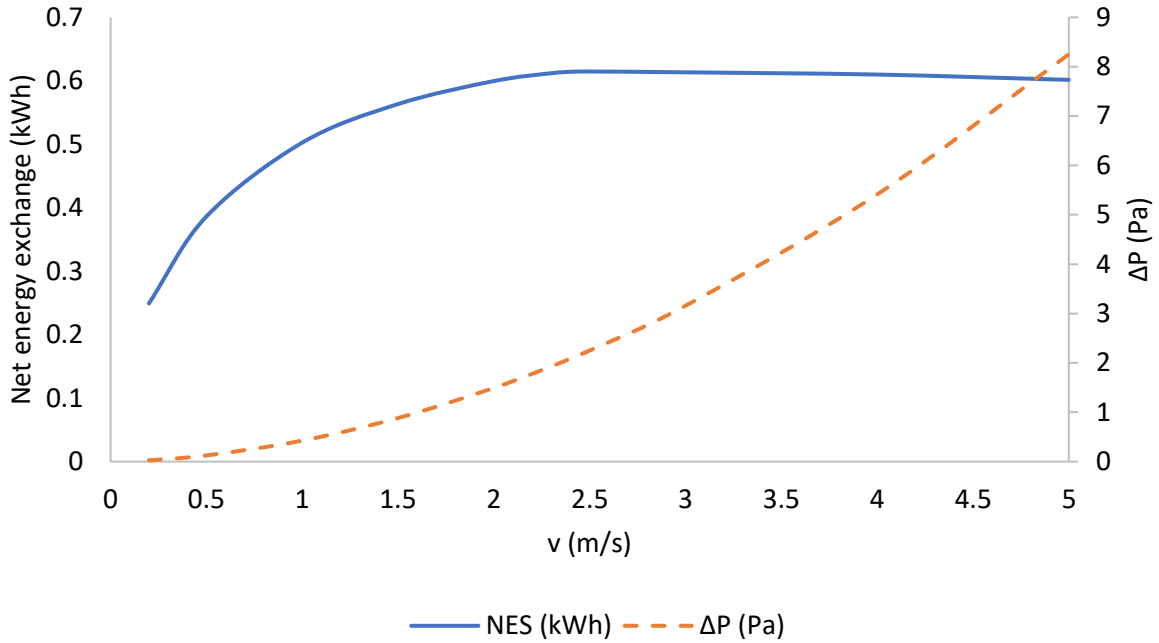


Figure 3.6 Net energy exchange and pressure changes

Figure 3.6 depicts that as air speed increased from 0.2 m/s to 2.5 m/s, the net energy exchange values also increased. However, for speeds above 2.5 m/s, net energy exchange decreased as the rate of fan energy consumption exceeded the rate of energy exchange. Therefore, in order to obtain the maximum net energy exchange, the optimal air speed was determined to be 2.5 m/s. Despite that, simulations were carried out using air speeds of 0 m/s (i.e., passive performance), 1 m/s, and 2 m/s for the parametric analysis. 2 m/s instead of 2.5 m/s was examined because the actual pressure loss caused by the fan is usually higher than the calculated amount, mostly as a result of the inlet and outlet covers of the channel, as well as the manifold, valves, and elbows in the system.

The air speed in the channel may change depending on the temperature difference between the air at the channel's inlet and outlet. Such variations are caused by changes in air density resulting from alterations in air temperature. Based on the fact that the maximum temperature difference between the inlet and outlet is only $\sim 1.7^{\circ}\text{C}$, resulting in a less than 1% change in air density from inlet to outlet [83], the study assumed that the volumetric flow rate within the

channel remains constant and that the air speed is not affected by such changes in air density from inlet to outlet.

3.3.4. Model validation

Yu et al. [73] investigated the thermal performance of a VBW. Heated by an external source, warm air with a fixed inlet temperature and a fixed speed, was introduced into hollow-core concrete blocks that were lined up to form serpentine air channels. The wall was ventilated every day between 9 a.m. and 5 p.m. For the remainder of the day, the wall worked naturally. An air conditioner maintained a constant temperature between 17°C and 18°C in the zone, although outdoor temperature fluctuations caused variations in the zone temperature. For validation purposes in this study, the developed numerical model is modified according to the parameters used in the experimental study. Main parameters include the supply air temperature, supply air speed, fixed zone temperature, ventilation period (i.e., when air circulation is active and when it is turned off), concrete block dimensions, wall area, and thermal properties of the wall. Furthermore, to represent the error between measured and simulated values, the coefficient variation of the root-mean square error (CV-RMSE) statistical measure is selected. CV-RMSE can be calculated using Eq. (3.23) [57].

$$CV - RMSE = \frac{\sqrt{\frac{\sum_{i=1}^n (y_i - \hat{y}_i)^2}{n}}}{\bar{y}} \quad (3.23)$$

where n is the number of data points; y_i is the measured value; \hat{y}_i is the simulated value; and \bar{y} is the average of all measured values.

Figure 3.7 illustrates the simulated and measured average wall surface temperature profiles over the 24-hour period. As shown in Figure 3.7, the simulated wall temperature closely followed the trend of measured wall surface temperature. However, some deviations of up to 0.45°C were observed, particularly between 10 a.m. and 4 p.m. These deviations could be caused by variations in the temperatures and speed of supply air and the zone temperature.

It is indicated by the CV-RMSE of 1.175% when comparing the model's simulated data (red line in Figure 3.7) to the actual measured data (blue dotted line in Figure 3.7) from the experiment. The comparison indicates that the numerical model developed in this study has sufficient accuracy for simulating the thermal performance of the VBW of interest.

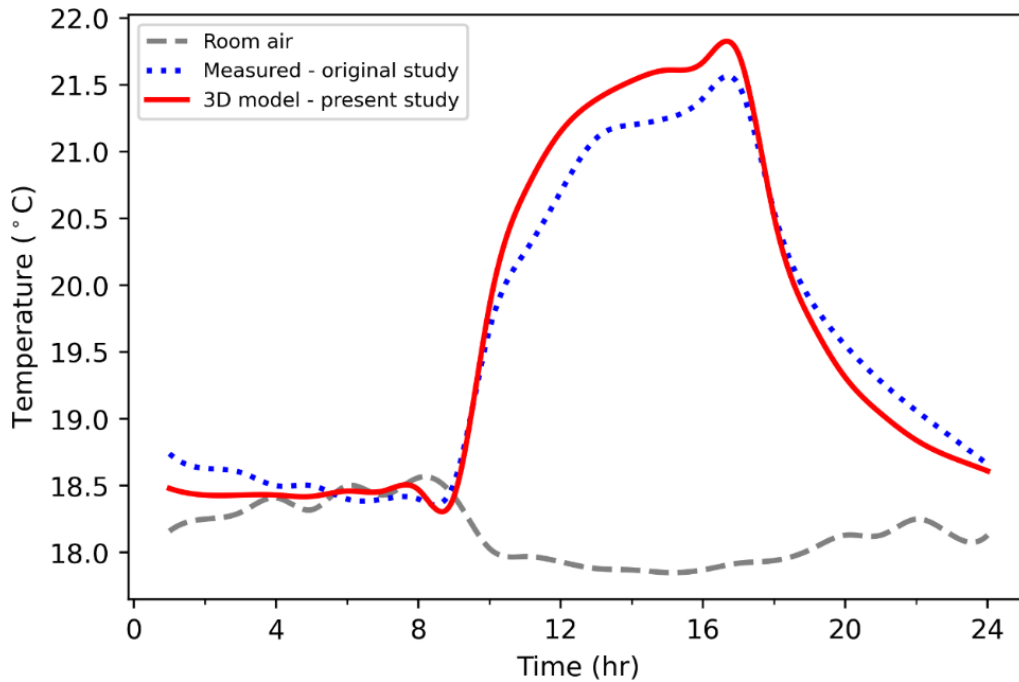


Figure 3.7 Measured and simulated average wall surface temperatures

3.4. Results and discussion

a) Typical-day thermal performance of a VBW; This part presents the average wall surface temperature, the heat flux density, and the total net energy exchange based on the following boundary conditions and parameters:

- i. Exterior and interior walls
- ii. Air speeds of 0 m/s, 1 m/s and 2 m/s
- iii. Different zone temperature profiles

In this part, the figures and descriptions are presented for a single zone temperature profile (minimum of 20°C and maximum of 26°C), an air speed of 2 m/s, and one wall strip. Results for other scenarios are tabulated in their respective sections.

b) Annual energy analysis of a VBW and a wood-frame wall for three Canadian cities

In this part, the energy performance of both exterior VBW and exterior wood-frame wall was compared over the course of a year, with a focus on the cold climate of Canada. Specifically, the results and descriptions in this annual energy analysis pertain to the city of Edmonton. Results for other Canadian cities such as Vancouver and Toronto can be found in [Appendix D](#).

3.4.1. *Typical-day thermal performance of VBW*

3.4.1.1. Exterior wall

3.4.1.1.1. Average wall surface temperature

Air speed and zone air temperature fluctuations have a significant impact on average wall surface temperature. In this study, as well as throughout the paper, the term "zone air temperature" is used based on the assumption that the room air temperature and the interior surfaces are at the same temperature. This assumption allows for treating the entire zone as having a single, consistent temperature, which is referred to as the zone air temperature. At an air speed of 2 m/s, Figure 3.8 illustrates the changes in zone air temperature and average wall surface temperature.

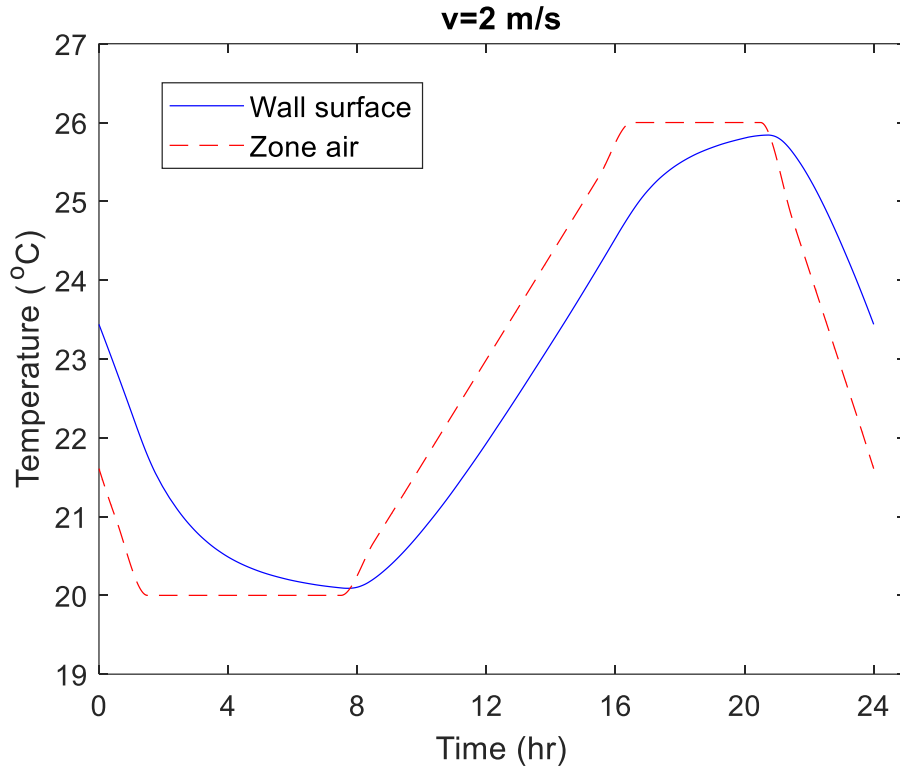


Figure 3.8 Zone air and average wall surface temperatures for an exterior VBW

In situations of strong heat exchange between the mass and the zone, the wall surface temperature closely follows the fluctuations in the zone air temperature. This is because the air inside the channel constantly transfers heat between the inner mass of the VBW and the zone. In the case of a wall that is warmer than the zone, as shown in Figure 3.8 (early in the morning and late at night), the circulating air takes heat from the mass and releases it to the zone. Rapid heat exchange occurs continuously between the wall and zone air, causing the wall temperature to decrease during the following hours, following the zone temperature. The larger difference between the minimum and maximum temperature of the wall indicates more thermal energy storage in the wall and effective heat exchange between the wall and the zone. As a result, more space heating and cooling load can be reduced and more stable zone temperature. Similarly, when a wall is colder than a zone (from morning to evening in Figure 3.8), the process is reversed. In contrast to significant swings in zone air temperature, a situation with insufficient

heat exchange will result in a smaller difference between the maximum and minimum wall temperatures. Therefore, the wall is unable to moderate the zone temperature effectively [16]. The zone temperature is predefined in this typical day analysis. However, the actual zone temperature would be different from the predefined values and be affected by the VBW.

Table 3.3 presents the minimum and maximum average wall interior surface temperatures, as well as the difference between the maximum and minimum wall surface temperature (which refers to ΔT from this point onwards) for different zone temperatures and air speeds.

Table 3.3 Maximum and minimum average wall interior surface temperatures for different zone temperatures and air speeds

Zone temperature (min/max) (°C)	Average wall surface temperature (°C)								
	$v=0$ m/s			$v=1$ m/s			$v=2$ m/s		
	min	max	max-min (ΔT)	min	max	max-min (ΔT)	min	max	max-min (ΔT)
20/26	21.2	24.2	3	20.4	25.5	5.1	20.1	25.9	5.8
20/24	21	23	2	20.3	23.7	3.4	20.2	24	3.8
20/22	20.4	21.6	1.2	20.3	22	1.7	20.2	22	1.8

According to Figure 3.8 and Table 3.3, a higher air speed leads to a stronger heat exchange between the wall and the zone, which results in a better moderation of zone air temperature. This is due to the fact that lower air speed decreases the heat transfer coefficient in the air channel. Thus, less heat is exchanged between the air and the wall, leading to a weak heat exchange between the wall and the zone. Additionally, Table 3.3 shows that a rise in zone peak temperature from 24°C to 26°C causes a 31% increase in ΔT for a fixed air speed. Increasing the air speed from 1 m/s to 2 m/s results in a 11% increase in ΔT for a given zone temperature

profile. Table 3.3 reveals that higher temperature fluctuation within the zone has a greater impact on ΔT than increasing air speed.

3.4.1.1.2. Heat flux density

The heat flux density (q) is defined as the rate of thermal energy (W) exchanged between the VBW and the zone per unit area of the VBW's exposed surface (m^2). A negative heat flux density indicates that the exterior surface or SAZ is cooling the zone at that particular time. In other words, the exterior surface temperature or SAZ temperature is lower than the zone temperature. Figure 3.9 illustrates the heat flux density for an air speed of 2 m/s. In Figure 3.9, "Convection+Radiation" represents the fluctuations in heat flux density between the wall surface and the zone by combining both convection and radiation effects. "Advection" solely shows the heat flux density between the supply air to zone and the zone air.

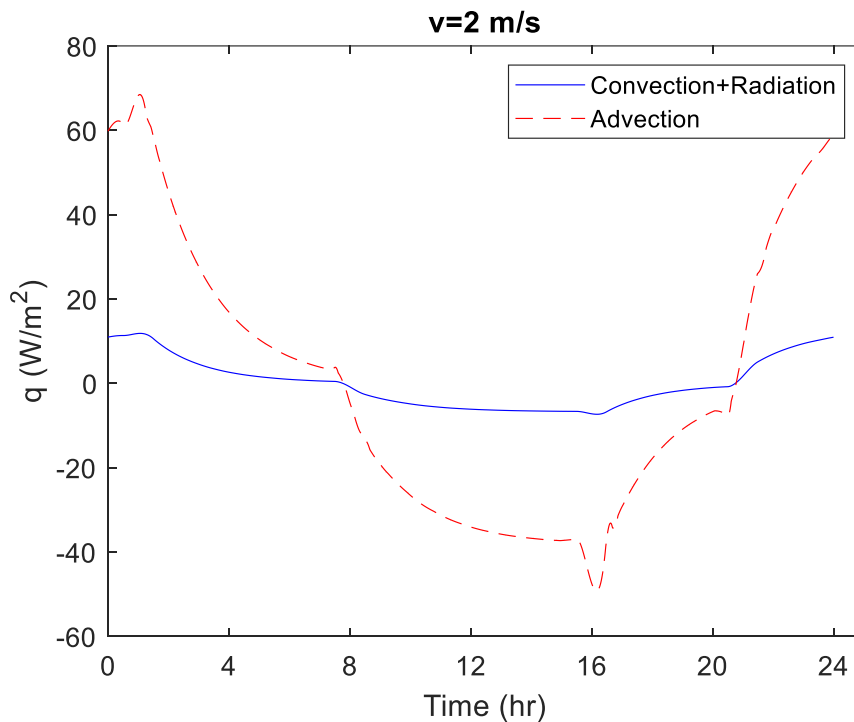


Figure 3.9 Heat flux for an exterior VBW over a 24-hour period

Figure 3.9 indicates that the VBW provides heating to the zone from 12 a.m. to 8 a.m. and also from 9 p.m. to 12 a.m. Cooling contributions were from 8 a.m. to 9 p.m. when the zone

temperature was on the rise. Eqs. (3.15) and (3.20) can be used to determine the heat flux density through the wall surface (i.e., convection and radiation) and the heat flux density through the SAZ (i.e., advection), respectively. Table 3.4 presents the minimum and maximum heat fluxes for different zone temperature profiles and air speeds.

Table 3.4 Heat fluxes for exterior VBW with cement plaster

Zone temperature (min/max) (°C)	Heat transfer mechanism	Heat flux density (min/max) (W/m ²)		
		<i>v</i> =0 m/s	<i>v</i> =1 m/s	<i>v</i> =2 m/s
20/26	Convection & radiation	-14.6/16.3	-9.1/14.1	-6.9/11.1
	Advection	0	-32.6/41.5	-48.6/67.8
20/24	Convection & radiation	-9.6/11.7	-6.1/10.4	-4.3/8.2
	Advection	0	-19.9/40.2	-21.5/52.5
20/22	Convection & radiation	-4.6/7.1	-3.1/6.4	-2.2/5.6
	Advection	0	-10.7/16.7	-16/24.6

Referring to Figure 3.9 and Table 3.4, it can be observed that maximum convection and radiation heat fluxes decrease with increasing air speed. On the other hand, at elevated air speeds, the maximum advection heat flux increases. Increasing the air speed shortens the time duration of heat exchange between the circulation air and the wall, resulting in minimal changes in air temperature. However, higher air speeds significantly enhance the convective heat transfer coefficient within the air channel, resulting in a higher rates heat exchange. When

analyzing the heat flux within the range of 0 m/s to 2 m/s for air speed, it was discovered that at air speeds smaller than 0.3 m/s, convection and radiation are the dominant heat transfer mechanisms when compared to advection.

3.4.1.1.3. Total energy exchange

Total energy exchange is measured as the accumulated heating and cooling energy (kWh) provided to a zone through surface and SAZ per unit area of the VBW's exposed surface (m²) over the course of a 24-hour period. The total energy exchange will include a 10% reduction, which is reflected in the values presented in Table 3.4. For walls with more than one column of blocks (same height of 2.47 m), total energy exchange can be determined by multiplying the results for one wall strip by the desired number of block columns.

Table 3.5 presents the total net energy exchange for different zone temperature profiles and air speeds. The total net energy exchange is calculated by deducting the fan's energy consumption from total energy exchange values.

Table 3.5 Total net energy exchange of the exterior VBW with cement plaster

Zone temperature (min/max) (°C)	Total net energy exchange (kWh/m ²)		
	<i>v</i> =0 m/s	<i>v</i> =1 m/s	<i>v</i> =2 m/s
20/26	0.2	0.49	0.57
20/24	0.13	0.33	0.39
20/22	0.06	0.17	0.21

For any given zone temperature profile, increasing the air speed from 0 m/s to 2 m/s, increased the total net energy exchange by 65%. Furthermore, for any given air speed, increasing the zone peak temperature from 22°C to 26°C, increased thermal energy storage by 67%. These findings demonstrate the significant impact of air speed and zone temperature swings on the total net energy exchange. The results reveal that significant thermal energy storage can be attributed to VBW, which in turn leads to efficient diurnal buffering and balancing of a zone's

heating and cooling loads. This effectiveness is particularly important during the shoulder seasons (e.g., spring and fall) in cold climate regions, when zones are more likely to experience substantial temperature fluctuations. Given these benefits, it is reasonable to infer that VBW can play a crucial role in maintaining comfortable indoor temperatures and reducing the overall thermal loads.

3.4.1.1.4. Impact of interior finishing layer on the thermal performance

Drywall, also known as gypsum board, and cement plaster have been extensively utilized as interior finishes on wall surfaces and studied in the literature [72, 79, 99-101]. Adding a layer on top of the interior surface of the wall has an effect on the rate of heat exchange between the zone air and the wall surface. This section examines the impact of three finishing layers, namely drywall, a thermal insulating material, and cement plaster, on the total net energy exchange between the zone and the exterior VBW. To assess the impact of a finishing layer on the performance of a VBW, simulations were conducted at both passive performance (i.e., $v=0$ m/s) and with an air speed of 2 m/s for all three typical-day zone air temperature profiles. Table 3.5 showed the simulation results of total net energy exchange for the VBW with cement plaster as the interior finishing layer.

Under passive performance, replacing cement plaster with drywall reduced total net energy exchange between the wall and the zone air by an average of approximately 16% across all zone air temperature profiles. When cement plaster layer was replaced by a layer of thermal insulation, total net energy exchange decreased by 45%. This roots in the fact that cement plaster has a higher thermal conductivity than other two materials, allowing it to transfer heat more efficiently through its surface, thereby facilitating better heat exchange between the wall surface and zone air throughout the day. When ventilation is turned on, the contribution of the exposed wall surface decreases. At an air speed of 2 m/s, replacing cement plaster with drywall and thermal insulation decreased total net energy exchange by an average of 10% and 16%,

respectively, across all zone air temperature profiles. Therefore, the influence of the finishing layer on energy exchange values decreases with increasing air speed. [Appendix E](#) presents the tabulated simulation results for the exterior VBW when drywall is used as the interior finishing layer.

3.4.1.2. Interior wall

3.4.1.2.1. Average wall surface temperature

As an interior wall, both sides of the VBW are exposed to the same zone temperature profile. Figure 3.10 shows changes in average wall surface temperature for an air speed of 2 m/s.

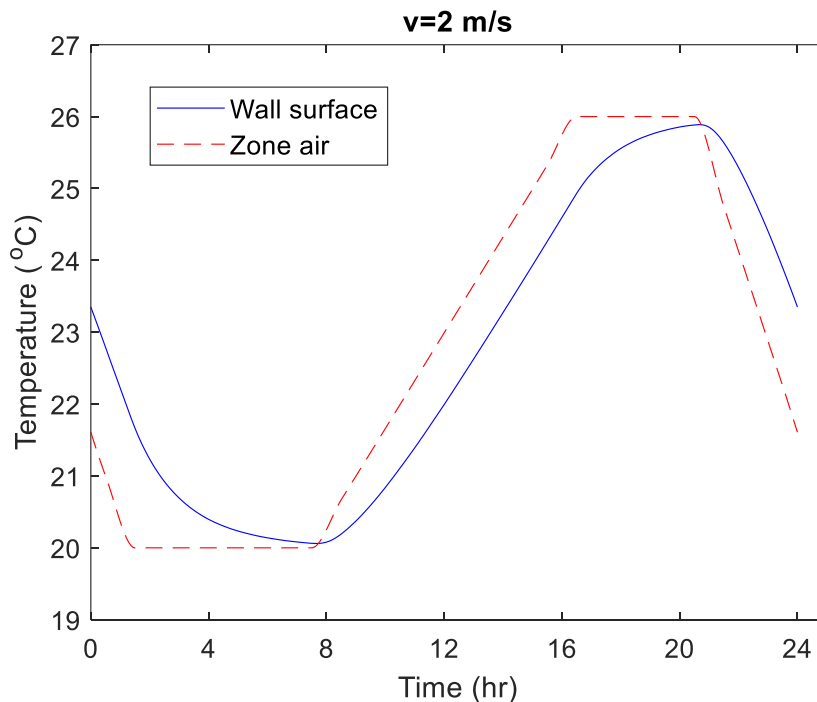


Figure 3.10 Zone air and average wall surface temperatures for an interior VBW

Table 3.6 presents the minimum and maximum interior wall surface temperatures, as well as the difference between the maximum and minimum (ΔT) for different zone temperatures and air speeds.

Table 3.6 Maximum and minimum average wall interior surface temperatures for different zone temperatures and air speeds

Zone temperature (min/max) (°C)	Average wall surface temperature (°C)								
	<i>v</i> =0 m/s			<i>v</i> =1 m/s			<i>v</i> =2 m/s		
	min	max	max- min (ΔT)	min	max	max- min (ΔT)	min	max	max- min (ΔT)
20/26	20.93	24.83	3.7	20.26	25.63	5.2	20.05	25.95	5.9
20/24	20.67	23.19	2.4	20.18	23.75	3.5	20.07	23.87	3.9
20/22	20.41	21.6	1.3	20.12	21.88	1.8	20.05	21.94	1.9

According to Figure 3.10 and Table 3.6, in an interior VBW, a greater ΔT was observed compared to an exterior VBW. This can be explained by the higher rates of convection and radiation through the surface. The increased exposed wall surface resulted in a stronger heat exchange between the wall and the zone.

3.4.1.2.2. Heat flux density

Figure 3.11 illustrates the change in heat flux density for an air speed of 2 m/s. The exposed surface area of an interior wall would be double that of an exterior wall, since the interior wall is exposed to the surrounding zone from two sides.

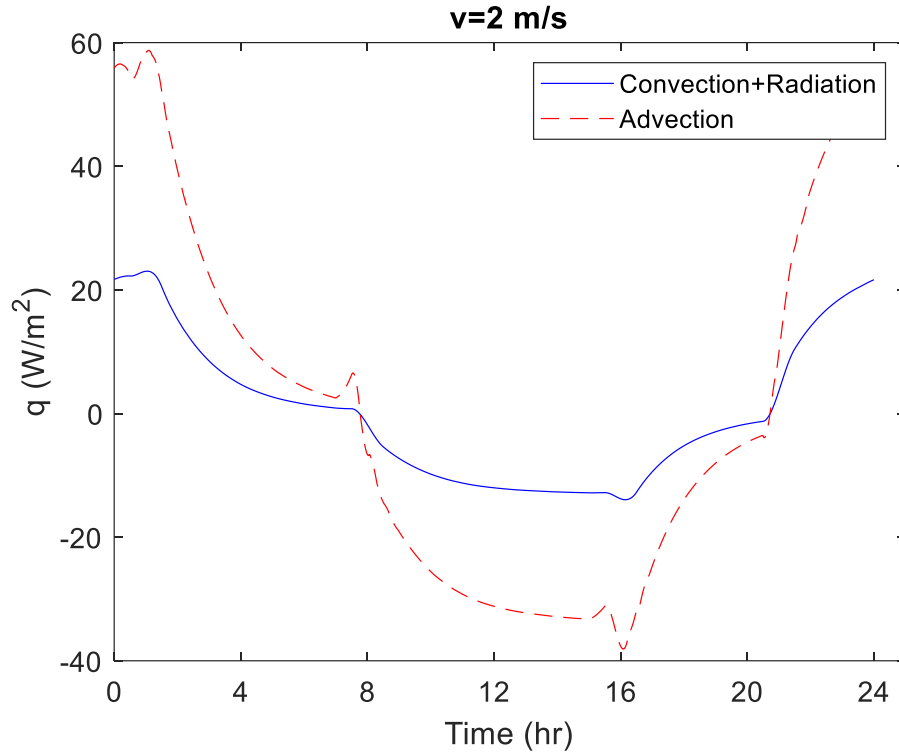


Figure 3.11 Heat flux changes for an interior VBW over a 24-hour period

Table 3.7 presents the minimum and maximum heat fluxes for different zone temperature profiles and air speeds.

Table 3.7 Heat fluxes for interior VBW with cement plaster

Zone temperature (min/max) (°C)	Heat transfer mechanism	Heat flux density (min/max) (W/m ²)		
		<i>v</i> =0 m/s	<i>v</i> =1 m/s	<i>v</i> =2 m/s
20/26	Convection & radiation	-30.6/38.9	-19/28.9	-14.4/23.9
	Advection	0	-34/35.6	-39.5/60
20/24	Convection & radiation	-20.3/27.3	-12.4/20.7	-9/16.9
	Advection	0	-20/25.6	-21.7/46.7
20/22	Convection & radiation	-10.5/15.3	-5.9/13.1	-4.6/11.5
	Advection	0	-8.5/16.7	-14.3/24.9

Interior walls are more affected by convection and radiation when it comes to heating and cooling, compared to exterior walls. Having analyzed the simulation results for heat flux density, convection and radiation have a greater contribution to the overall heat flux to the zone than advection, when air speed is less than 0.8 m/s. This is attributed to the fact that both surfaces of the interior wall are exposed to the Zone air. This causes the convection and radiation heat fluxes to increase significantly, making them the dominant heat transfer mechanisms over advection. However, when air speed exceeds 0.8 m/s, advection's share of the total heat flux becomes greater than that of convection and radiation. Additionally, regardless of air speed, the wall continues to provide heat to the zone until 8 a.m. when the zone temperature is kept at 20°C. Also, the wall continues to deliver cooling energy to the zone until 8-9 p.m. as the temperature within the zone rises to 26°C. There is a small heating contribution from the wall in the late night as the zone temperature decreases. For all zone temperature profiles, as the air speed increases, the advection heat flux increases while the convection and radiation heat fluxes decrease.

3.4.1.2.3. Total net energy exchange

Table 3.8 presents the changes in total net energy exchange based on different zone temperature profiles and air speeds for an interior wall.

Table 3.8 Total net energy exchange of interior VBW with cement plaster

Zone temperature (min/max) (°C)	Total net energy exchange (kWh/m ²)		
	<i>v</i> =0 m/s	<i>v</i> =1 m/s	<i>v</i> =2 m/s
20/26	0.46	0.64	0.72
20/24	0.3	0.43	0.48
20/22	0.16	0.21	0.24

The total net energy exchange for an interior VBW compared to an exterior VBW varies depending on air speed, with the potential to exchange 8-33% more energy for all zone air temperature profiles. However, as the peak temperatures within the zone decrease, the energy exchange also decreases by an average of 66%. This is because higher temperature rises within the zone allow for more efficient charging and discharging of thermal mass, which improves space heating and cooling.

3.4.1.2.4. Impact of interior finishing layer on the thermal performance

To evaluate the influence of an interior surface finishing layer on the performance of an interior VBW, simulations were conducted at both passive performance (i.e., $v=0$ m/s) and with an air speed of 2 m/s for all three typical-day zone air temperature profiles. Table 3.8 presented the simulation results for energy exchange values of interior VBW with cement plaster as the interior finishing layer. Under passive performance, replacing the cement plaster layer with drywall reduced total net energy exchange by an average of approximately 14% across all zone air temperature profiles. Additionally, at an air speed of 2 m/s, replacing cement plaster with drywall decreased total net energy exchange by an average of approximately 9% for all zone air temperature profiles.

3.4.2. Annual energy analysis for VBW and wood-frame wall

The impacts of VBW and wood-frame walls on space heating and cooling loads are compared over the course of a year. In order to evaluate the thermal performance of a VBW versus a traditional wood-frame wall, two indicators of performance were introduced: assisting heating and assisting cooling. These measures refer to the amount of thermal energy stored in each wall that contributes to reduced space heating and cooling needed over the course of a year.

Furthermore, to prevent unwanted cooling in the zone during the winter, the air circulation is turned off when the temperature of the walls falls below 20°C. Throughout the remainder of the year, a 2 m/s air speed is maintained for ventilation. The following annual energy analysis is conducted based on TMY data for three Canadian cities (i.e., Edmonton, Vancouver, and Toronto) from 1996 to 2015. Data for solar radiation and meteorological elements is provided as part of the TMY data for a given location for a period of one year. Annual performance of the VBW for Edmonton is presented in the following paragraphs. The performance for the cities of Vancouver and Toronto are in [Appendix D](#).

Edmonton, located in western Canada, is the capital city of the province of Alberta. As one of the northernmost large cities in North America, Edmonton experiences freezing winters and sunny summers. With more than 2200 hours of sunshine per year, Edmonton ranks among the sunniest cities in Canada [102].

Figure 3.12 depicts the outdoor temperature, predicted indoor temperature, and the VBW surface temperature for three representative days in winter.

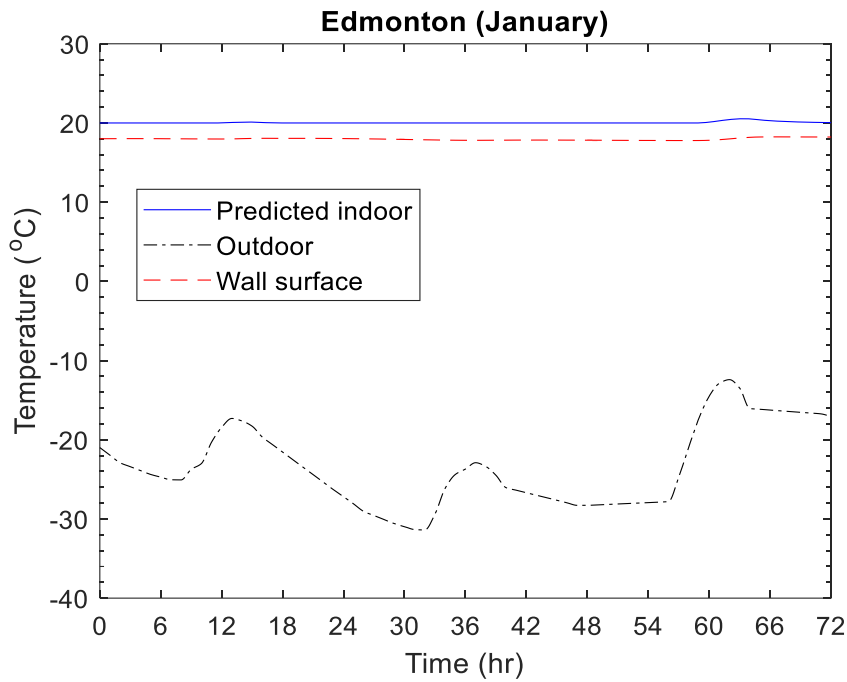


Figure 3.12 Outdoor, predicted indoor, and VBW surface temperatures for Edmonton, January

As illustrated in Figure 3.12, the outdoor temperature ranged from -32°C to nearly -13°C during a selected three-day period in winter. Indoor temperatures, however, were largely kept between 20°C and 20.5°C . The extremely cold outdoor temperature caused the wall surface to experience temperatures between 17.8°C and 18.2°C due to significant heat loss through the back of the wall. In the absence of temperature variations within the zone, the wall does not contribute to heating or cooling the zone, particularly when the outdoor temperature is below freezing.

Figure 3.13 illustrates the heat flux of the VBW and wood-frame wall for three representative days in winter.

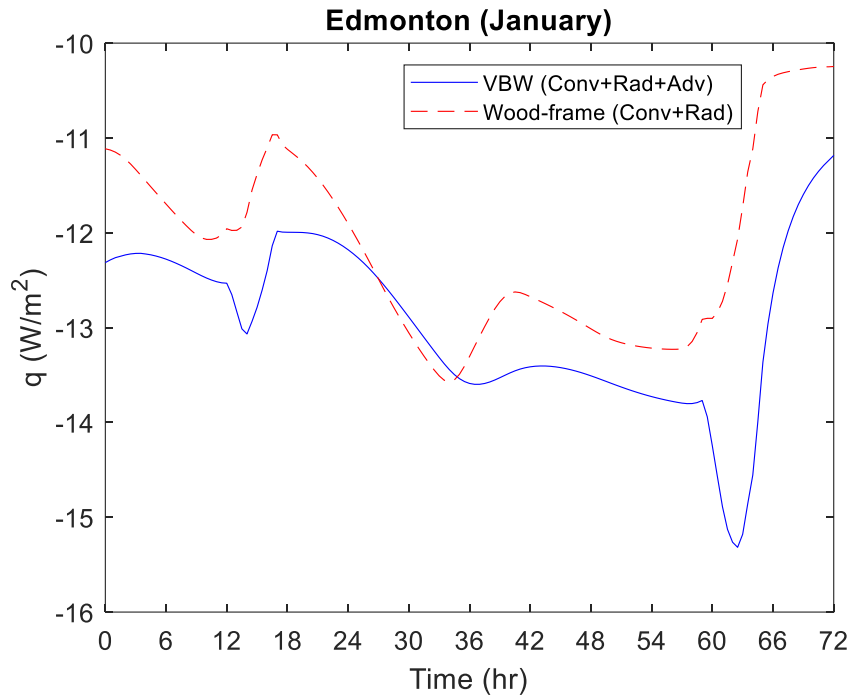


Figure 3.13 Heat flux of the VBW and wood-frame wall for Edmonton, January

As shown in Figure 3.13, both walls contributed to the unwanted cooling of the zone since their surface temperatures were lower than the zone temperature throughout the three-day period. Furthermore, the ventilation system was turned off for the entire time as the temperature of the VBW was below 20°C. Therefore, the only heat exchange between the VBW and the zone occurred through the wall surface. The heat flux density for a wood-frame wall changed rapidly in response to indoor temperature changes, with a short time lag. However, the VBW's high thermal inertia meant that it took longer to observe temperature changes on the wall surface. For most hours, both walls had nearly identical surface temperatures, with a maximum temperature difference of 0.2°C, due to minimal indoor temperature changes resulting in approximately the same heat flux density. However, between hours 59 and 63 in Figure 3.13 (i.e., 11 a.m. to 3 p.m. on the third day), the indoor temperature increased by approximately 0.7°C due to a significant outdoor temperature increase. Consequently, the wood-frame wall surface temperature increased rapidly due to changes in indoor and outdoor temperatures.

Although the VBW's surface temperature also increased during those hours, the indoor temperature increased at a faster rate than the VBW temperature. Therefore, the VBW's heat flux density reached its minimum at hour 63 (i.e., a dip in the blue line in Figure 3.13) due to the higher temperature difference between the surface and the zone air.

Figure 3.12 and Figure 3.13 suggest that when the indoor temperature remains stable and outdoor temperature drops significantly during winter, both walls will provide little or no heating and cooling contributions. In these cases, the heating systems should work as normal to maintain the desired temperature in the zone.

During summer, the walls show different behavior compared to winter due to greater variations in indoor temperature, higher outdoor temperature, and increased levels of solar radiation. Figure 3.14 shows the outdoor temperature, predicted indoor temperature, and surface temperature of VBW for three representative days in summer.

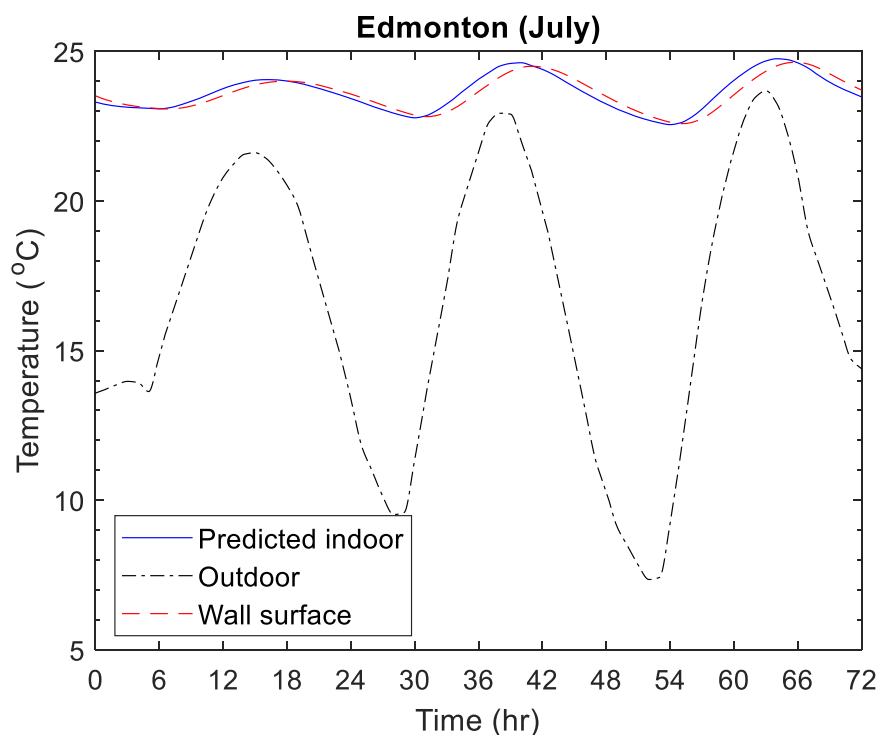


Figure 3.14 Outdoor, predicted indoor, and VBW surface temperatures for Edmonton, July

As depicted in Figure 3.14, outdoor temperatures are subject to large fluctuations in warm months. During the three-day period, the outdoor temperature varied between 7°C and 23°C. In most hours, this fluctuation in outdoor temperature caused the indoor temperature to fluctuate between 22.5°C and 25°C. The influence of variations in indoor temperature can be observed in the heating and cooling contributions of the VBW during the day. Heat storage within the VBW during hotter hours, when indoor temperature rises, can result in cooling contributions. Subsequently, the VBW's high thermal inertia allows for the gradual release of heat during the cooler periods of the night and early morning, when indoor temperature decreases.

Figure 3.15 illustrates the heat flux of VBW and wood-frame wall for three representative days in summer.

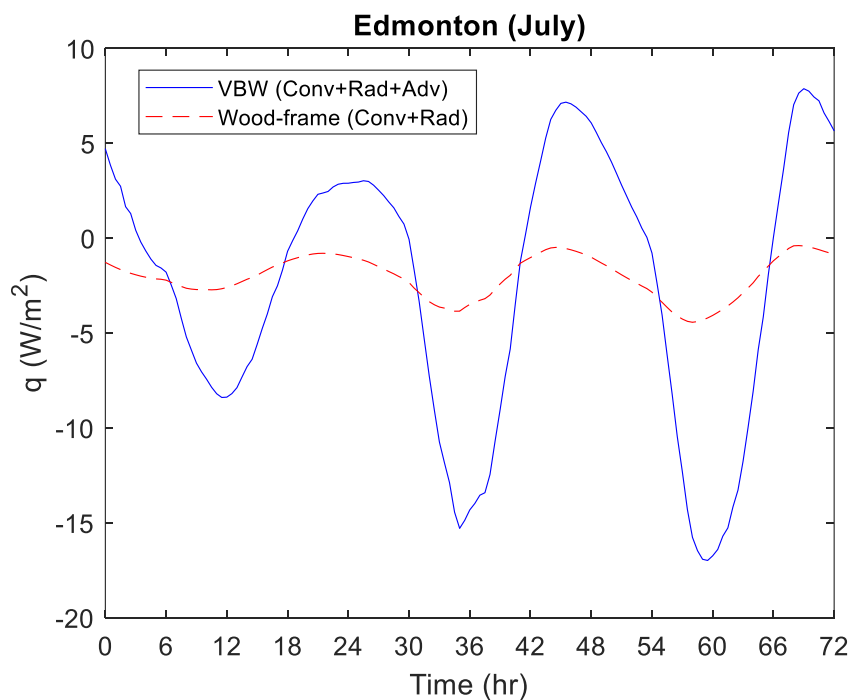


Figure 3.15 Heat flux of the VBW and wood-frame wall for Edmonton, July

Figure 3.15 shows that VBW contributes to both heating and cooling during the cold and hot hours, respectively. This can be attributed to the high thermal capacity and inertia of the

wall, which are capable of compensating for supply and demand mismatches by storing excess thermal energy and gradually releasing it to the zone. Conversely, an exterior wood-frame wall cannot contribute to the heating and cooling of the zone compared to VBWs especially in the cooling seasons. This is primarily due to the lack of ability to store heat in wood-frame walls and the absence of an advection heat transfer mechanism. Indeed, advection plays a crucial role in the heating and cooling of zones at air speeds exceeding 0.3 m/s, as compared to convection and radiation. Furthermore, wall temperature is primarily affected by the indoor temperature. Therefore, changes in indoor temperature that are dependent upon the indoor temperature, outdoor temperature and the GHI in the past timestep, can also contribute significantly to the amount of energy delivered to the zone and therefore reduction of space thermal loads.

Table 3.9 presents the monthly total assisting heating and cooling achieved by both walls for Edmonton based on the criteria defined in Table 3.2.

Table 3.9 Monthly total assisting heating and cooling achieved by both walls for Edmonton

Month	Wood-frame wall			VBW					
	H* (kWh/ /m ²)	C #1** (kWh/ m ²)	C #2*** (kWh/ m ²)	<i>v</i> =2 m/s			<i>v</i> =0 m/s		
				H (kWh/ m ²)	C #1 (kWh/ m ²)	C #2 (kWh/m ²)	H (kWh/ m ²)	C #1 (kWh/ m ²)	C #2 (kWh/ m ²)
January	0	0	0	0.4	0	0	0	0	0
February	0	0	0	0.6	0	0	0	0	0
March	0	0	0	1	0	0	0	0	0
April	0.01	0	0	2.3	0	0.05	0.02	0	0.01
May	0.07	0.005	0.03	3	0.2	1.1	0.4	0.1	0.3
June	0.14	0.012	0.05	3.1	0.4	2.2	0.9	0.2	0.7
July	0.22	0.04	0.15	3.6	1.3	3.5	1.6	0.7	1.4
August	0.19	0.01	0.07	3.3	0.6	3	0.9	0.4	0.8
September	0.04	0.003	0.03	2.7	0.3	1.5	0.6	0.2	0.5
October	0.02	0	0	2.1	0	0.13	0.03	0	0.03
November	0	0	0	1.2	0	0	0	0	0
December	0	0	0	0.3	0	0	0	0	0

Total (kWh/m²/year)	0.7	0.1	0.3	23.6	2.8	11.5	4.5	1.6	2.8
Fan energy consumption (kWh/year)		-			0.56			-	

*Heating

**Cooling – scenario 1

***Cooling – scenario 2

Zone temperature fluctuation occurs as the outdoor temperature experiences lows and highs throughout the day, resulting in assisting heating when the zone temperature decreases and assisting cooling when the zone temperature rises. Across all months in a year, as shown in Table 3.9, July provides the most heating and cooling energy to the zone, largely due to the heightened temperature fluctuations within the zone during this month. Furthermore, cooling scenario #2 provides more cooling energy than scenario #1, owing to the inclusion of additional criteria in the calculation. During the colder months of November through March, neither wall provides assisting cooling as the outside temperature never exceeds 20°C. Additionally, For Edmonton, the total heating energy consistently exceeds the total cooling energy, largely due to the very cold climate conditions in Edmonton, where the outside temperature is lower than 20°C for most of the year.

Table 3.9 demonstrates that a wood-frame wall has limited capacity to provide heating and cooling energy, largely because of its structural composition and its inability to store and release heat during the day. Conversely, the VBW exhibits a notable capacity for assisting with heating and cooling energy in the zone, owing to its significant heat storage ability, as compared to a wood-frame wall. When using an air speed of 2 m/s for ventilation, replacing a wood-frame wall with a VBW leads to a total assisting heating and cooling of 35 kWh/m² (wall area) for Edmonton, Canada throughout the year. Passive performance (i.e., v=0 m/s) results in a significant reduction in total heating and cooling energy when compared to an air speed of 2 m/s. Specifically, a reduction of 80%, 42%, and 74% was observed in total heating, total

cooling in scenario 1, and total cooling in scenario 2, respectively. Results for other Canadian cities such as Vancouver and Toronto can be found in [Appendix D](#).

3.5. Conclusion

This Chapter aimed to evaluate the thermal performance of a VBW. In order to determine the thermal performance, the average wall temperature, the heat flux from and to the wall, and the amount of energy that could be saved by using VBW were calculated. The performance was assessed using two main approaches: 1) the typical-day thermal performance of a VBW under different boundary conditions, zone temperatures, and air speeds; and 2) the energy analysis of an exterior VBW and a traditional wood-frame wall over a one-year period with emphasis on the cold climate of Canada. Findings for the typical-day approach were investigated based on a parametric analysis of the zone temperature profile and air speed to determine their effect on the thermal performance of a VBW. A similar experimental study in the literature was used to validate the proposed numerical model. Findings revealed that by increasing the peak zone temperature as well as the air speed, the heat exchange between the wall and the zone could be increased over the course of one day for both exterior and interior VBWs. In addition, when the air speed was increased from 0 m/s to 2 m/s for an exterior VBW, thermal energy storage rose by 67% for any given zone temperature. In a similar manner, the total energy exchange for the interior VBW went up by 22% on average when the air speed rose from 0 m/s to 2 m/s. For all temperature profiles, an interior VBW can save 8-33% more energy than an exterior VBW. Moreover, the simulation results of annual energy analysis showed that substituting a traditional wood-frame wall with a VBW can yield a total assisting heating and cooling of 35 kWh/m² (wall area) for Edmonton, Canada throughout the year.

Chapter 4 Conclusion

The escalating energy use for heating and cooling in residential buildings has become a worry among scholars, designers, and policy makers. Natural Resources Canada reveals that space heating and cooling consume 66% of a building's total energy. Therefore, this thesis aimed to reduce thermal loads by investigating the implementation of active TES in walls.

Chapter 2 evaluated the cooling potentials of a DCW-wall system composed of copper pipes embedded in a thermally massive wall and to provide a general guideline for condensation prevention. The DCW-wall performance was studied through a sensitivity analysis of pipe configuration, pipe spacing, zone temperature, and water supply temperature. The study showed that higher cooling capacity and delivered cooling energy could be achieved with smaller pipe spacing, lower water inlet temperature, and thinner walls. The serpentine configuration had the highest cooling potential among all configurations, while the spiral counterflow configuration had the most uniform wall surface temperature, important for both thermal comfort and condensation prevention. Subsequently, a conservative, yet simple guideline was recommended to prevent condensation. Keeping the indoor RH level less than 53.8% would make condensation less likely regardless of operation scenario. The cooling energy from the simulated DCW-wall system was compared with the actual cooling energy demand for residential buildings in Toronto, Canada. It was found that the DCW-wall system with spiral configuration was capable of supplying up to ~11 % of the annual energy demand for space cooling.

In Chapter 3, the thermal performance of a VBW with airflow to a zone was investigated. Two methods were used to evaluate the performance: a typical-day analysis based on different boundary conditions (i.e., interior, and exterior walls), zone temperatures, and air speeds; and an annual energy analysis, which compares the thermal performance of an exterior VBW with an exterior wood-frame wall in three cities of Canada. Simulation results from the typical-day

analysis showed that increasing the peak zone temperature and air speed improved the heat exchange rate between the wall and the zone for both exterior and interior VBWs. Additionally, increasing air speed in an exterior VBW resulted in significant reduction in space heating and cooling loads, while an interior VBW showed a moderate improvement in thermal load reduction with higher air speed compared to its passive performance. An annual energy analysis showed that substituting a wood-frame wall with a VBW can yield a total assisting heating and cooling of 35 kWh/m² (wall area) for Edmonton, Canada throughout the year.

4.1. Future work

The numerical models for DCW-wall system and VBW can be improved by conducting experiments and analyzing the results. Real-time zone temperature data can be obtained through experiments or real-time estimation methods. Moreover, once experiments have been conducted and a large dataset has been collected, machine learning techniques can be utilized to identify the most influential parameters and estimate the behavior of the system under more operation and boundary scenarios. Furthermore, the performance of combined passive and active TES systems can be assessed. Direct solar irradiance on a wall while the hydronic or ventilated system is operating is an example of the combination of both passive and active TES.

Additionally, sensitivity analyses for the VBW and DCW-wall systems can consider more parameters. There are various thermal conductivities and pipe types to be used in the analysis of the DCW-wall system. Performance can be further evaluated by comparing results in cold, temperate, and hot climate regions. In sensitivity analysis of a VBW system, multiple parameters can be considered, such as core and face shell thickness variations and air path configurations. In addition, to make an accurate comparison between VBW and wood-frame walls, different wood-frame designs with varying framing factors should be examined.

References

1. Jackson, R.B., et al., *Global energy growth is outpacing decarbonization*. Environmental Research Letters, 2018. **13**(12): p. 120401.
2. Dadoo, A., L. Gustavsson, and R. Sathre, *Building energy-efficiency standards in a life cycle primary energy perspective*. Energy and Buildings, 2011. **43**(7): p. 1589-1597.
3. Edenhofer, O., et al., *Change 2014: Mitigation of Climate Change. Contribution of Working Group III to the Fifth Assessment Report of the Intergovernmental Panel on Climate Change*. 2014.
4. IEA, *Perspectives for the clean energy transition*. 2019, International Energy Agency Paris, France.
5. IEA. *Insights Brief: Space Cooling*. 2017 [cited 2022 December, 13]; Available from: <https://www.iea.org/reports/insights-brief-space-cooling>.
6. Yang, L., H. Yan, and J.C. Lam, *Thermal comfort and building energy consumption implications—a review*. Applied energy, 2014. **115**: p. 164-173.
7. Chen, S., et al., *The impacts of occupant behavior on building energy consumption: A review*. Sustainable Energy Technologies and Assessments, 2021. **45**: p. 101212.
8. Levesque, A., et al., *How much energy will buildings consume in 2100? A global perspective within a scenario framework*. Energy, 2018. **148**: p. 514-527.
9. Levesque, A., R.C. Pietzcker, and G. Luderer, *Halving energy demand from buildings: The impact of low consumption practices*. Technological Forecasting and Social Change, 2019. **146**: p. 253-266.
10. Heier, J., C. Bales, and V. Martin, *Combining thermal energy storage with buildings—a review*. Renewable and Sustainable Energy Reviews, 2015. **42**: p. 1305-1325.
11. De Gracia, A. and L.F. Cabeza, *Phase change materials and thermal energy storage for buildings*. Energy and Buildings, 2015. **103**: p. 414-419.
12. Dincer, I., *On thermal energy storage systems and applications in buildings*. Energy and buildings, 2002. **34**(4): p. 377-388.
13. Alva, G., Y. Lin, and G. Fang, *An overview of thermal energy storage systems*. Energy, 2018. **144**: p. 341-378.
14. Verbeke, S. and A. Audenaert, *Thermal inertia in buildings: A review of impacts across climate and building use*. Renewable and sustainable energy reviews, 2018. **82**: p. 2300-2318.
15. Balaras, C., *The role of thermal mass on the cooling load of buildings. An overview of computational methods*. Energy and buildings, 1996. **24**(1): p. 1-10.
16. Chen, Y., K.E. Galal, and A.K. Athienitis, *Integrating hollow-core masonry walls and precast concrete slabs into building space heating and cooling*. Journal of building engineering, 2016. **5**: p. 277-287.
17. Babiak, J., B.W. Olesen, and D. Petras, *Low temperature heating and high temperature cooling: REHVA GUIDEBOOK No 7*. 2007.
18. Behrendt, B., *Possibilities and Limitations of Thermally Activated Building Systems: Simply TABS and a Climate Classification for TABS*. 2016.
19. Lehmann, B., et al., *Thermally activated building systems (TABS): Energy efficiency as a function of control strategy, hydronic circuit topology and (cold) generation system*. Applied Energy, 2011. **88**(1): p. 180-191.
20. Edenhofer, O., et al., *Intergovernmental Panel on Climate Change (IPCC): mitigation of climate change. Contribution of working group III to the fifth assessment report of the intergovernmental panel on climate change*. Cambridge, United Kingdom and New York, NY. 2014, USA: Cambridge University Press.

21. Andreou, A., et al., *Decomposing the drivers of residential space cooling energy consumption in EU-28 countries using a panel data approach*. Energy and Built Environment, 2020. **1**(4): p. 432-442.
22. Dutta, S. and C.M. Hussain, *Sustainable Fuel Technologies Handbook*. 2020: Academic Press.
23. Mugnini, A., F. Polonara, and A. Arteconi, *Energy flexibility curves to characterize the residential space cooling sector: The role of cooling technology and emission system*. Energy and Buildings, 2021. **253**: p. 111335.
24. Santamouris, M. and D. Kolokotsa, *Passive cooling dissipation techniques for buildings and other structures: The state of the art*. Energy and Buildings, 2013. **57**: p. 74-94.
25. Bulut, H. and M.A. Aktacir, *Determination of free cooling potential: A case study for Istanbul, Turkey*. Applied Energy, 2011. **88**(3): p. 680-689.
26. International Energy Agency (IEA), *Ventilative Cooling*. Status and recommendations for better implementation of ventilative cooling in standards, legislation and compliance tools (Background Report), 2018.
27. Katili, A.R., R. Boukhanouf, and R. Wilson. *Space cooling in buildings in hot and humid climates—a review of the effect of humidity on the applicability of existing cooling techniques*. in *14th International Conference on Sustainable Energy Technologies “SET”*. 2015.
28. Guo, X. and M. Hendel, *Urban water networks as an alternative source for district heating and emergency heat-wave cooling*. Energy, 2018. **145**: p. 79-87.
29. van der Hoek, J.P., et al., *Energy recovery from the water cycle: Thermal energy from drinking water*. Energy, 2018. **162**: p. 977-987.
30. Ahmad, J.I., et al., *Maximizing Thermal Energy Recovery from Drinking Water for Cooling Purpose*. Energies, 2021. **14**(9): p. 2413.
31. Prybysh, R., et al., *Experimental Study on the Palatability Impacts of Potable Water as a Hydronic Medium*. Water, 2018. **10**(2): p. 218.
32. Babiak, J. and G. Vagiannis. *Thermally Activated Building System (TABS): Efficient cooling and heating of commercial buildings*. in *Congreso, Climamed*. 2015.
33. Ma, P., L.-S. Wang, and N. Guo, *Energy storage and heat extraction—From thermally activated building systems (TABS) to thermally homeostatic buildings*. Renewable and Sustainable Energy Reviews, 2015. **45**: p. 677-685.
34. Romani, J., A. de Gracia, and L.F. Cabeza, *Simulation and control of thermally activated building systems (TABS)*. Energy and Buildings, 2016. **127**: p. 22-42.
35. Chung, W.J., et al., *Control of Thermally Activated Building System Considering Zone Load Characteristics*. Sustainability, 2017. **9**(4): p. 586.
36. Guerrero, M., et al. *Evaluation of the behavior of an innovative thermally activated building system (TABS) with PCM for an efficient design*. in *E3S Web of Conferences*. 2019. EDP Sciences.
37. Antonopoulos, K., M. Vrachopoulos, and C. Tzivanidis, *Experimental and theoretical studies of space cooling using ceiling-embedded piping*. Applied Thermal Engineering, 1997. **17**(4): p. 351-367.
38. Xie, J.-l., Q.-y. Zhu, and X.-h. Xu, *An active pipe-embedded building envelope for utilizing low-grade energy sources*. Journal of Central South University, 2012. **19**(6): p. 1663-1667.
39. Shin, M.S., et al., *Design of radiant floor heating panel in view of floor surface temperatures*. Building and Environment, 2015. **92**: p. 559-577.

40. Romani, J., L.F. Cabeza, and A. de Gracia, *Development and experimental validation of a transient 2D numeric model for radiant walls*. Renewable Energy, 2018. **115**: p. 859-870.
41. Šimko, M., et al., *Testing of a Radiant Wall Cooling System with Pipes Coupled to Aerated Blocks*. Periodica Polytechnica Mechanical Engineering, 2022. **66**(1): p. 59-66.
42. Krajčík, M. and O. Šikula, *The possibilities and limitations of using radiant wall cooling in new and retrofitted existing buildings*. Applied Thermal Engineering, 2020. **164**: p. 114490.
43. Krajčík, M., et al., *Thermal performance of a radiant wall heating and cooling system with pipes attached to thermally insulating bricks*. Energy and Buildings, 2021. **246**: p. 111122.
44. Šimko, M., M. Krajčík, and O. Šikula. *Radiant wall cooling with pipes arranged in insulation panels attached to facades of existing buildings*. in *E3S Web of Conferences*. 2019. EDP Sciences.
45. Samuel, D.L., S.S. Nagendra, and M.P. Maiya, *Parametric analysis on the thermal comfort of a cooling tower based thermally activated building system in tropical climate—An experimental study*. Applied Thermal Engineering, 2018. **138**: p. 325-335.
46. ASHRAE, *2016 ASHRAE Handbook-HVAC Systems and Equipment (IP Edition)*. 2016: ASHRAE.
47. Kappel, K. and T. Grechenig. "show-me" water consumption at a glance to promote water conservation in the shower. in *Proceedings of the 4th international conference on persuasive technology*. 2009.
48. Beal, C.D. and R.A. Stewart, *Identifying residential water end uses underpinning peak day and peak hour demand*. Journal of Water Resources Planning and Management, 2014. **140**(7): p. 04014008.
49. Cole, G. and R.A. Stewart, *Smart meter enabled disaggregation of urban peak water demand: precursor to effective urban water planning*. Urban Water Journal, 2013. **10**(3): p. 174-194.
50. Legget, R. and F. Peckover, *SOIL TEMPERATURE STUDIES—A PROGRESS REPORT*. 1949.
51. Tham, S., et al., *Indoor temperature and health: a global systematic review*. Public Health, 2020. **179**: p. 9-17.
52. Oetomo, A., et al., *Indoor temperatures in the 2018 heat wave in Quebec, Canada: exploratory study using Ecobee smart thermostats*. JMIR formative research, 2022. **6**(5): p. e34104.
53. Patankar, S.V., *Numerical heat transfer and fluid flow*. 2018: CRC press.
54. Bergman, T.L., et al., *Fundamentals of heat and mass transfer*. 2011: John Wiley & Sons.
55. Baldinelli, G., et al., *Transient heat transfer in radiant floors: a comparative analysis between the lumped capacitance method and infrared thermography measurements*. Journal of Imaging, 2016. **2**(3): p. 22.
56. Merabtine, A., et al., *Experimental and multidimensional numerical analysis of the thermal behavior of an anhydrite radiant slab floor heating system: A multi-objective sensitivity study*. Energy and Buildings, 2018. **174**: p. 619-634.
57. FEMP, M., *Guidelines: Measurement and Verification for Federal Energy Projects, Version 3.0*. Energy Efficiency and Renewable Energy, 2008.
58. Xing, D., et al., *A critical review of passive condensation prevention for radiant cooling*. Building and Environment, 2021. **205**: p. 108230.

59. Xie, D., et al., *Numerical analysis of temperature non-uniformity and cooling capacity for capillary ceiling radiant cooling panel*. *Renewable Energy*, 2016. **87**: p. 1154-1161.
60. Ning, B., et al., *Cooling capacity improvement for a radiant ceiling panel with uniform surface temperature distribution*. *Building and Environment*, 2016. **102**: p. 64-72.
61. Environmental Protection Agency, W., DC. Office of Radiation and I. Air, *Mold remediation in schools and commercial buildings*. 2001: ERIC Clearinghouse.
62. Cholewa, T., et al., *On the heat transfer coefficients between heated/cooled radiant floor and room*. *Energy and Buildings*, 2013. **66**: p. 599-606.
63. Cholewa, T., et al., *On the heat transfer coefficients between heated/cooled radiant ceiling and room*. *Applied Thermal Engineering*, 2017. **117**: p. 76-84.
64. Natural Resources Canada, *Energy Fact Book 2019–2020*. 2019, Natural Resources Canada Ottawa.
65. Statistics Canada. *Household energy consumption, Canada and provinces*. 2019 [cited 2022 August 15]; Available from: <https://www150.statcan.gc.ca/t1/tbl1/en/tv.action?pid=2510006001>.
66. Purushothama, B., *Humidification and ventilation management in textile industry*. 2010: CRC Press.
67. Government of Canada. *Air Conditioning Your Home*. 2016 [cited 2023 February 1]; Available from: <https://www.nrcan.gc.ca/energy-efficiency/energy-star-canada/about/energy-star-announcements/publications/air-conditioning-your-home/6051>.
68. Government of Canada. *Weather, Climate, and Hazard - Historical data*. 2021 [cited 2022 August 15]; Available from: https://climate.weather.gc.ca/historical_data/search_historic_data_e.html.
69. Olsthoorn, D., et al., *Abilities and limitations of thermal mass activation for thermal comfort, peak shifting and shaving: A review*. *Building and Environment*, 2017. **118**: p. 113-127.
70. Bouvenot, J.-B. and M. Egg. *Numerical And Experimental Study Of A Supply Air Wall Based On Integrated Insulation Clay Hollow Blocks*. in *Journal of Physics: Conference Series*. 2021. IOP Publishing.
71. Huang, J., J. Yu, and H. Yang, *Effects of key factors on the heat insulation performance of a hollow block ventilated wall*. *Applied Energy*, 2018. **232**: p. 409-423.
72. Yu, J., J. Yang, and C. Xiong, *Study of dynamic thermal performance of hollow block ventilated wall*. *Renewable Energy*, 2015. **84**: p. 145-151.
73. Yu, T., et al., *Experimental and numerical studies on dynamic thermal performance of hollow ventilated interior wall*. *Applied Thermal Engineering*, 2020. **180**: p. 115851.
74. Bunn, R., *Termodeck: the thermal flywheel*. *Building Services Engineering Research and Technology*; (United Kingdom), 1991. **13**(5).
75. Labat, M., et al., *Indoor thermal behaviour of an office equipped with a ventilated slab: a numerical study*. *Journal of Building Performance Simulation*, 2021. **14**(3): p. 227-246.
76. Chen, Y., K.E. Galal, and A.K. Athienitis, *Design and operation methodology for active building-integrated thermal energy storage systems*. *Energy and buildings*, 2014. **84**: p. 575-585.
77. Barnaby, C., D. Nall, and E. Dean, *Structural mass cooling in a commercial building using hollowcore concrete plank*. *Proc. Annu. Meet.-Am. Sect. Int. Sol. Energy Soc.;* (United States), 1980. **5**(CONF-801016-(Vol. 2)).
78. Russell, M. and P. Surendran, *Influence of active heat sinks on fabric thermal storage in building mass*. *Applied energy*, 2001. **70**(1): p. 17-33.

79. Zmeureanu, R. and P. Fazio, *Thermal performance of a hollow core concrete floor system for passive cooling*. Building and environment, 1988. **23**(3): p. 243-252.
80. Zhou, J., T. Yu, and B. Lei, *Experimental study on the influence of solar heat gain on the thermal performance of hollow ventilated interior wall*. Journal of Solar Energy Engineering, 2022: p. 1-34.
81. Canadian Concrete Masonry Producers' Association (CCMPA). *Empirical Masonry Design Guidelines*. 2022 [cited 2022 October 8]; Available from: <https://ccmpa.ca/wp-content/uploads/2012/02/8-EmpiricalMasonryDsgn.pdf>.
82. IRC, N., *National energy code of Canada for buildings*. Ottawa, On: Government of Canada, 2020.
83. ASHRAE, *ASHRAE handbook-Fundamentals*. 2005: ASHRAE.
84. Bisegna, F., et al., *Influence of insulating materials on green building rating system results*. Energies, 2016. **9**(9): p. 712.
85. Canadian Centre for Occupational Health and Safety (CCOHS). *Temperature condition at workplace - Legislation*. [cited 2022 October 8,]; Available from: https://www.ccohs.ca/oshanswers/phys_agents/temp_legislation.html.
86. Jaakkola, J., O. Heinonen, and O. Seppänen, *Sick building syndrome, sensation of dryness and thermal comfort in relation to room temperature in an office building: need for individual control of temperature*. Environment international, 1989. **15**(1-6): p. 163-168.
87. Ontario regulation. *Ontario Residential Tenancies Act*. 2006 [cited 2022 October 8]; Available from: <https://www.ontario.ca/laws/regulation/060516>.
88. Noguchi, M., et al. *Net zero energy homes of the future: A case study of the EcoTerra™ house in Canada*. in *Renewable Energy Congress, Glasgow, Scotland*. 2008.
89. Bergman, T.L., et al., *Introduction to heat transfer*. 2011: John Wiley & Sons.
90. Travis, Q.B. and L.W. Mays, *Relationship between hazen-william and colebrook-white roughness values*. Journal of Hydraulic Engineering, 2007. **133**(11): p. 1270-1273.
91. Chanson, H., *Hydraulics of open channel flow*. 2004: Elsevier.
92. Tayşi, N. and S. Abid, *Temperature distributions and variations in concrete box-girder bridges: experimental and finite element parametric studies*. Advances in Structural Engineering, 2015. **18**(4): p. 469-486.
93. ISO, *11855-2: 2012 (E) Building Environment Design-Design, Dimensioning, Installation and Control of Embedded Radiant Heating and Cooling Systems. Part 2: Determination of the Design Heating and Cooling Capacity*. International Organization for Standard, Geneve, Switzerland, 2012.
94. Shinoda, J., et al., *A review of the surface heat transfer coefficients of radiant heating and cooling systems*. Building and Environment, 2019. **159**: p. 106156.
95. Barton, P., C. Beggs, and P. Sleight, *A theoretical study of the thermal performance of the TermoDeck hollow core slab system*. Applied Thermal Engineering, 2002. **22**(13): p. 1485-1499.
96. Yang, J., J. Yu, and C. Xiong, *Heat transfer analysis of hollow block ventilated wall based on CFD modeling*. Procedia Engineering, 2015. **121**: p. 1312-1317.
97. Yu, J., et al., *A semi-dynamic heat transfer model of hollow block ventilated wall for thermal performance prediction*. Energy and Buildings, 2017. **134**: p. 285-294.
98. Streeter, V. and B.K. WE, *Fluid mechanics*. WCB McGraw-Hill. Inc. Boston, 1998.
99. Li, J., et al., *Effect of the insulation materials filling on the thermal performance of sintered hollow bricks*. Case studies in thermal engineering, 2018. **11**: p. 62-70.
100. Pierquet, P., J.L. Bowyer, and P. Huelman, *Thermal performance and embodied energy of cold climate wall systems*. Forest Products Journal, 1998. **48**(6): p. 53.

101. Sassine, E., et al. *Thermal performance of lightweight concrete applications in building envelopes in Lebanon*. in *Building Simulation*. 2021. Springer.
102. CurrentResults. *Sunniest cities in Canada*. [cited 2022 November 18th]; Available from: <https://www.currentresults.com/Weather-Extremes/Canada/sunniest-cities.php>.
103. Qasass, R., M. Gorgolewski, and H. Ge, *Timber framing factors in Toronto residential house construction*. *Architectural Science Review*, 2014. **57**(3): p. 159-168.
104. Canadian Mortgage Housing and Corporation (CMHC). *Wood frame envelopes. Best practice guide: Building Technology*. 2001; Available from: <https://publications.gc.ca/site/eng/9.647239/publication.html>
105. Canadian Mortgage Housing and Corporation (CMHC). *Canadian wood-frame house construction*. 2013; Available from: <https://publications.gc.ca/site/eng/9.700100/publication.html>

Appendix A – Calculation of thermal transmittances in DCW-wall system

U_{P1} , U_{P2} , and U_{P3} can be calculated using Eqs. (A.1) to (A.3).

$$U_{P1} = \pi D_i \times L_f \times h_{water} \quad (A.1)$$

$$U_{P2} = \frac{2\pi \times L_f \times \lambda_{pipe}}{\ln\left(\frac{D_o}{D_i}\right)} \quad (A.2)$$

$$U_{P3} = \frac{2\pi \times L_f \times \lambda_{wall}}{\ln\left(\frac{1.08 \times W_f}{D_o}\right)} \quad (A.3)$$

D_o and W_f stand for the outside diameter of the pipe and the width of the wall node in the direction transverse to the flow, respectively. h_{water} , λ_{tube} , and λ_{wall} represent the water convective heat transfer coefficient; pipe and wall thermal conductivity. h_{water} can be obtained by using Eq. (A.4) [54].

$$h_{water} = \frac{Nu \times \lambda_{water}}{D_i} \quad (A.4)$$

where λ_{water} and Nu are water thermal conductivity and Nusselt number. Depending on the flow regime (i.e., laminar, or turbulent), Nusselt number can take different values. Eqs. (A.5) and (A.6) determine the Nusselt number [54].

$$Nu = 4.364 \text{ (Laminar flow; } Re \leq 2300) \quad (A.5)$$

$$Nu = \frac{\frac{f}{8}(Re-1000)Pr}{1+12.7\left(\frac{f}{8}\right)^{0.5}(Pr^{2/3}-1)} \text{ (Turbulent flow; } 3000 \leq Re \leq 5 \times 10^6 \text{ \& } 0.5 \leq Pr \leq 2000) \quad (A.6)$$

Re is the Reynolds number, Pr is the Prandtl number, and f is the friction factor. Eqs. (A.7) to (A.9) can be used to calculate Re , Pr , and f [54].

$$Re = \frac{v \times D_i}{\vartheta} \quad (A.7)$$

$$Pr = \frac{\vartheta}{\lambda_{water}/(\rho C_p)_{water}} \quad (\text{A.8})$$

$$fr = (0.79 \times \text{Ln}(Re) - 1.64)^{-2} \quad (\text{A.9})$$

where v and ϑ denote the fluid speed and fluid kinematic viscosity, respectively.

Appendix B – Wood-frame wall

The overall thermal resistance of a wood-frame wall is primarily determined by the framing factor (FF) and the applied insulations. The FF of a wood-frame wall corresponds to the ratio of the wood's surface area (studs, top plates, bottom plates, etc.) to the total wall's surface area. The FF can vary from 6.3% to more than 40% depending on the type of exterior wall and its components [103]. Actual wall FF is usually higher due to junction between walls or added pieces of wood with the purpose of increasing the safety margin. An average FF for a house is defined as the total walls framing area divided by the total area of the walls. The average FF is recommended to be between 19% and 23% [103]. Typically, a higher FF can be achieved by increasing the openings in a wall. The Canadian Wood Council and Canadian Mortgage and Housing Corporation (CMHC) [104] suggest that, typically, about 15% of a wood-frame wall area consists of the framing material, depending on stud spacing and layout. In this situation, the FF can be increased by reducing the space between studs and/or by using double bottom plates when the concrete topping is applied to the floor [105]. In some cases, wall is comprised of cripples, window headers, studs, a bottom plate, and two top plates, whereas in other cases, king studs, door headers, T-walls, trimmers, and corners can be added to the wall. As a result, these components can significantly increase the framing factor.

Moreover, rigid, or semi-rigid insulation (i.e., continuous insulation) at the back of the wall, and the use of 2×6 studs or in some cases 2×8 studs, would improve the thermal performance of these types of walls. According to the CMHC [104], rigid or semi-rigid insulation has proven to be the most cost-effective method of enhancing thermal performance and minimizing thermal bridges.

In this study, an exterior wood-frame wall (2×6 nominal size, 1.5×5.5 actual size) with double top plates, one bottom plate, and studs spaced at 16 inches on-center was modelled. An

FF of 13% was calculated for the modelled wall. Figure B.1 shows the front view of the wood-frame wall (i.e., wood frame and insulation) and its discretization in three directions.

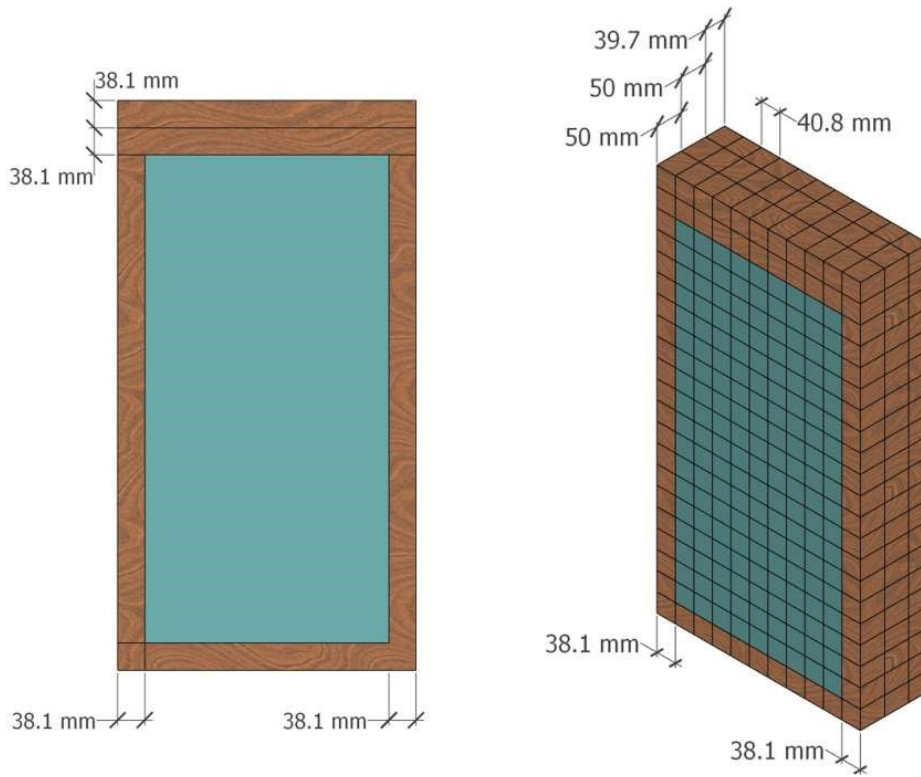


Figure B.1 Front view of the wood-frame wall and its discretization in three directions

As shown in Figure B.1, the length of all the CVs in the studs is the same, however it differs from the length of other CVs in the plates and insulation. Also, the height of all CVs in the top and bottom plates is equal, but different from the height of all other CVs. The discretization of other continuous layers (i.e., dry wall, plywood, and rigid insulation) is identical to the discretization shown in Figure B.1. A schematic of the wood-frame wall is depicted in Figure B.2.

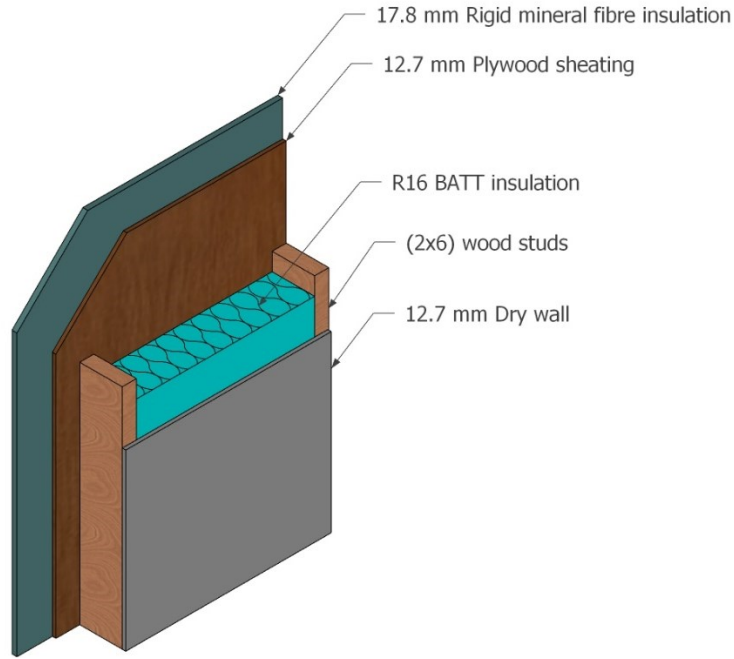


Figure B.2 A schematic of the Wood-frame wall

The isothermal plane and parallel method was utilized to determine the effective RSI value of the wood-frame wall [82]. Initially, the RSI value of the wood studs and insulation in the cavity was determined using the parallel method, and subsequently, the value was combined with RSI values of the remaining layers (isothermal plane method) to obtain the effective RSI value of the wood-frame wall.

The thermal resistance of the wood stud and insulation can be obtained using Eq. (B.1).

$$RSI_{wood-insulation} = \frac{1}{\frac{FF}{RSI_{wood}} + \frac{1 - FF}{RSI_{insulation}}} \quad (B.1)$$

where FF is the framing factor (i.e., 0.13), RSI_{wood} is the thermal resistance of the wood-studs, $RSI_{insulation}$ is the thermal resistance of the insulation placed in the cavity. The effective RSI value of the entire wall can be determined using Eq. (B.2).

$$RSI_{effective} = RSI_{Drywall} + RSI_{wood-insulation} + RSI_{Plywood} + RSI_{Rigid\ insulation} \quad (B.2)$$

Appendix C – Predicted and measured indoor temperatures in annual energy analysis

Figure C.1 to Figure C.3 compare the predicted indoor temperature with measured indoor temperature of EcoTerra house for some typical days.

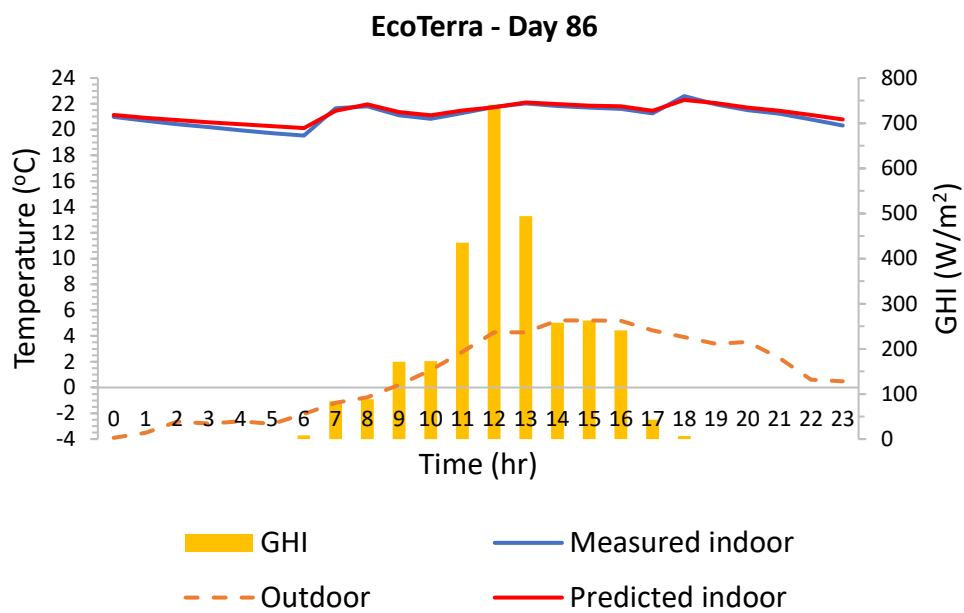


Figure C.1 Measured and predicted average indoor temperature for EcoTerra house-day 86

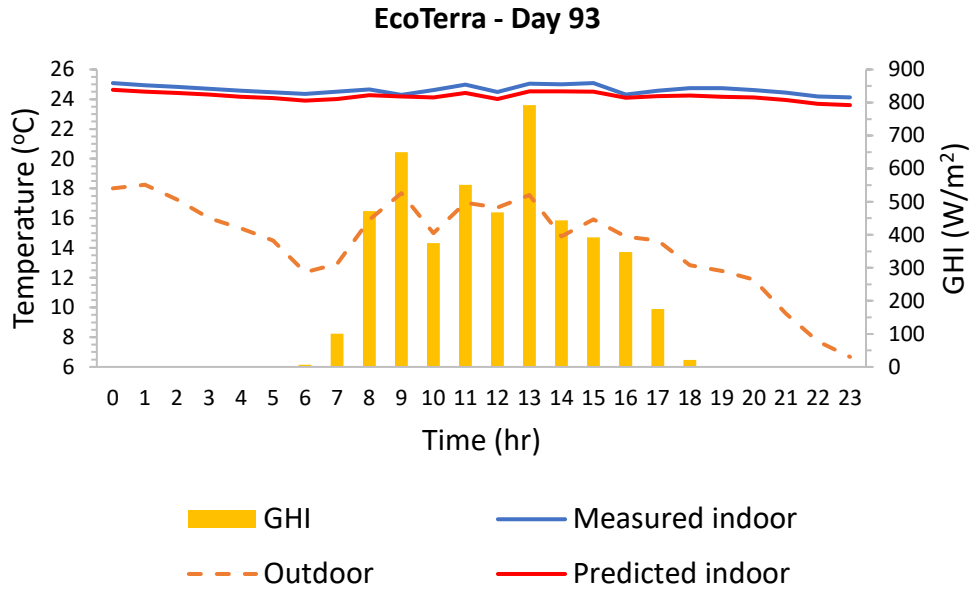


Figure C.2 Measured and predicted average indoor temperature for EcoTerra house-day 93

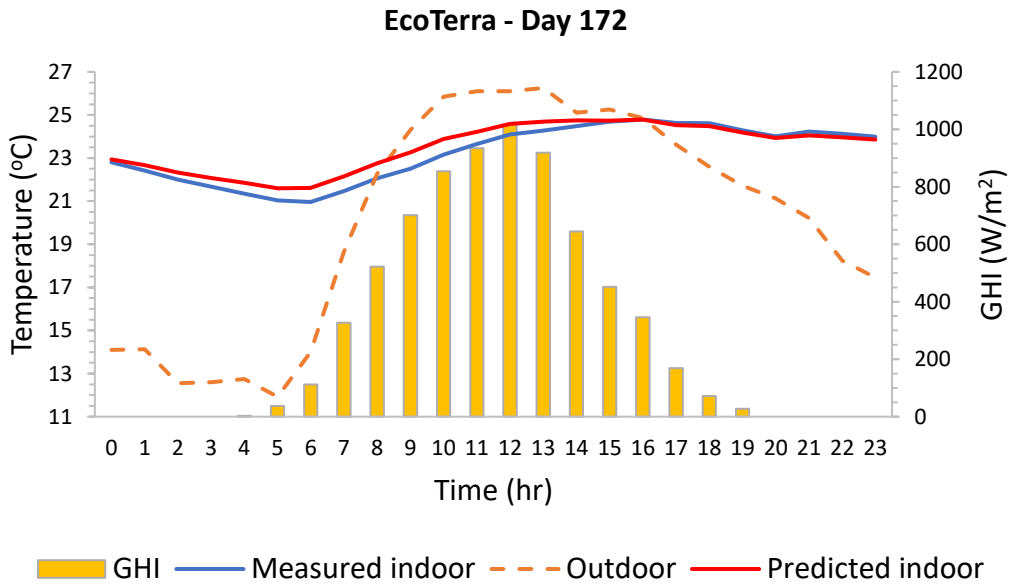


Figure C.3 Measured and predicted average indoor temperature for EcoTerra house-day 172

Figure C.1 to Figure C.3 demonstrate a strong correlation between the predicted indoor temperature data and the recorded indoor temperature data from the EcoTerra house.

Appendix D – Annual energy analysis for Vancouver and Toronto

a) Vancouver

Vancouver is located in the west of Canada and is known for its mild, oceanic climate. In the following, the main findings from the plots and Tables are explained. Figure D.1 depicts the outdoor temperature, predicted indoor temperature, and the VBW surface temperature for three representative days in winter.

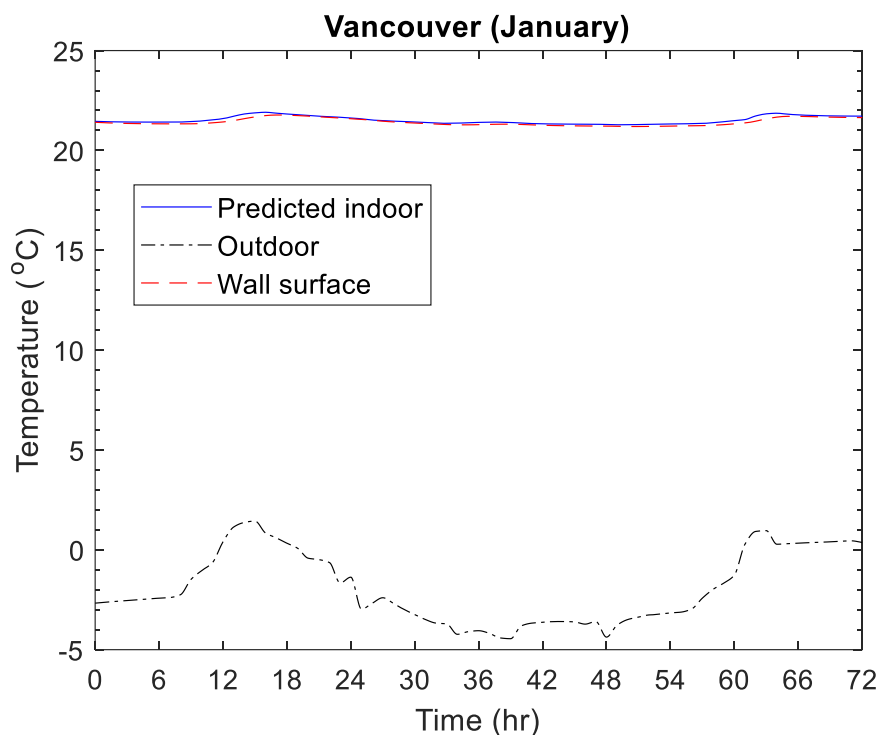


Figure D.1 Outdoor, predicted indoor, and VBW surface temperatures for Vancouver, January

Winters in Vancouver are warmer than those in Edmonton. In Figure D.1, the wall surface temperature was lower than the indoor temperature during the sunny hours when the indoor temperature began to rise resulting in cooling contributions. However, during the cold hours of the day, neither cooling nor heating contributions were made.

Figure D.2 shows the heat flux of the VBW and wood-frame wall for three representative days in winter.

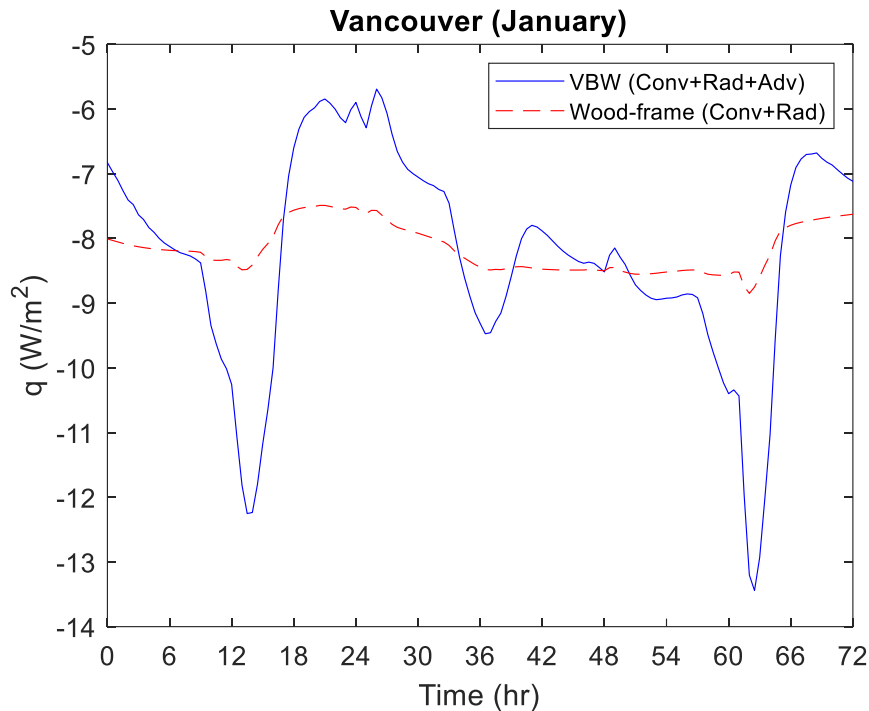


Figure D.2 Heat flux of the VBW and wood-frame wall for Vancouver, January

Figure D.2 shows that the VBW and wood-frame wall both contribute to cooling the zone during the entire three-day period. Nevertheless, the VBW provided more cooling during the sunny hours than the wood-frame wall due to its higher storage capacity and the significant role played by advection. During cold hours, the VBW contributed a lower level of cooling than a wood-frame wall. Given that the wall temperature remains consistently above 20°C over the course of three days, the ventilation switches on and operates continuously. Consequently, during periods of increased temperature difference between the indoor environment and the wall, such as from hour 9 to 17 and hour 59 to 66, the heat flux density of the VBW falls to more negative values in comparison to a wood-frame wall, owing to the predominant influence of advection on total heat flux density compared to the convection and radiation.

Figure D.3 illustrates the outdoor temperature, predicted indoor temperature, and the VBW surface temperature for three representative days in summer.

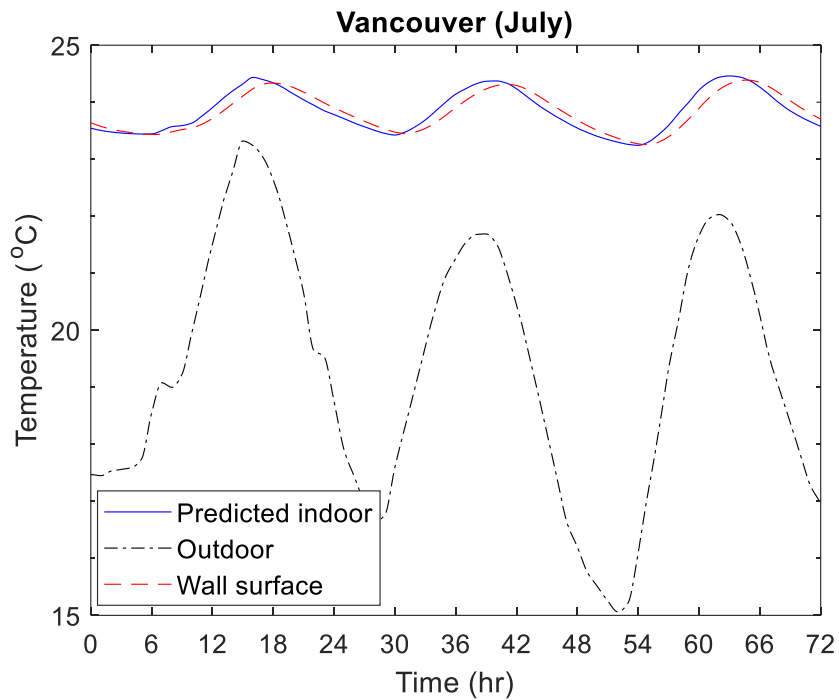


Figure D.3 Outdoor, predicted indoor, and VBW surface temperatures for Vancouver, July

As a result of more significant fluctuations in the outdoor temperature, the indoor temperature experiences pronounced swings throughout the day. Figure D.3 shows heating contributions during cold hours and cooling contributions during sunny hours.

Figure D.4 shows the changes in heat flux for the VBW and wood-frame wall in Vancouver, for three representative days in summer.

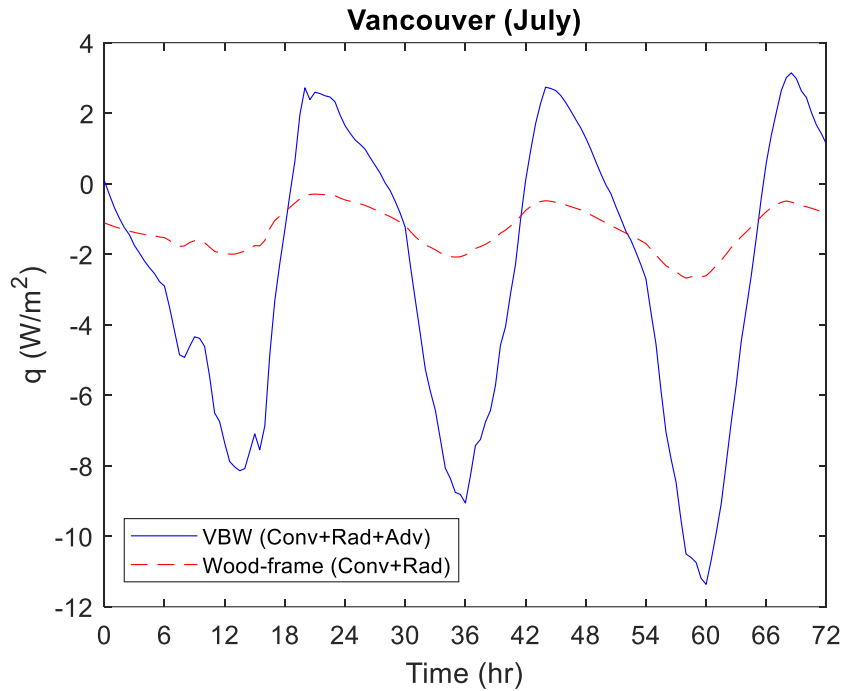


Figure D.4 Heat flux of VBW and wood-frame wall for Vancouver, July

The wood-frame wall only provided a small amount of cooling energy to the zone for the entire three-day period as shown in Figure D.4. The VBW, however, contributed a significant amount of heating and cooling during the day, which assisted in better regulating the zone temperature during the day.

Table D.1 presents the monthly total assisting heating and cooling achieved by both walls for Vancouver.

Table D.1 Monthly total assisting heating and cooling achieved by both walls for Vancouver

Month	Wood-frame wall			VBW					
	H* (kWh/ m ²)	C #1** (kWh/ m ²)	C #2*** (kWh/ m ²)	<i>v</i> =2 m/s			<i>v</i> =0 m/s		
				H (kWh/ m ²)	C#1 (kWh/ m ²)	C #2 (kWh/m ²)	H (kWh/ m ²)	C #1 (kWh/ m ²)	C #2 (kWh/ m ²)
January	0	0	0	0.8	0	0	0	0	0
February	0	0	0	1	0	0	0	0	0
March	0	0	0	1.4	0	0	0	0	0
April	0.005	0	0	1.8	0	0.03	0.004	0	0.01

May	0.05	0	0	2.1	0	0.7	0.2	0	0.15
June	0.1	0.01	0.03	2.3	0.3	1.3	0.5	0.3	0.4
July	0.2	0.04	0.09	2.9	0.7	2.8	1.1	0.6	1
August	0.2	0.03	0.07	2.7	0.7	2.6	1	0.4	1
September	0.1	0.001	0.001	1.9	0.01	1.1	0.1	0.02	0.04
October	0.01	0	0	1.3	0	0.13	0	0	0
November	0	0	0	1	0	0	0	0	0
December	0	0	0	0.9	0	0	0	0	0
Total (kWh/m²/year)	0.4	0.1	0.2	20.1	1.7	8.7	2.9	1.3	2.5
Fan energy consumption (kWh/year)		-			0.77			-	

*Heating

**Cooling – scenario 1

***Cooling – scenario 2

Across all months in a year, as shown in Table D.1, July provides the most heating and cooling energy to the zone, largely due to the heightened temperature fluctuations within the zone during this month. Furthermore, similar to Edmonton, cooling scenario #2 provides more cooling energy than scenario #1. Moreover, in Vancouver, fan energy consumption is greater than in Edmonton, as the fan is operated for more hours throughout the year due to the wall temperature experiencing more hours above 20°C compared to Edmonton.

When using an air speed of 2 m/s for ventilation, replacing a wood-frame wall with a VBW results in a total assisting heating and cooling of ~31 kWh/m² (wall area) for Vancouver, Canada throughout the year. Passive performance (i.e., v=0 m/s) results in a significant reduction in total heating and cooling energy when compared to an air speed of 2 m/s. Specifically, a reduction of 86%, 35%, and 70% was observed in total heating, total cooling in scenario 1, and total cooling in scenario 2, respectively.

b) Toronto

Toronto is the capital city of Ontario, a province in eastern Canada. On average, Toronto enjoys more than 2000 hours of bright sunshine each year, making it one of the top ten major cities in

Canada in terms of sunny hours [102]. In contrast to Vancouver, Toronto has colder and longer winters.

For Toronto, merely the plots and the monthly total energy exchange values are presented. More discussion can be found in the related analyses for Edmonton and Vancouver.

Figure D.5 shows the outdoor temperature, predicted indoor temperature, and the VBW surface temperature for three representative days in winter.

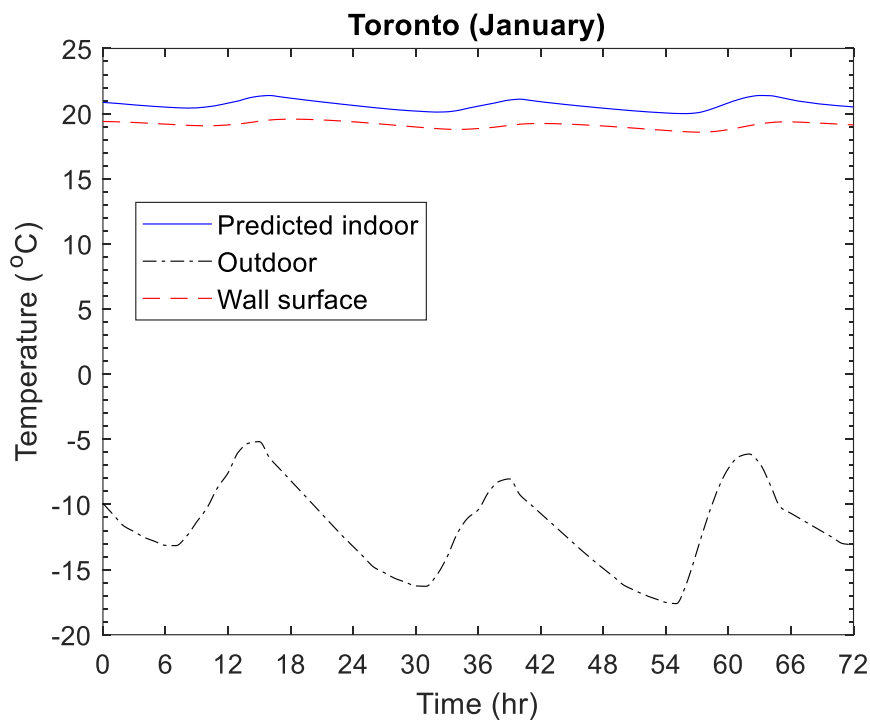


Figure D.5 Outdoor, predicted indoor, and VBW surface temperatures for Toronto, January
Figure D.6 shows the changes in heat flux for the VBW and wood-frame wall in Toronto, for three representative days in summer.

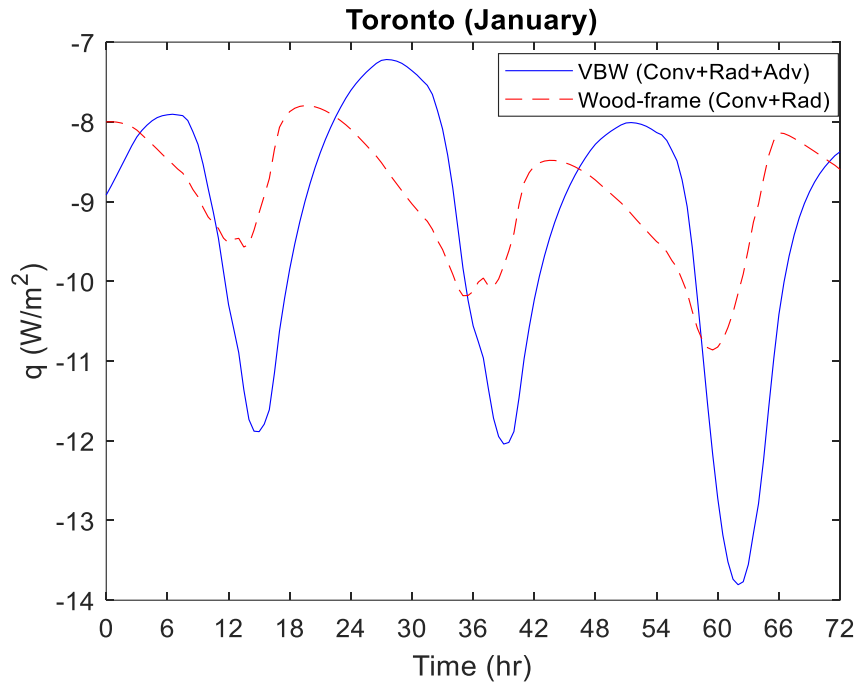


Figure D.6 Heat flux of the VBW and wood-frame wall for Toronto, January

Figure D.7 shows the outdoor temperature, predicted indoor temperature, and the VBW surface temperature for three representative days in summer.

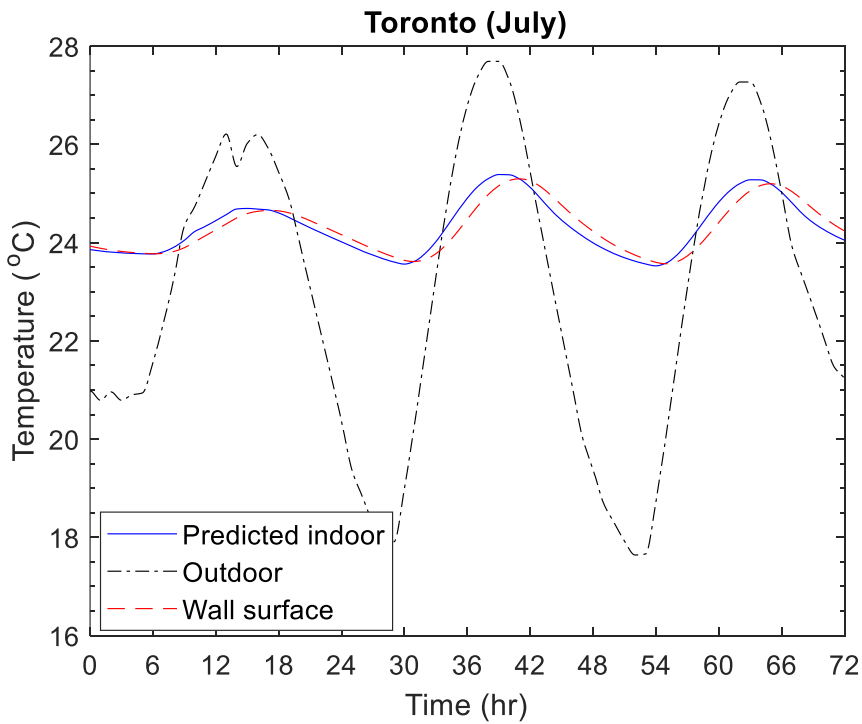


Figure D.7 Outdoor, predicted indoor, and VBW surface temperatures for Toronto, July

Figure D.8 depicts the changes in heat flux for the VBW and wood-frame wall in Toronto, for three representative days in summer.

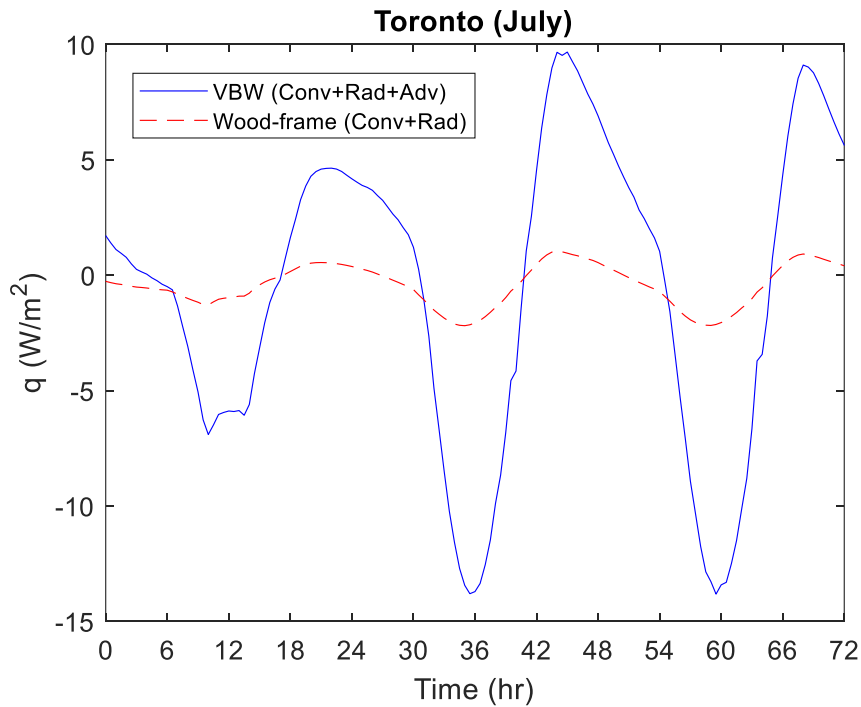


Figure D.8 Heat flux of VBW and wood-frame wall for Toronto, July

Table D.2 presents the monthly total assisting heating and cooling achieved by both walls for Toronto.

Table D.2 Monthly total assisting heating and cooling achieved by both walls for Toronto

Month	Wood-frame wall			VBW					
	H* (kWh/ m ²)	C #1** (kWh/ m ²)	C #2*** (kWh/ m ²)	<i>v</i> =2 m/s			<i>v</i> =0 m/s		
				H (kWh/ m ²)	C#1 (kWh/ m ²)	C #2 (kWh/m ²)	H (kWh/ m ²)	C #1 (kWh/ m ²)	C #2 (kWh/ m ²)
January	0	0	0	0.8	0	0	0	0	0
February	0	0	0	0.9	0	0	0	0	0
March	0	0	0	1.6	0	0	0	0	0
April	0	0	0	1.8	0	0	0	0	0

May	0.05	0.01	0.03	2.6	0.3	1.5	0.06	0.03	0.05
June	0.1	0.04	0.07	2.9	0.8	3.2	0.3	0.2	0.4
July	0.2	0.09	0.15	2.9	2.8	4	1.3	1	1.3
August	0.2	0.05	0.1	2.9	2.3	3.7	1.2	0.7	1.1
September	0.05	0.03	0.07	2.3	0.7	2.3	0.9	0.2	0.6
October	0.02	0	0	1.5	0	0.13	0	0	0.03
November	0	0	0	1.2	0	0	0	0	0
December	0	0	0	1	0	0	0	0	0
Total (kWh/m²/year)	0.6	0.2	0.4	22.4	6.9	14.8	3.8	2.2	3.5
Fan energy consumption (kWh/year)		-			0.72			-	

*Heating

**Cooling – scenario 1

***Cooling – scenario 2

Across all months in a year, as shown in Table D.2, July provides the most heating and cooling energy to the zone. In line with other cities, assisted cooling energy-scenario 1 shows that the total amount is consistently lower than total heating energy. However, unlike Edmonton and Vancouver, Toronto's cooling energy-scenario 2 reveals that cooling energy surpasses heating energy during the summer months of June, July, and August. This indicates that Toronto experienced numerous hours when outdoor temperatures exceeded 20°C, and VBW supplied cooling to the area during this period.

When using an air speed of 2 m/s for ventilation, replacing a wood-frame wall with a VBW leads to a total assisting heating and cooling of 44 kWh/m² (wall area) for Toronto, Canada throughout the year. Passive performance (i.e., v=0 m/s) results in a significant reduction in total heating and cooling energy when compared to an air speed of 2 m/s. Specifically, a reduction of 80%, 42%, and 74% was observed in total heating, total cooling in scenario 1, and total cooling in scenario 2, respectively.

Appendix E – A typical-day performance with drywall as the interior surface finishing

In this appendix, the results for the typical-day performance of the VBW with drywall as the interior surface finishing are presented. The following figures are associated with the exterior VBW with considering an air speed of 2 m/s and peak zone air temperature of 26°C.

Figure E.1 shows the average wall surface temperature. Results for other scenarios are tabulated in Table E.1.

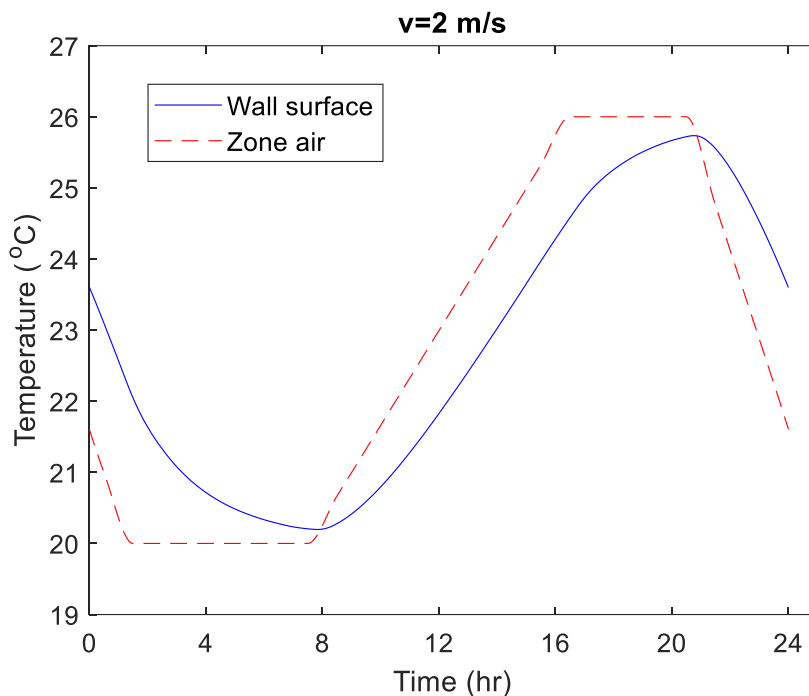


Figure E.1 Zone air and average wall surface temperatures for an exterior VBW with dry wall finishing

Table E.1 Maximum and minimum average wall interior surface temperatures for different zone temperatures and air speeds – Dry wall as the finishing layer

Zone temperature (min/max) (°C)	Average wall surface temperature (°C)		
	$v=0$ m/s	$v=1$ m/s	$v=2$ m/s

	min	max	max-min (ΔT)	min	max	max-min (ΔT)	min	max	max-min (ΔT)
20/26	21.1	24	2.9	20.4	25.4	5	20.1	25.7	5.6
20/24	21	22.9	1.9	20.2	23.5	3.3	20.3	23.9	3.6
20/22	20.4	21.5	1.1	20.3	21.7	1.4	20.2	21.9	1.7

Figure E.2 shows heat flux density changes for VBW with dry wall as the interior finishing.

Table E.2 shows the results for other scenarios.

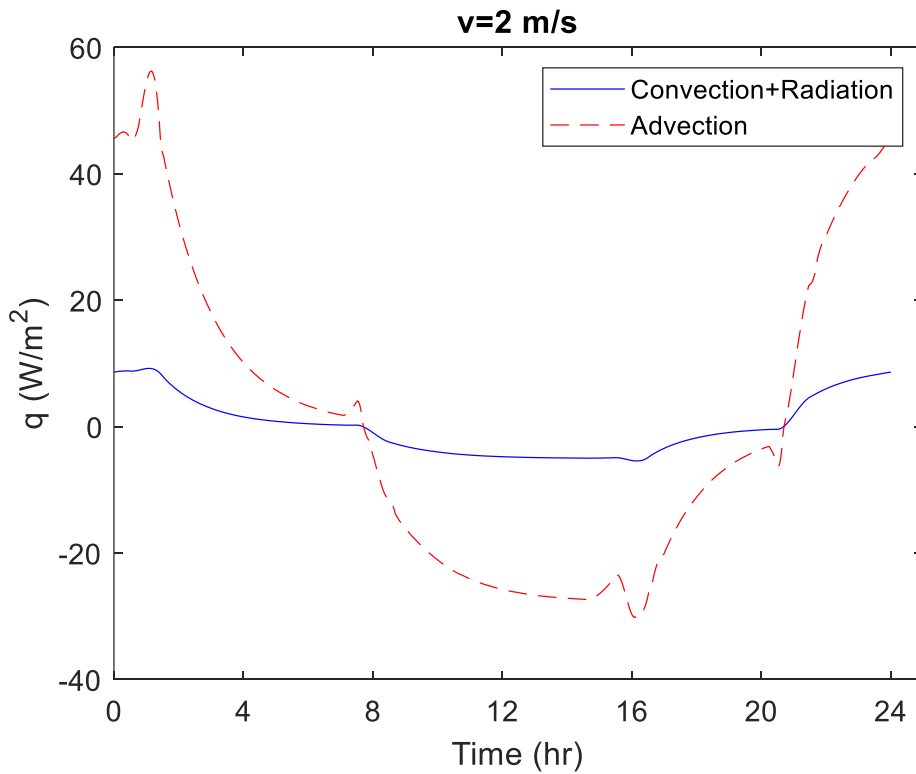


Figure E.2 Heat flux changes for an exterior VBW with dry wall finishing over a 24-hour period

Table E.2 Heat fluxes for an exterior VBW – Dry wall as the finishing layer

Zone temperature (min/max) (°C)	Heat transfer mechanism	Heat flux density (min/max) (W/m ²)		
		<i>v</i> =0 m/s	<i>v</i> =1 m/s	<i>v</i> =2 m/s
20/26	Convection & radiation	-13/13.7	-8/11.7	-5.4/9.1
	Advection	0	-26.5/39.1	-30.1/55.2
20/24	Convection & radiation	-8.3/10.1	-5.2/8.5	-3.6/6.7
	Advection	0	-19.3/29.3	-20/35.6
20/22	Convection & radiation	-4.2/6.2	-2.6/5.4	-2/4.7
	Advection	0	-10.1/16.5	-15.9/24.2

Table E.3 presents the total energy exchange between VBW and zone when dry wall was selected as the interior finishing layer.

Table E.3 Total net energy exchange of the exterior VBW – Dry wall as the finishing layer

Zone temperature (min/max) (°C)	Total net energy exchange (kWh/m ²)		
	<i>v</i> =0 m/s	<i>v</i> =1 m/s	<i>v</i> =2 m/s
20/26	0.17	0.43	0.51
20/24	0.11	0.29	0.35
20/22	0.05	0.15	0.19